

# Polyakov loop modeling for hot QCD

Kenji Fukushima,<sup>1</sup> and Vladimir Skokov<sup>2</sup>

<sup>1</sup>Department of Physics, The University of Tokyo, 7-3-1 Hongo, Bunkyo-ku, Tokyo 113-0033, Japan

<sup>2</sup>Riken-BNL Research Center, Brookhaven National Laboratory, Upton, New York 11973, USA

August 4, 2017

## Abstract

We review theoretical aspects of quantum chromodynamics (QCD) at finite temperature. The most important physical variable to characterize hot QCD is the Polyakov loop, which is an approximate order parameter for quark deconfinement in a hot gluonic medium. Additionally to its role as an order parameter, the Polyakov loop has rich physical contents in both perturbative and non-perturbative sectors. This review covers a wide range of subjects associated with the Polyakov loop from topological defects in hot QCD to model building with coupling to the Polyakov loop.

## Contents

<b>1</b>	<b>Introduction</b>	<b>2</b>
<b>2</b>	<b>Hot QCD, Polyakov Loop, and Confinement</b>	<b>4</b>
2.1	Quantizing Hot QCD . . . . .	4
2.2	Center Symmetry . . . . .	7
2.3	Strong Coupling Potential for the Polyakov Loop . . . . .	9
2.4	Perturbative Potential for the Polyakov Loop . . . . .	11
2.5	Gauge Configurations and Center Symmetry Restoration . . . . .	14
2.5.1	$Z(N_c)$ domain walls . . . . .	14
2.5.2	$Z(N_c)$ bubbles and calorons . . . . .	16
<b>3</b>	<b>Phase Transition in the Pure Gluonic Theory</b>	<b>18</b>
3.1	Polyakov Loop Models . . . . .	19
3.1.1	Parametrizing the Polyakov loop potential . . . . .	19
3.1.2	Inverted Weiss potential . . . . .	20
3.1.3	Mean-field approximation of a matrix model . . . . .	21
3.2	Large $N_c$ Limit . . . . .	23
3.2.1	Gross-Witten phase transition . . . . .	23
3.2.2	Effective matrix theory . . . . .	26
3.2.3	Weakly coupled theory on a small 3-sphere . . . . .	29

<b>4</b>	<b>Coupling to Quarks</b>	<b>31</b>
4.1	Polyakov Loop Potential from Quarks . . . . .	32
4.2	Polyakov Loop in Chiral Models . . . . .	33
4.2.1	PNJL model . . . . .	33
4.2.2	PQM model . . . . .	40
4.2.3	Critical point with heavy quarks . . . . .	42
4.3	Systems at Finite Baryon Density . . . . .	43
4.3.1	Sign problem . . . . .	43
4.3.2	Heavy-dense model . . . . .	45
4.3.3	Roberge-Weiss phase transition with imaginary chemical potential . . . . .	45
4.4	Deformed QCD with Center Symmetry . . . . .	47
4.4.1	Canonical ensemble . . . . .	47
4.4.2	Center twisted flavors . . . . .	49
4.4.3	Center-stabilized QCD . . . . .	49
<b>5</b>	<b>Phenomenological Implications</b>	<b>51</b>
5.1	Higher Cumulants and Polyakov Loop Fluctuations . . . . .	51
5.2	Semi-QGP Regime . . . . .	54
<b>6</b>	<b>Summary</b>	<b>56</b>

# 1 Introduction

Quantum Chromodynamics, which is commonly abbreviated as QCD, is a fundamental theory of the strong interaction composed from quarks and gluons. Gluons belong to the adjoint representation of the color  $SU(3)$  group, while quarks are in the color fundamental representation. Conventionally the quark color index runs over red, green, and blue, in analogy to “three primary colors” in nature. Although this is a departure from reality, it is nevertheless useful to change the number of colors  $N_c$  arbitrarily. Then the gluonic part in QCD is described by the  $SU(N_c)$  pure Yang-Mills theory. We will refer to the pure Yang-Mills theory as simply the “pure gluonic theory” throughout this review. We note that QCD reduces to the pure gluonic theory in the heavy-quark limit, i.e. the limit with all quark masses sent to infinity, which is often called the quenched limit.

The research area dedicated to reveal microscopic details for the QCD vacuum structure and QCD phase transitions when the system is equilibrated at finite temperature,  $T$ , has been very rich and active. The main subject of this review is focused on the physics of an order parameter of such a hot gluonic system, that is called the Polyakov loop named after the inventor [1]. Regarding the longstanding problem of color confinement in QCD, the Polyakov loop provides us with a useful view point especially on the following question: what causes color confinement? Precisely speaking, the problems of “quark” confinement and “gluon” confinement should be considered separately. For quark confinement in the pure gluonic theory, the Wilson loop in the fundamental representation is an well-defined measure of confinement, demonstrating the expected area law in the quark confined phase. To realize the area law, the QCD vacuum should accommodate highly disturbed gauge configurations; such an extremal case is approached in the limit of strong gauge coupling, as was first elucidated by Wilson [2]. In the strong coupling limit, gauge fluctuations at each spacetime point become independent of adjacent ones. Actually, the strong coupling expansion in gauge theory has clear resemblance to the high- $T$  expansion in (classical) spin models. This analogy is naturally understood in terms of the Polyakov loop; the finite- $T$  counterpart of the Wilson loop is the Polyakov loop correlation function, and the area law of the Wilson loop is recapitulated as an exponentially decaying behavior of the Polyakov loop correlation function, which is reminiscent of the spin correlation function in the *disordered* state. As a matter of

fact, the Polyakov loop effective model for the hot pure gluonic theory takes a form of a classical spin model with inverted temperature. In this sense the confined phase at low  $T$  can be regarded as a dual of the spin disordered state at high  $T$ . Such a picture of quark confinement from the point of view of condensed matter physics is quite useful for us to deepen our understanding of confinement.

The Polyakov loop provides additional benefits for investigations of the quark confinement. The disordered state is by definition a state with large fluctuations, and the question is what microscopic quanta can bring such fluctuations into the system. We know that magnetic domains and associated domain-walls are microscopic contents in the ordered and disordered states in spin systems; thus, it is natural to consider a gluonic counterpart, namely, the dynamics of the  $Z(N_c)$  domain-walls. Interestingly, the  $Z(N_c)$  domain-wall is a solution of the classical equation of motion *including* thermal fluctuation corrections. At the same time, we also know that the pure gluonic theory accommodates other solutions of the classical equation of motion, i.e. instantons. The finite- $T$  extended instantons are specifically called the calorons (meaning “caloric” instantons at finite  $T$ ) and the Polyakov loop varies on caloron configurations. Thus, the calorons are nothing but the  $Z(N_c)$  bubbles and the condensation of those bubbles may cause quark confinement. Originally, the instantons were supposed to be responsible for chiral symmetry breaking and quark confinement [3, 4] but the phenomenological model building for confinement based on an instanton liquid picture was not very successful before the relatively recent discovery of new calorons that have a non-trivial boundary condition of the Polyakov loop at large distance. These intriguing developments will be closely discussed in Sec. 2. We note, however, that it is not realistic to cover all relevant topics and background foundations within this single review. As a pragmatic approach, we shall make a decision not to reiterate fairly well-known parts of the Polyakov loop related physics, for which the readers can easily find comprehensive reviews. Let us here recommend several articles; for center symmetry and the classification of possible phase transitions, Ref. [5] is the most comprehensive review based on the classic paper [6]. Some updates for the classification are found in Ref. [7]. For the theoretical formulation of hot QCD, including discussion on the Polyakov loop and the calorons, Ref. [8] provides a complete description, and for a modern review on hot QCD, see also Ref. [9] which contains unique considerations on the meaning of the Polyakov loop. Here, in this review, we will not dwell on the physics of relativistic heavy-ion collision in which a new state of hot QCD matter, i.e. a quark-gluon plasma (QGP) is created in the laboratory. Interested readers can consult Refs. [10, 11, 12] for phenomenological implications of the Polyakov loop to the QGP physics. Several established textbooks are also available to study the heavy-ion collision physics [13, 14, 15, 16]. One might be wondering why we do not touch the lattice-QCD results in this review. This is because there are already thorough reviews by the authors from lattice-QCD groups [17] including recent proceedings [18, 19]. In this review, we pay more of our attention to semi-analytical sides of the Polyakov loop physics, particularly about the theoretical formulations of deconfinement in the pure gluonic theory as addressed in Sec. 3; we also try to make the present review be different from others, although we cannot avoid a partial overlap to keep this review as self-containing as possible.

Now, turning from the pure gluonic theory to QCD with dynamical quarks, which is the main subject in Sec. 4, new possible applications open. Although the physical meaning of the Polyakov loop as an order parameter is the most transparent in the pure gluonic theory, it also captures general screening properties of any colored excitations, and hence, the thermal excitations of quarks in QCD should be dictated by the Polyakov loop to a significant degree. This is the underlying idea behind the development of the Polyakov loop augmented chiral effective models, such as the Nambu–Jona-Lasinio (NJL) model and the quark-meson (QM) model. This is an active field of research covering many interesting subjects of hot QCD matter; there is also a multitude of interesting results from the chiral model studies which cannot be covered in this review in full. Therefore, again, we shall take a pragmatic strategy of not discussing all related works but picking up some selected topics only. In particular, we will put our emphasis on rather analytical aspects of the model studies and the implication to the sign problem of the Dirac determinant at finite density, which also includes recently developing topics such as the

determination of the Polyakov loop effective potential and the semi-QGP regime. Because the Polyakov loop is more sensitive to deconfinement rather than the chiral sector, though they couple to each other through the Polyakov loop, our descriptions of the chiral symmetry breaking and restoration will be minimal in this review. Interested readers can easily find background materials; the classic reviews on the chiral physics can be found following Refs. [20, 21] and the state-of-the-art review including inhomogeneous phases is Ref. [22]. Since we already mentioned that the QCD vacuum has a condensed matter analogy, it is not surprising that chiral models also have the condensed matter interpretation, which is known from the very early times traced back to Nambu and Jona-Lasinio [23]. In this context readers may want to consult review articles on condensed matter physics aspects of chiral symmetry in QCD [24, 25].

## 2 Hot QCD, Polyakov Loop, and Confinement

We explain the quantization procedure for QCD following the standard procedure outlined in Ref. [8] and supplemented with the field theoretical treatment of the ghost boundary condition. The Polyakov loop arises from the free energy in the presence of a test color charge. We then proceed to discussions on underlying symmetry that governs the behavior of the Polyakov loop. For the rest of this section, we see various concrete examples of the Polyakov loop calculations using perturbative and non-perturbative methods.

### 2.1 Quantizing Hot QCD

We will evade going into mathematical subtleties of QCD quantization, as the standard perturbative procedure to quantize hot QCD would suffice for our present purpose. The QCD Lagrangian density in Minkowskian spacetime consists of the pure gluonic part and the quark part as

$$\mathcal{L}(x) = -\frac{1}{4}F_{\mu\nu}^a(x)F^{\mu\nu a}(x) + \bar{\psi}(x)(i\not{D} - m)\psi(x), \quad (1)$$

where the flavor trace is implicitly understood (with  $m$  being a quark mass matrix in flavor space). Our convention for the field strength tensor is  $F_{\mu\nu}^a = \partial_\mu A_\nu^a - \partial_\nu A_\mu^a + gf^{abc}A_\mu^b A_\nu^c$  in terms of gluon fields  $A_\mu^a(x)$ . We can then read the canonical momenta from the Lagrangian density as

$$\Pi_A^{ia}(x) = \frac{\partial\mathcal{L}}{\partial(\partial_0 A_i^a(x))} = -F^{0ia}(x) = -\partial^0 A^{ia}(x), \quad (2)$$

$$\pi_\psi(x) = \frac{\partial\mathcal{L}}{\partial(\partial_0\psi(x))} = i\psi^\dagger(x). \quad (3)$$

Several remarks are necessary here. Because  $\pi_\psi(x)$  does not involve any time derivative, we need to calculate the Dirac brackets to quantize such a constrained system. It is known, however, that the correct answer is obtained in a simplified prescription in which only  $\psi(x)$  is treated as a dynamical variable and  $\bar{\psi}(x)$  or  $\psi^\dagger(x)$  is regarded as its canonical momentum. Another problem is that there is no canonical momentum for  $A_0^a(x)$  because the antisymmetric tensor  $F_{\mu\nu}^a$  cannot accommodate the term  $\partial_0 A_0^a(x)$  by definition. Therefore, we impose the so-called Weyl gauge fixing condition,  $A_0^a = 0$ , which is used for the second equality in Eq. (2). With these canonical momenta we proceed with the Legendre transformation to find the QCD Hamiltonian density as

$$\mathcal{H} = -\frac{1}{2}\Pi_{A_i}^a\Pi_A^{ia} + \frac{1}{4}F_{ij}^a F^{ija} - i\pi_\psi\gamma^0[-i\gamma^i(\partial_i - igA_i) + m]\psi. \quad (4)$$

Now that the Hamiltonian density is explicitly given, we can write down the QCD ‘‘partition function’’ at finite temperature  $T$  as follows;

$$Z_{\text{QCD}} = \text{tr} e^{-\beta H} = \int \mathcal{D}A_i \mathcal{D}\psi \langle A_i - \psi | e^{-\beta H} \mathcal{P}_G | A_i, \psi \rangle . \quad (5)$$

Here, the Hamiltonian  $H$  represents  $H = \int d^3x \mathcal{H}$ . The anti-periodic boundary condition imposed as  $\int \mathcal{D}\psi \langle -\psi | \cdots | \psi \rangle$  is attributed to our convention for the fermionic complete set;  $1 = \int \mathcal{D}\psi |\psi\rangle \langle \psi|$ . It is quite important to note that  $\mathcal{P}_G$  is needed to project states out to satisfy the Gauss law, which eliminates gauge uncertainty in the time evolution.

The Gauss law operator is a generator for the gauge transformation and it acts on the field coherent states as

$$\mathcal{G}^a(\mathbf{x}) | A_i, \psi \rangle = \left( D_i \Pi_A^{ia} - ig \pi_\psi t^a \psi \right) | A_i, \psi \rangle , \quad (6)$$

which should be vanishing for physical states selected by  $\mathcal{P}_G$ . We note that  $t^a$ 's are elements of  $\text{su}(N_c)$  algebra in the fundamental representation. Then, we can introduce a Lagrange multipliers  $\Theta^a(\mathbf{x})$  to express  $\mathcal{P}_G$  in the following way,

$$\mathcal{P}_G = \int \mathcal{D}\Theta \mu[\Theta] \exp \left[ -i \int d^3x \Theta^a(\mathbf{x}) \mathcal{G}^a(\mathbf{x}) \right] , \quad (7)$$

where  $\mu[\Theta]$  represents an appropriate integration measure. If we adopt a gauge invariant measure or the Haar measure for the  $\text{SU}(N_c)$  group integration, as is obvious from discussions above, the gauge is completely fixed and then  $\mu[\Theta]$  turns out to coincide with the Faddeev-Popov determinant in a certain gauge. In many cases it would be more convenient to formulate quantized QCD with more general Faddeev-Popov determinant rather than a special choice of the gauge fixing as we have employed above. For this purpose we extend the interpretation of  $\mu[\Theta]$  to include the gauge fixing constraint and the Faddeev-Popov determinant. We then insert the projection operator at each ‘‘thermal time’’ slice and convert the partition function into a functional representation of

$$\begin{aligned} Z_{\text{QCD}} &= \lim_{n \rightarrow \infty} \int \mathcal{D}A_i \mathcal{D}\psi \langle A_i, -\psi | \left( e^{-\frac{\beta}{n} H} \mathcal{P}_G \right)^n | A_i, \psi \rangle \\ &= \int_{(\text{anti-})\text{periodic}} \mathcal{D}A_\mu \mathcal{D}\psi \mathcal{D}\bar{\psi} \delta(G[A]) \det \left( D_\mu^a \frac{\partial G}{\partial A_\mu^a} \right) e^{-S_G[A] - S_F[A, \bar{\psi}, \psi]} , \end{aligned} \quad (8)$$

where the gluon fields are periodic,  $A_\mu(x_4 = \beta) = A_\mu(x_4 = 0)$ , while the quark fields are anti-periodic,  $\psi(x_4 = \beta) = -\psi(x_4 = 0)$ . We note that we renamed as  $\Theta \rightarrow A_4$  and  $i\pi_\psi \gamma^0 \rightarrow \bar{\psi}$  and replaced  $\mu[\Theta]$  with a conventional set in the Faddeev-Popov quantization procedure with an arbitrary gauge fixing function  $G[A]$ . As a consequence of above manipulations, the theory appears in Euclidean spacetime and the corresponding actions are

$$S_G = \int^\beta d^4x \frac{1}{4} F_{\mu\nu}^a F_{\mu\nu}^a , \quad S_F = \int^\beta d^4x \bar{\psi} (i\not{D} - m) \psi , \quad (9)$$

with a short-handed notation;  $\int^\beta d^4x \equiv \int_0^\beta dx_4 \int d^3x$ . For Dirac matrices in the Euclidean space, we use the same convention as in the standard textbook [14] where  $\gamma_4^E = i\gamma^0$  and  $\gamma_i^E = \gamma^i$ , so that  $\{\gamma_\mu^E, \gamma_\nu^E\} = -2\delta_{\mu\nu}$ , which is sometimes referred to as the anti-Hermitian convention, for all  $\gamma_\mu^E$ 's are anti-Hermitian matrices. Hereafter we use only the Euclidean notation throughout this review and drop the superscript E. We also comment that, according to the above-mentioned convention, the covariant derivative should be changed from  $\partial_i - igA_i$  in original Minkowskian spacetime to  $\partial^i + igA^i$  in the imaginary-time formalism. We, however, keep using the common convention  $\partial_i - igA_i$  in both

cases by changing the sign of  $g$ . Also at finite chemical potential  $\mu$ , we can simply replace  $\partial_4 \rightarrow \partial_4 - \mu$ . This means that the chemical potential is to be identified as an imaginary component of the Euclidean gauge field, i.e.,  $\mu \sim -\text{Im}(gA_4)$ .

In frequency space the periodic boundary condition for  $A_\mu$  and the anti-periodic boundary condition for  $\psi$  imply that the frequencies for  $A_\mu$  and  $\psi$  are discretized as  $\omega_n = 2\pi nT$  (bosonic Matsubara frequency) and  $\omega_n = 2\pi(n + 1/2)T$  (fermionic Matsubara frequency), respectively. Following the well-known trick with auxiliary fields we can reformulate Eq. (8) into a more familiar form with ghost  $c$  and anti-ghost  $\bar{c}$  fields. Then, it is quite non-trivial which of the periodic and anti-periodic boundary conditions the ghost fields should obey. From an intuitive argument that the ghost contributions should cancel unphysical polarizations in  $A_\mu$ , one would presume that the ghost fields should be periodic, but the question is how to justify it from the field theoretical point of view. To this end, we should have started with the BRST quantized Hamiltonian in Minkowskian spacetime instead of choosing the Weyl gauge. In the BRST quantization procedure, similarly to  $\mathcal{P}_G$ , the physical states are picked up by the operator  $\mathcal{P}_{\text{BRST}}$  that projects out states with zero ghost number. Then, using the BRST charge  $Q_B$  and the ghost number  $Q_C$ , the quantized QCD partition function takes the following form [26]:

$$Z_{\text{QCD}} = \text{tr} \left[ (1 - \{Q_B, R\}) e^{-\pi Q_C} e^{-\beta H} \right], \quad (10)$$

with some operator  $R$  that has the ghost number  $-1$  (where an exact form of  $R$  is irrelevant here). Because  $\mathcal{P}_{\text{BRST}} = 1 - \{Q_B, R\}$  already selects only  $Q_C = 0$  states out, the insertion of  $e^{-\pi Q_C} = 1$  is formally trivial, but its presence significantly simplifies the final form. Then,  $\{e^{-\pi Q_C}, Q_B\} = 0$  follows from  $e^{i\pi} = -1$  and the algebra,  $[Q_C, Q_B] = -iQ_B$ . Hence, owing to the insertion  $e^{-\pi Q_C}$ , the  $\{Q_B, R\}$  part in Eq. (10) does not contribute. Thus, the partition function is  $Z_{\text{QCD}} = \text{tr}(e^{-\pi Q_C - \beta H})$ , in which the remnant of  $\mathcal{P}_{\text{BRST}}$  is interpreted as a ghost chemical potential, namely,  $\mu_{\text{ghost}} = i\pi T$ . This imaginary chemical potential shifts the ‘‘fermionic’’ Matsubara frequency of the ghost fields by  $-\pi T$ , so that the ghost fields have the ‘‘bosonic’’ Matsubara frequency after all (see discussions in Ref. [26] for more details).

Let us now evaluate the free energy  $F_q(\mathbf{r})$  when a static test quark is placed at  $\mathbf{x} = \mathbf{r}$ . The Gauss law constraint is modified as

$$\mathcal{G}^a(\mathbf{x})|A_i, \psi; q^b(\mathbf{r})\rangle = \left[ D_i \pi_A^{ia} - ig\pi_\psi t^a \psi + gt^a \delta^{ab} \delta(\mathbf{x} - \mathbf{r}) \right] |A_i, \psi; q^b(\mathbf{r})\rangle. \quad (11)$$

The color-averaged free energy is then given by [27, 28]

$$e^{-\beta F_q(\mathbf{r})} = \int \mathcal{D}A_i \mathcal{D}\psi \sum_{a=1}^{N_c} \langle A_i, -\psi; q^a(\mathbf{r}) | e^{-\beta H} \mathcal{P}_G | A_i, \psi; q^a(\mathbf{r}) \rangle = \langle \text{tr}_c L_3(\mathbf{r}) \rangle, \quad (12)$$

where  $\text{tr}_c$  explicitly indicates that this trace is taken in color space only. Here,  $L(\mathbf{r})$  is called the Polyakov loop [1] defined as

$$L_3(\mathbf{r}) = \mathcal{P} \exp \left[ ig \int_0^\beta dx_4 A_4(\mathbf{r}, x_4) \right] \quad (13)$$

in the fundamental representation. The path ordering  $\mathcal{P}$  appears naturally from the construction of the path integral. Replacing  $A_4 = A_4^a t^a$  with  $A_4^a T^a$ , where  $T^a$  are elements of  $\text{su}(N_c)$  algebra in the adjoint representation, we can also define the adjoint Polyakov loop  $L_8$  likewise.

The free energy  $F_{q\bar{q}}(\mathbf{r})$  in the presence of a static test quark at  $\mathbf{x} = 0$  and a static test anti-quark at  $\mathbf{x} = \mathbf{r}$  can also be computed by taking the color average separately for the quark and the anti-quark

$$e^{-\beta F_{q\bar{q}}(\mathbf{r})} = \langle \text{tr}_c L_3^\dagger(\mathbf{r}) \text{tr}_c L_3(0) \rangle. \quad (14)$$



Furthermore, it would be convenient to define the traced Polyakov loops and its expectation values for general representation  $\mathcal{R}$  as

$$\ell_{\mathcal{R}}(\mathbf{x}) = \frac{1}{d_{\mathcal{R}}} \text{tr}_c L_{\mathcal{R}}(\mathbf{x}), \quad \Phi_{\mathcal{R}}(\mathbf{x}) = \langle \ell_{\mathcal{R}}(\mathbf{x}) \rangle. \quad (15)$$

Here,  $d_{\mathcal{R}}$  denotes the dimension of the representation  $\mathcal{R}$ , so that  $\ell_{\mathcal{R}}$  becomes the unity for vanishing gauge field (apart from renormalization). For the quark dynamics we mostly deal with the fundamental (triplet) representation only, and we often drop the subscript 3 and use simplified notations in this review such as  $\ell = \frac{1}{N_c} \text{tr}_c L$  and  $\Phi = \langle \ell \rangle$  and so on. Finally we here make a quick remark that  $\Phi_{\mathcal{R}}$  takes a real-valued number in general, while  $\ell_{\mathcal{R}}$  can be complex. We will discuss this point in detail when we consider finite-density systems.

## 2.2 Center Symmetry

The Polyakov loop is a gauge invariant quantity and nevertheless it is sensitive to the boundary condition of the gauge transformation. Under the gauge transformation with a transformation matrix  $V(x) \in \text{SU}(N_c)$ , the gluon fields change as

$$A_{\mu}(x) \rightarrow A'_{\mu}(x) = V(x) \left( A_{\mu}(x) - \frac{1}{ig} \partial_{\mu} \right) V^{\dagger}(x), \quad (16)$$

which does not affect the action. However, the boundary condition may be changed by the boundary property of  $V(x)$ . In principle we can abandon the periodicity of  $A'_{\mu}(x)$ , and then the theory is put on a different manifold than  $S^1 \times R^3$  (see Ref. [29] for such an example). If we prefer to keep the same computational rules on the same manifold, we need to extend the meaning of symmetry including the manifold structure. This would require,

$$A'_{\mu}(x_4 = \beta) = A'_{\mu}(x_4 = 0). \quad (17)$$

What is interesting is that this requirement for  $A'_{\mu}(x)$  does not necessarily impose the periodicity of  $V(x)$ , that is, a twisted boundary condition is allowed as

$$V(x_4 = \beta) = z_k \cdot V(x_4 = 0), \quad z_k = e^{i2\pi k/N_c} \quad (18)$$

for  $k = 0, 1, \dots, N_c - 1$ . It should be noted that  $\det(z_k V) = (z_k)^{N_c} \det V = 1$ . Because  $z_k$ 's belong to the center group  $Z_{N_c}$  of the  $\text{SU}(N_c)$  gauge group, the invariance under such a gauge transformation with a twist by  $z_k$  is called center symmetry [6].

It would be instructive to take an example of  $V(x)$  to deepen some intuitive understanding on center symmetry. The simplest example would be

$$V(x_4) = \text{diag} \left[ e^{i2\pi k x_4 / (\beta N_c)}, e^{i2\pi k x_4 / (\beta N_c)}, \dots, e^{-i2\pi(N_c-1)k x_4 / (\beta N_c)} \right], \quad (19)$$

which belongs to  $\text{SU}(N_c)$  for any  $x_4$ . Obviously  $V(x_4 = 0) = 1_{N_c \times N_c}$  and  $V(x_4 = \beta) = z_k V(0)$ . Then,  $A_4$  is shifted by this center twisted gauge transformation  $V$  as

$$A_4 \rightarrow A'_4 = A_4 - \frac{2\pi}{g\beta N_c} \text{diag} [k, k, \dots, -(N_c - 1)k]. \quad (20)$$

Therefore, the center transformation amounts to a discretized displacement in  $A_4$ , and usually such a constant shift or the so-called large gauge transformation is not relevant for physical quantities. However, it is quite easy to see from the definition (13) that the Polyakov loop changes as

$$L_3 \rightarrow L'_3 = z_k \cdot L_3. \quad (21)$$

As long as center symmetry is not broken, therefore, the Polyakov loop expectation value,  $\Phi_3$ , is zero, and this leads to the following conclusion [see Eq. (12)];

$$(\text{center symmetry}) \rightarrow \Phi_3 = 0 \rightarrow F_q = \infty, \quad (22)$$

which is interpreted as realization of *quark confinement*. To summarize the above discussions, the fundamental Polyakov loop expectation value is an order parameter for center symmetry breaking, and the confined phase corresponds to the center symmetric vacuum.

It would be an interesting question what happens for gluons in the adjoint representation. Using an identity,  $\text{tr}L_8 = |\text{tr}L_3|^2 - 1$ , we see that, with a decomposition to the disconnected part as  $\langle |\text{tr}L_3|^2 \rangle = N_c^2 \Phi_3^2 + \langle |\text{tr}L_3|^2 \rangle_c$ , the adjoint Polyakov loop is always non-zero, i.e.

$$\Phi_8 = \frac{N_c^2}{N_c^2 - 1} \Phi_3^2 + \frac{1}{N_c^2 - 1} (\langle |\text{tr}L_3|^2 \rangle_c - 1). \quad (23)$$

We can give a clear interpretation for the fact that  $\Phi_8$  is not necessarily zero even in the center symmetric vacuum in which  $\Phi_3 = 0$ ; (test) gluons can be always screened by gluons (in a medium) to form a color singlet with a finite energy, while it was impossible for a test quark in a gluonic medium. In other words, gluons are not sensitive to the center of the gauge group (note that the adjoint representation is not a faithful representation by the center of the original group). The important message is that we cannot construct an order parameter for *gluon confinement* in this way. However, Eq. (23) implies that  $\Phi_8$  can behave like an order parameter  $\propto \Phi_3^2$  in the large  $N_c$  limit and it may approximately work even for  $N_c = 3$ .

One might have thought that  $\Phi$  looks like a spin variable and the confined phase may well be characterized by a disordered state in a corresponding spin system. The possible connection between hot QCD and spin systems would be transparent in the original argument by Polyakov [1]. For the rest of this subsection, we will take a quick look at the original idea, which is actually quite useful to understand why the QCD *disordered* state appears in *low T*. To address a possible phase transition of quark deconfinement at high  $T$ , it is first indispensable to setup a theoretical description of confined matter at low  $T$ . One way to do this is to use the strong coupling expansion. In the leading order of the strong coupling expansion in the Hamiltonian formalism, only the chromo-electric fields  $\sim g^2 E^2$  contribute to the partition function and the chromo-magnetic fluctuations  $\sim g^{-2} B^2$  are negligible. The leading-order QCD partition function at temperature  $T$  reads;

$$Z_{\text{QCD}} = \sum_{\{\mathbf{n}(\mathbf{x})\}} \exp \left[ -\frac{g^2}{2T} \sum_{\mathbf{x}} \mathbf{n}(\mathbf{x})^2 \right] \delta(\nabla \cdot \mathbf{n}), \quad (24)$$

where  $\mathbf{n}(\mathbf{x})^2$  denotes an electric flux squared with the trace over color implicitly taken. At strong coupling the gauge group is irrelevant and even the compact U(1) theory realizes confinement via Dirac monopoles. In what follows let us consider the simple compact U(1) gauge theory and only the quantized Dirac strings for  $\mathbf{n}(\mathbf{x})$  discarding continuous fluctuations. Now, for notational simplicity, we choose the lattice spacing so that  $\mathbf{n}(\mathbf{x})$  is quantized to be integral numbers. The delta functional constraint represents the Gauss law, for which we can introduce an auxiliary field  $\phi$  as  $\delta(\nabla \cdot \mathbf{n}) \rightarrow \int \mathcal{D}\phi \mu(\phi) \exp[i \sum \phi(\nabla \cdot \mathbf{n})]$ . Clearly,  $\phi$  plays the same role as  $\Theta$  in our previous discussions and it should be interpreted as  $A_4$  after all.

Using Poisson's resummation formula,

$$\sum_{n=-\infty}^{\infty} f(x + nT) = \frac{1}{T} \sum_{m=-\infty}^{\infty} \tilde{f}(k/T) e^{i2\pi kx/T}, \quad (25)$$



where  $\tilde{f}(k)$  is a Fourier transform of  $f(x)$ , we can rewrite the partition function, apart from irrelevant overall constants, as

$$Z_{\text{QCD}} = \int \mathcal{D}\phi \mu(\phi) \sum_{\{\mathbf{m}(\mathbf{x})\}} \exp \left[ -\frac{T}{2g^2} \sum_{\mathbf{x}} (\nabla\phi - 2\pi\mathbf{m})^2 \right]. \quad (26)$$

This is a well-known form of the Villain approximated XY spin model. If the coefficient  $T/(2g^2)$  is large enough to suppress large amplitude fluctuations, the Villain approximation works good, and then we can make an approximation on the above expression to go *back* to the XY spin model;

$$Z_{\text{QCD}} \approx \int \mathcal{D}\phi \mu(\phi) \exp \left( \frac{T}{g^2} \sum_{\text{n.n.}} \mathbf{S}_i \cdot \mathbf{S}_j \right), \quad (27)$$

where the nearest neighbor interaction arises from discretized  $\nabla$  on the lattice and  $\mathbf{S}_i = (\cos \phi_i, \sin \phi_i)$ . In this way we can see that the QCD partition function at strong coupling is mapped onto the XY spin model with the temperature  $\propto 1/T$ . In fact, Poisson's resummation formula connects dual theories with inverse coupling and temperature, and this clearly explains why the confined phase in low- $T$  QCD looks like a disordered phase that usually appears in high- $T$  spin systems. We can readily identify the order parameter for spontaneous magnetization in this XY model;  $\langle S_x \rangle = \langle \cos \phi \rangle$ , which is nothing but the traced Polyakov loop expectation value.

## 2.3 Strong Coupling Potential for the Polyakov Loop

The Hamiltonian formalism is suitable to clarify the physical contents of the dual spin-like theory, as we saw in the previous subsection, but is not very convenient practically for more systematic expansions. Here, let us see another strong coupling expansion to calculate the effective potential for the Polyakov loop [30, 31, 32, 33, 34]. The strategy is straightforward; first we integrate all spatial gauge fluctuations and leave only  $A_4$  unintegrated, and second, we analyze the phase transition in the mean-field approximation.

In the lattice gauge theory the partition function is formulated in terms of the link variables,  $U_\mu(\mathbf{x}) = e^{-igaA_\mu(\mathbf{x})}$ , and the plaquettes,  $U_{\mu\nu}(\mathbf{x}) = U_\mu(\mathbf{x})U_\nu(\mathbf{x} + \hat{\mu})U_\mu^\dagger(\mathbf{x} + \hat{\nu})U_\nu^\dagger(\mathbf{x})$ . Then, the  $A_4$  or  $U_4$  unintegrated partition function is defined as

$$Z[U_4] = \int \mathcal{D}U_i \exp \left[ \frac{1}{g^2} \sum_{\mathbf{x}, \mu > \nu} \text{tr}_c(U_{\mu\nu} + U_{\mu\nu}^\dagger) \right]. \quad (28)$$

In the leading order of the strong coupling expansion, the first nonzero term appears from the contribution of  $N_c$  plaquettes aligned straightly along the  $x_4$  direction, i.e.

$$Z[U_4] \sim \exp \left[ \left( \frac{1}{g^2 N_c} \right)^{N_\tau} \sum_{\text{n.n.}} \text{tr} L_3^\dagger(\mathbf{x}') \cdot \text{tr} L_3(\mathbf{x}) \right], \quad (29)$$

where  $L(\mathbf{x}) = \prod_{x_4} U_4(\mathbf{x}, x_4)$  is the Polyakov loop on the lattice and  $N_\tau$  is the number of sites along the periodic  $x_4$  direction. Because  $T = 1/(N_\tau a)$  and the string tension in the strong coupling limit is  $\sigma = a^{-2} \ln(g^2 N_c)$  (with  $a$  being the lattice spacing), we can write the nearest neighbor interaction strength with physical quantities, and the Polyakov loop effective theory, that is exactly the counterpart of the XY model in Eq. (27), takes the following form;

$$Z = \int \mathcal{D}L \exp \left[ J \sum_{\text{n.n.}} \ell_3^*(\mathbf{x}') \cdot \ell_3(\mathbf{x}) \right] \quad (J = N_c^2 e^{-\beta\sigma a}), \quad (30)$$

which defines an effective matrix model. We will closely discuss the properties of this model in a later section and here we see a phase transition in the simplest mean-field (tree-level) approximation.

If  $J$  is very small, the Polyakov loop expectation value should be zero, which is caused by the group integration. Therefore, it is crucial to include the effect of the group integration that favors the confined phase. We can actually take account of this by including the Haar measure in the effective potential, which is sometimes called the Vandermonde determinant interaction, for the  $SU(N_c)$  Haar measure is given by the Vandermonde determinant. Then, the effective potential is,

$$V[\Phi_3] = -6J|\Phi_3|^2 - \ln H[\Phi_3], \quad (31)$$

where  $H[\Phi_3]$  represents the Haar measure whose concrete shape simplifies in the Polyakov gauge in which  $A_4$  is diagonal and static. In this gauge we can parametrize  $A_4$  as

$$A_4 = \frac{2\pi}{g\beta} \text{diag}(q_1, q_2, \dots, q_{N_c}) \quad \left( \sum_i q_i = 0 \right). \quad (32)$$

Then, the  $SU(N_c)$  Haar measure associated with the Polyakov loop integration reads,

$$H[q] = \prod_{\mathbf{x}, i < j} \left| e^{i2\pi q_i(\mathbf{x})} - e^{i2\pi q_j(\mathbf{x})} \right|^2. \quad (33)$$

For the color  $SU(2)$  case we can write the Polyakov loop as  $\Phi_3 = \langle \cos(\pi q) \rangle$  using  $q_1 = q/2$  and  $q_2 = -q/2$ . This expression reminds us of  $\langle S_x \rangle$  in the XY model that is dual to hot QCD in the Hamiltonian formalism. We note that the Polyakov loop (even before taking the expectation value) always takes a real value in the  $SU(2)$  case, reflecting the pseudo-real property of the  $SU(2)$  group. In this case, according to Eq. (33), the Haar measure is  $H[q] = \sin^2(\pi q)$  and in the mean-field approximation we have  $H[\Phi] = 1 - \Phi_3^2$ . The effective potential including the Haar measure contribution is thus,

$$V[\Phi_3] = -6J\Phi_3^2 - \ln(1 - \Phi_3^2) \simeq (1 - 6J)\Phi_3^2 + O(\Phi_3^4) \quad [\text{for } SU(2) \text{ case}], \quad (34)$$

from which we can easily understand that a second-order phase transition occurs at the critical coupling,  $J_c = 1/6$ . The potential behavior near  $J_c$  is plotted in the left of Fig. 1. It is important to point out that the perturbative vacuum at  $\Phi_3 = 1$  (or  $A_4 = 0$ ) is singular and can never be realized at finite energy. For the color  $SU(3)$  case  $\ell_3$  is generally a complex number, though  $\Phi_3$  is real. This may in principle induce  $\bar{\Phi}_3 \neq \Phi_3$  where  $\bar{\Phi}_3 = \langle \ell_3^* \rangle$ . Then, again from Eq. (33) for the  $SU(3)$  Haar measure, the effective potential in the mean-field approximation reads,

$$V[\Phi_3] = -6J\bar{\Phi}_3\Phi_3 - \ln[1 - 6\bar{\Phi}_3\Phi_3 + 4(\bar{\Phi}_3^3 + \Phi_3^3) - 3(\bar{\Phi}_3\Phi_3)^2] \quad [\text{for } SU(3) \text{ case}]. \quad (35)$$

We note that we can safely postulate  $\bar{\Phi}_3 = \Phi_3$  as long as the charge parity symmetry holds (that is the case for the pure gluonic theory). Because of the presence of the cubic terms,  $\bar{\Phi}_3^3$  and  $\Phi_3^3$ , the above effective potential has a first-order phase transition at  $J_c \simeq 0.773$ . The potential behavior near  $J_c$  is plotted in the right of Fig. 1.

So far, we have seen that the perturbative vacuum of  $A_4 = 0$  has an infinite barrier and its realization is prohibited in the strong coupling calculation. Interestingly enough, one can conversely prove that  $A_4 = 0$  is always the ground state once the Haar measure is removed by hand from the partition function [35], or in short, one could say; no Haar measure, no confinement! This observation strongly suggests that the Haar measure is the driving-force for quark confinement.

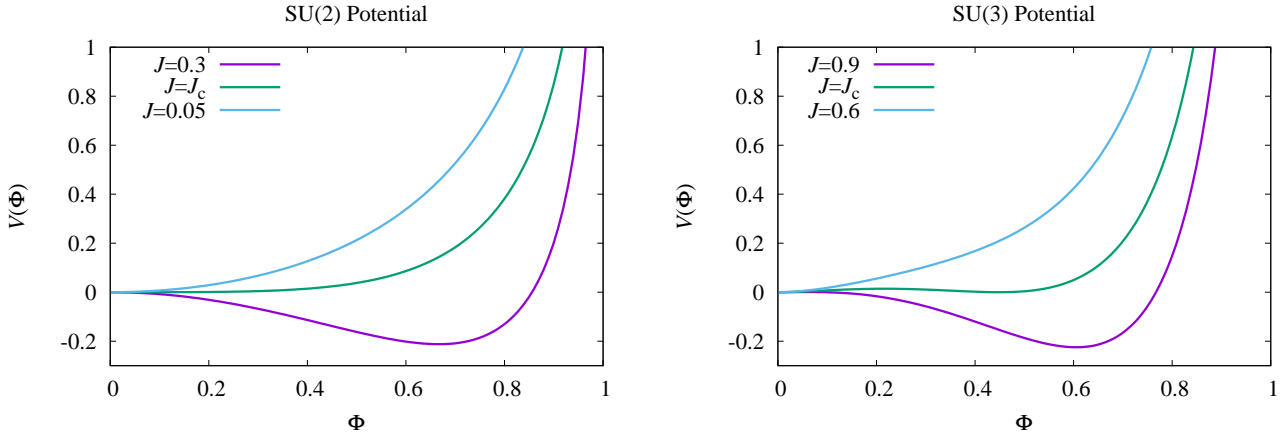


Figure 1: SU(2) (left) and SU(3) (right) effective potentials as a function of the Polyakov loop  $\Phi$  around the critical value of  $J$ .

## 2.4 Perturbative Potential for the Polyakov Loop

The perturbative vacuum is by definition empty with  $A_\mu = 0$ , and nevertheless, the Polyakov loop there is  $\Phi = 1$ , and this means that center symmetry must be spontaneously broken around  $A_4 = 0$  in the deconfined phase at high enough temperature. In other words, if we evaluate the Polyakov loop effective potential perturbatively, we should find a local minimum at  $A_4 = 0$ . Let us confirm this in what follows below.

To achieve this goal, let us specify the gauge fixing condition and the concrete matrix representation of the  $\mathfrak{su}(N_c)$  algebra. The most convenient choice for systematic higher-order calculations should be the covariant background gauge for the gauge fixing and the ladder basis for the representation. In the background field method, the gauge fields are split into the quantum fluctuations  $\mathcal{A}_\mu$  and the background fields  $A_{B\mu}$ , and the covariant background field gauge is chosen by the condition,

$$D_{B\mu}\mathcal{A}_\mu = 0. \quad (36)$$

Then, from the residual symmetry of the effective action  $\Gamma[\bar{A}, A_B]$  defined on top of the background  $A_{B\mu}^a$ , one can prove that  $\Gamma[\bar{A}, A_B] = \Gamma[\bar{A} = \bar{A} + A_B]$ , where  $\Gamma[\bar{A}]$  is the standard effective action that we want to know. From this we see  $\Gamma[A_B] = \Gamma[\bar{A} = 0, A_B]$ . This implies that we can obtain the effective action by integrating the quantum fluctuations out around the background fields. Because we are interested in the effective potential for the Polyakov loop, we should take only the temporal component of the background fields and rename it in the same way as in Eq. (32), i.e.

$$A_{B4} = \frac{2\pi}{g\beta} \text{diag}(q_1, q_2, \dots, q_{N_c}) = \frac{2\pi}{g\beta} \sum_{i=1}^{N_c} q_i \delta_i \quad \left( \sum_i q_i = 0 \right), \quad (37)$$

where, for convenience, we define matrices as

$$(\delta_i)^{ab} = \begin{cases} 1 & (a = b = i) \\ 0 & (\text{otherwise}) \end{cases}. \quad (38)$$

For the evaluation of the covariant derivative  $D_{B4}$ , the ladder basis is quite convenient for systematic higher-order calculations [36]. The elements of the Cartan subalgebra in the ladder basis are defined as

$$(t_{(n,n)})^{ab} = \frac{\delta^{ab}}{\sqrt{2n(n+1)}} \times \begin{cases} 1 & (a \leq n) \\ -n & (a = n+1) \\ 0 & (n+2 \leq a \leq N_c) \end{cases} \quad (39)$$

and off-diagonal ladder elements for  $i \neq j$  are

$$(t_{(i,j)})^{ab} = \frac{1}{\sqrt{2}} \delta^{ai} \delta^{bj} . \quad (40)$$

and then it is easy to show the following commutation relations,

$$[\delta_i, t_{(j,k)}] = (\delta_{ij} - \delta_{ik}) t_{(j,k)} , \quad [t_{(i,j)}, t_{(k,l)}] = \frac{1}{2} \delta_{il} \delta_{jk} (\delta_i - \delta_j) . \quad (41)$$

Using these commutation relations we can express the covariant derivative as

$$D_{B_4} \mathcal{A}_\mu = \partial_4 \mathcal{A}_\mu - ig [A_{B_4}, \mathcal{A}_\mu] = \partial_4^{(i,j)} \mathcal{A}_\mu^{(i,j)} t_{(i,j)} , \quad (42)$$

where  $\partial_4^{(i,j)} = \partial_4 - 2\pi i \delta_{\mu 4} q_{ij}$  with  $q_{ij} = q_i - q_j$ . We note that  $A_{B_4}$  or  $q_{ij}$  appears like a colored imaginary chemical potential. Then, the one-loop integration with respect to  $\mathcal{A}_\mu$  and the ghost fields leads to the following effective potential,

$$V_{\text{glue}}[q] = \frac{1}{2} \text{tr} \ln [(\partial_4^{(i,j)})^2 + \nabla^2] \cdot \text{tr}(\delta_{\mu\nu}) - \text{tr} \ln [(\partial_4^{(i,j)})^2 + \nabla^2] = \text{tr} \ln [(\partial_4^{(i,j)})^2 + \nabla^2] . \quad (43)$$

Here the first term multiplied by four polarizations  $\text{tr}(\delta_{\mu\nu})$  results from  $\mathcal{A}_\mu$  fluctuations and the second term from the ghost fluctuations that eliminate two unphysical polarizations out from the gluon fluctuations. From the observation that  $q_{ij}$  is an imaginary chemical potential, we can immediately conclude that the above trace in momentum space becomes the grand canonical partition function with an imaginary chemical potential, that is,

$$V_{\text{glue}}[q] = 2V \int \frac{d^3 p}{(2\pi)^3} \sum_{i>j} \left[ \ln(1 - e^{-\beta|\mathbf{p}|+2\pi i q_{ij}}) + \ln(1 - e^{-\beta|\mathbf{p}|-2\pi i q_{ij}}) \right] . \quad (44)$$

We can carry out this momentum integration explicitly, which yields,

$$V_{\text{glue}}^{\text{Weiss}}[q] = \frac{4\pi^2 V}{3\beta^3} \sum_{i>j} (q_{ij})_{\text{mod}1}^2 [(q_{ij})_{\text{mod}1} - 1]^2 . \quad (45)$$

This is often called the (GPY-)Weiss potential [8, 37, 38] (there are many derivations and generalizations of the Weiss potential; for example, see Refs. [39, 40] for the heat kernel expansion approach to the one-loop effective action). The modulo operation is defined as  $(q)_{\text{mod}1} = q - \lfloor q \rfloor$ , where  $\lfloor \dots \rfloor$  denotes the floor function.

Surprisingly the recent extension of this result to 2-loop order [41] showed that the shape of the potential remains the same as in Eq. (45).

The Weiss potential has a periodic nature for  $q_{ij}$ , that is already obvious in Eq. (44);  $q_{ij}$  or the imaginary chemical potential generally appears as an angle variable. This periodic property is attributed to center symmetry that is a symmetry associated with a discretized displacement in  $A_4$  as we discussed in Eq. (20).

First let us consider the SU(2) case, for which there is only one independent variable;  $q_1 = q/2$  and  $q_2 = -q/2$ . Then, the SU(2) Weiss potential has a periodic shape as depicted in the left of Fig. 2. We note that the Polyakov loop in this case is  $\Phi = \cos(\pi q)$  (just like the case at strong coupling), and so a minimum at the perturbative vacuum  $q = 0$  corresponds to  $\Phi = 1$ , and center symmetry is spontaneously broken there. The next minimum at  $q = 1$  is a center transformed point with  $\Phi = -1$ . One might think that the perturbation theory may be reformulated around  $q = 1$  equivalently, but as we see later, the quark one-loop potential favors  $q = 0$  and the perturbative vacuum must be identified

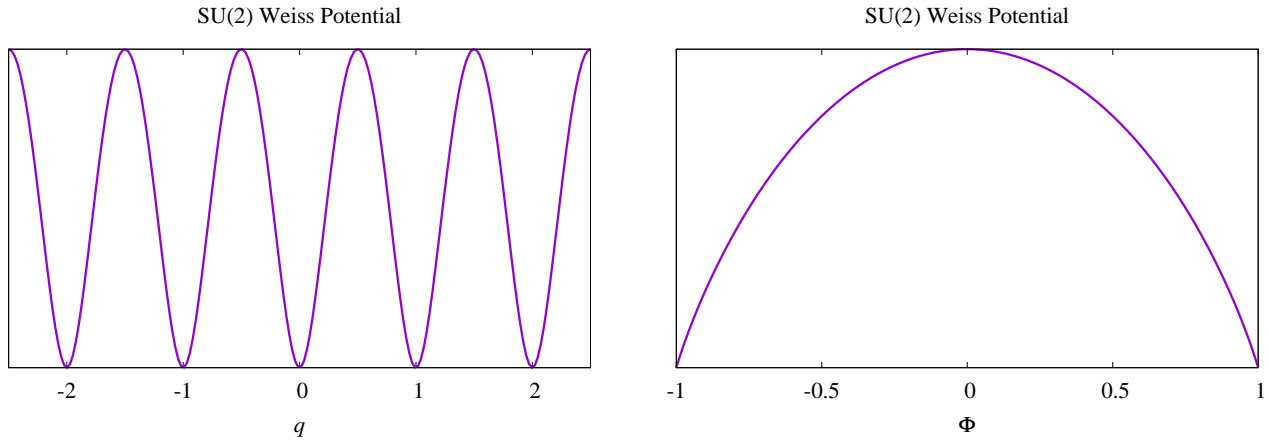


Figure 2: SU(2) Weiss potential as a function of  $q$  (left) and  $\Phi$  (right).

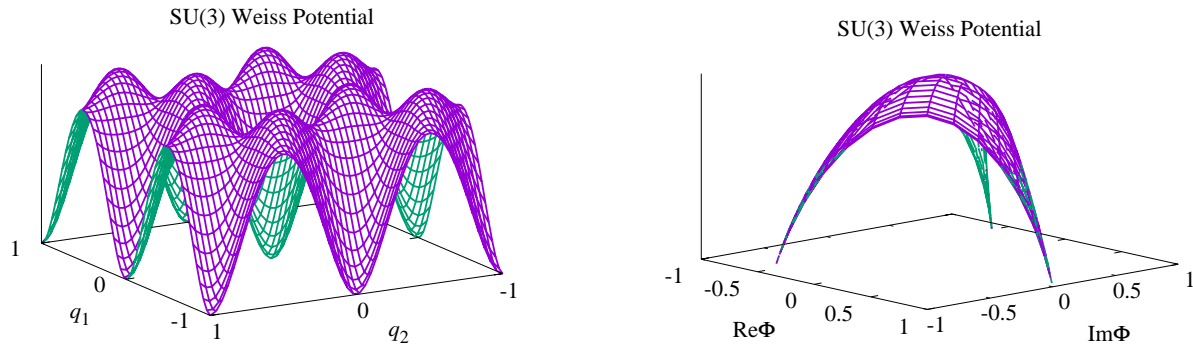


Figure 3: SU(3) Weiss potential as a function of  $q_1$  and  $q_2$  (left) and  $\text{Re}\Phi$  and  $\text{Im}\Phi$  (right).

at  $q = 0$  if we assume continuity between the pure gluonic theory and the massive limit of QCD. It is straightforward to change the variable from  $q$  to  $\Phi$ , and the SU(2) Weiss potential as a function of  $\Phi$  is plotted in the right of Fig. 2. We can see that the potential minima are located at  $\Phi = \pm 1$ , but these points of  $\Phi = \pm 1$  look singular unlike the left of Fig. 2. Such singular character originates from the Jacobian from  $q$  to  $\Phi$ , namely,  $dq/d\Phi = -1/[\pi \sin(\pi q)]$ , which diverges at  $\Phi = \pm 1$ . This observation of the potential shape is important when we want to consider the effect of the Polyakov loop fluctuations in physical observables.

Next, the generalization to the SU(3) case is easy to understand. Now, for the graphical purpose, we choose  $q_1$  and  $q_2$  as independent variables and set  $q_3 = -q_1 - q_2$  to draw the SU(3) Weiss potential in the left of Fig. 3. We see that one of the minima is certainly located at the perturbative vacuum  $q_1 = q_2 = 0$  and there are degenerate minima at the center transformed points. It is not clear which minimum has what value of the Polyakov loop, and so let us change the variables from  $q_1$  and  $q_2$  to  $\text{Re}\Phi$  and  $\text{Im}\Phi$  as shown in the right of Fig. 3. In this case, three points,  $\Phi = 1, e^{2\pi i/3}, e^{4\pi i/3}$ , are degenerate and connected by center transformation, among which  $\Phi = 1$  is favored by quark loop contributions.

In this way we have confirmed that the perturbative vacuum at  $A_4 = 0$  should be certainly identified as an ordered state with spontaneous center symmetry breaking. The potential curvature around the potential minimum characterizes how strongly symmetry is broken; in other words, the Debye screening mass stabilizes the perturbative vacuum. From the explicit expression (45) we can infer the potential

curvature or the Debye screening mass  $m_E$  as

$$\frac{V_{\text{glue}}[q]}{\beta V} = \frac{4\pi^2}{3\beta^4} \sum_{i>j} (q_{ij})^2 + O(q^3) = m_E^2 \text{tr}(A_4^2) = m_E^2 \left(\frac{2\pi T}{g}\right)^2 \sum_i q_i^2 \Rightarrow m_E^2 = \frac{N_c}{3} g^2 T^2, \quad (46)$$

where we used  $\sum_{i>j} (q_{ij})^2 = N_c \sum_i q_i^2$ . We can continue such an analysis to read higher-order interaction terms. The cubic term has an infrared singular origin from infinite sum over ring diagrams (at zero Matsubara frequency), and we next go to quartic order; suppose that the one-loop effective action has quartic terms such as  $\lambda_E (\text{tr} A_4^2)^2 + \bar{\lambda}_E \text{tr} A_4^4$ , we can infer  $\lambda_E$  and  $\bar{\lambda}_E$  from the Weiss potential (45) as

$$\lambda_E = \frac{g^4}{4\pi^2}, \quad \bar{\lambda}_E = \frac{N_c g^4}{12\pi^2}. \quad (47)$$

These are exactly the coefficients that appear in the so-called electrostatic QCD (EQCD).

## 2.5 Gauge Configurations and Center Symmetry Restoration

In the perturbative regime at high  $T$  the Debye screening is the physical origin of center symmetry breaking and deconfinement. Then, one would ask the following question; what is the physical origin of confinement at low  $T$ ? We have seen in Sec. 2.3 that the Haar measure or the ghost determinant is responsible for confinement in the strong coupling limit, but confinement should persist even at weak coupling as long as  $T$  is low enough. We are now addressing typical gauge configurations as microscopic mechanisms to restore center symmetry.

### 2.5.1 $Z(N_c)$ domain walls

Slightly above the critical temperature  $T_c$ , it is a natural anticipation that the spatial regions are divided into domains with different center elements just like the formation of magnetized domains in the spin systems near  $T_c$ . The possibility of domain-wall formation was pursued historically in the cosmological context [42] and in the heavy-ion collision experiment recently [43], which is one concrete manifestation of a more general idea of the semi-QGP that will be argued in Sec. 5.2.

Now that we have the explicit form of the Weiss potential, it is easy to find a domain-wall solution of the equation of motion [44, 45]. Let us find the  $Z(2)$  domain wall along the  $z$  direction for the color  $SU(2)$  case. We take the boundary condition as  $q(z = -\infty) = 0$  (i.e.  $\Phi = 1$ ) and  $q(z \rightarrow \infty) = 1$  (i.e.  $\Phi = -1$ ). The effective action with the kinetic term added should be

$$\Gamma_{\text{glue}}[q] = L_x L_y \int_{-L_z/2}^{L_z/2} dz \left\{ \frac{2\pi^2}{g^2 \beta} \left[ \frac{dq(z)}{dz} \right]^2 + \frac{4\pi^2}{3\beta^3} q(z)^2 [1 - q(z)]^2 \right\}. \quad (48)$$

Because we are thinking of a limited range  $0 \leq q \leq 1$ , we do not have to put the modulo operator. The equation of motion leads to the following solution;

$$q_c(z) = \frac{1}{1 + \exp\left(-\sqrt{\frac{2}{3}} g T z\right)}, \quad (49)$$

which is, together with the corresponding Polyakov loop value, plotted in the left of Fig. 4. We can evaluate the on-shell value of the effective action as

$$\Gamma_{\text{glue}}[q_c] = \sigma_t (\beta L_x L_y) = \frac{4\pi^2 T^2}{3\sqrt{6}g} L_x L_y. \quad (50)$$



In this way we can estimate the interface surface tension  $\sigma_t$  of the  $Z(2)$  domain-wall perturbatively, which can be generalized to  $SU(N_c)$  as [44, 45]

$$\sigma_t = \frac{4(N_c - 1)\pi^2 T^3}{3\sqrt{3}N_c g}. \quad (51)$$

It is important to note that the center domain-wall is accompanied by the magnetic loop or the 't Hooft loop that is a dual of the Wilson loop [46].

To have an intuitive feeling about how the center domain-wall and the 't Hooft loop are linked, it would be useful to consider the following transformation matrix in the Abelian part,

$$V(z') = \exp \left[ - \int d\mathbf{x} \delta(z - z') \frac{\delta}{\delta a_z(\mathbf{x})} \right]. \quad (52)$$

In the same manner as  $A_4^3$ , we defined  $a_z$  from  $A_z^3 = \frac{2\pi}{g} a_z$ . Because  $V(x)$  is a shift operator, the unitary transformation (not the gauge transformation) leads to

$$a'_z(\mathbf{x}) = a_z(\mathbf{x}) - \delta(z - z'). \quad (53)$$

Thus, if we define the Wilson loop as  $W = \exp(ig \int dz A_z^3 \frac{\sigma_3}{2})$ , it is easy to show,

$$V(z') W V^\dagger(z') = e^{-i\pi\theta(z-z')} W. \quad (54)$$

Actually, in the canonical quantization,  $\delta/\delta a_z$  is nothing but  $-i\frac{2\pi}{g} E_z$  and then the matrix can be rewritten in a form of the surface integral on  $z = z'$  as  $V(z') = \exp[i\frac{2\pi}{g} \int dS_z E_z(z')]$ . To pick up such an electric flux, we can regard this expression of  $V$  as a dual counterpart of the Wilson loop with magnetic loops on the edges of the  $xy$  plane. In this sense,  $V$  is called the 't Hooft loop, named after the pioneer who studies such a *disordered* parameter first [46].

Now let us see that  $V(z')$  turns out to be a creation operator of the center domain-wall at  $z = z'$ , which can be understood from the computation of the expectation value,  $\langle V(z') \rangle$ . In the functional integration we should replace  $\delta/\delta a_z$  by  $\Pi_z$  which should be integrated out, and after all we reach an expression,  $\langle V(z') \rangle = e^{-\tilde{\Gamma}}$ , where

$$\tilde{\Gamma} = L_x L_y \int_{-L_z/2}^{L_z/2} dz \left\{ \frac{2\pi^2}{g^2 \beta} \left[ \frac{dq(z)}{dz} - \delta(z - z') \right]^2 + \frac{4\pi^2}{3\beta^3} q(z)^2 [1 - q(z)]^2 \right\} \Bigg|_{\text{minimizing } q}. \quad (55)$$

Here, an additional term by  $\delta(z - z')$  imposes the boundary condition as  $q(z \rightarrow -\infty) = 0$  and  $q(z \rightarrow +\infty) = 1$  for a configuration that minimizes the above effective action. We already know such a configuration that is the center domain-wall, and then the expectation value of  $V$  reads,

$$\langle V \rangle = e^{-\sigma_t \beta L_x L_y}. \quad (56)$$

We note that the above expression implies that the 't Hooft loop shows the area law in the deconfined phase at high temperature. So, unlike the string tension in the Wilson loop,  $\sigma_t$  in the 't Hooft loop is a perturbatively calculable quantity. For the non-perturbative calculation in the lattice-QCD simulation, instead of using the definition of  $V$  in an operator form, one can impose a domain-wall boundary condition as argued in Ref. [47].

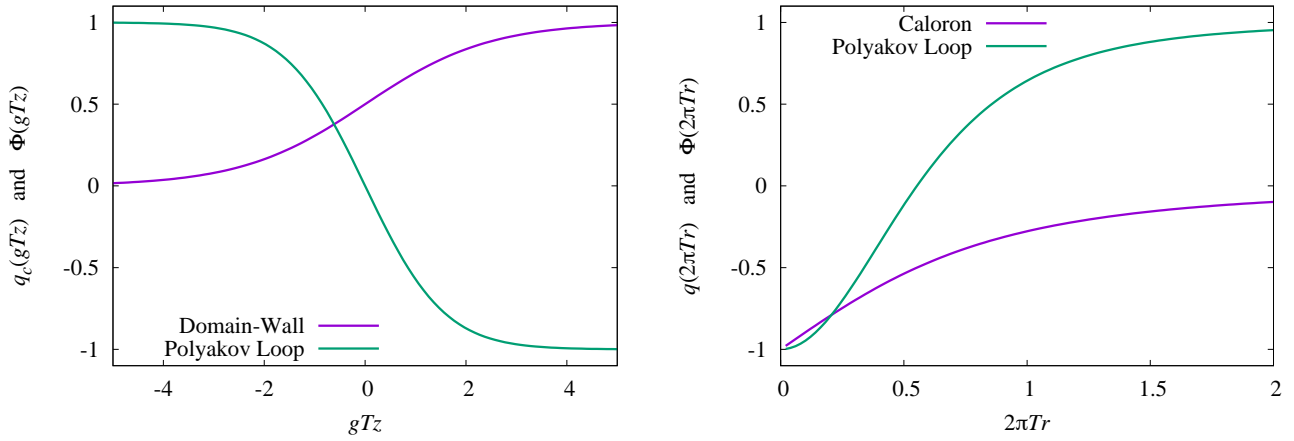


Figure 4: SU(2) domain-wall solution and associated Polyakov loop distribution (left) and SU(2) caloron solution and associated Polyakov loop distribution for  $\rho' = 1$  (i.e.  $\rho = 1/(2\pi T)$ ) (right).

### 2.5.2 $Z(N_c)$ bubbles and calorons

In the thermodynamic limit an infinitely large domain-wall solution is not stable because its action or energy diverges with  $L_x L_y \rightarrow \infty$ . Therefore, in reality, a number of finite-size domain-walls distribute in space, and its length becomes large only near  $T_c$  where the surface tension is suppressed.

Away from  $T_c$ , rather a picture of instanton distributions should be a favorable interpretation of disordered state, for the instanton action stays finite. At finite temperature the temporal or thermal direction should be periodically closed, and to construct periodic instantons, one can place multi-instantons along the  $x_4$  axis. Let us focus on the SU(2) case only in what follows, but the generalization to SU( $N_c$ ) is simple; we can consider all possible combinations of SU(2) subgroups in SU( $N_c$ ) and embed instantons there.

The single SU(2) instanton centered at  $z$  is written as

$$A_\mu(x) = \frac{1}{2} \bar{\eta}_{\mu\nu} \partial_\nu \ln \phi(x), \quad \phi(x) = 1 + \frac{\rho^2}{(x_4 - z_4)^2 + |\mathbf{x} - \mathbf{z}|^2} \quad (57)$$

with the 't Hooft symbols,  $\eta_{\mu\nu} = \eta_{\mu\nu}^a \sigma^a = -i(\sigma_\mu \bar{\sigma}_\nu - \delta_{\mu\nu})$  and  $\bar{\eta}_{\mu\nu} = \bar{\eta}_{\mu\nu}^a \sigma^a = -i(\bar{\sigma}_\mu \sigma_\nu - \delta_{\mu\nu})$ , where  $\sigma_\mu = (1, i\boldsymbol{\sigma})$  and  $\bar{\sigma}_\mu = (1, -i\boldsymbol{\sigma})$  are the quaternion bases. For the Polyakov loop calculation the most useful relation is  $\bar{\eta}_{4i}^a = \delta_{ia}$ . By putting infinitely many instantons at  $z_4 + n\beta$ , the Harrington-Shepard instanton configuration that satisfies the finite- $T$  periodic boundary condition is obtained by Eq. (57) with a modified  $\phi(x)$ , that is [8],

$$\phi(x) = 1 + \frac{\pi T \rho^2}{|\mathbf{x} - \mathbf{z}|} \cdot \frac{\sinh(2\pi T |\mathbf{x} - \mathbf{z}|)}{\cosh(2\pi T |\mathbf{x} - \mathbf{z}|) - \cos(2\pi T |x_4 - z_4|)}. \quad (58)$$

It is easy to see that Eq. (58) immediately reduces to Eq. (57) in the low- $T$  limit and this  $\phi(x)$  has a period  $1/T$  in terms of  $x_4$ . This finite- $T$  instanton is commonly called the ‘‘caloron’’ indicating that this special instanton is manifested in a thermal or caloric environment. It is then an interesting question how the Polyakov loop value behaves in the presence of a caloron. We can calculate this using the explicit components of the 't Hooft symbols;  $\bar{\eta}_{4i} = \bar{\eta}_{4i}^a \sigma^a = \sigma^i$ . Thus, for a caloron whose center is  $z = 0$ , the  $x_4$  integral of the eigenvalue of  $A_4$  simplifies as

$$\int_0^\beta dx_4 |A_4| = \frac{1}{2} \int_0^\beta dx_4 \frac{d}{dr} \ln \phi(r, x_4) = -\pi \left[ 1 - \frac{\rho'^2 (r' \cosh r' - \sinh r') + 2r'^2 \sinh r'}{r' \sqrt{2(r'^2 + \frac{\rho'^4}{4})(\cosh 2r' - 1) + 2\rho'^2 r' \sinh 2r'}} \right], \quad (59)$$

where  $r' = 2\pi T r$  and  $\rho' = 2\pi T \rho$  are, respectively, the rescaled dimensionless radial coordinate and instanton size. The Polyakov loop in the SU(2) case is simply given cosine of the above integrated  $A_4$  (where  $g$  is absorbed in the normalization of  $A_4$ ) and the numerical profile is shown in the right of Fig. 4. From this figure it is clear that  $\Phi = -1$  at the caloron center  $r = 0$  and  $\Phi \rightarrow +1$  at infinity  $r \rightarrow \infty$ . Therefore, calorons are identified as Z(2) bubbles and can disturb center elements to realize a disordered and thus center symmetric ground state.

It is an intriguing attempt to seek for an extension of calorons with different asymptotic behavior; by introducing an additional parameter  $\omega$  in the SU(2) case, if  $L(r \rightarrow \infty) \rightarrow e^{i2\pi\omega\sigma_3}$  is realized, the asymptotic value of the traced Polyakov loop approaches  $\Phi \rightarrow \cos(2\pi\omega)$ . Such a caloron solution has been discovered and it is called the Kraan, van Baal [48, 49] and Lee, Lu [50, 51] (KvBLL) solution. Intuitively speaking, this new caloron is a generalization of the Harrington-Shepard solution with a gauge rotation by  $e^{i2\pi\omega\sigma_3}$  among temporally aligned multi-instantons. Such a construction in the so-called algebraic gauge does not respect the periodicity along the thermal axis, and a gauge transformation by  $\Omega = e^{-i2\pi T\omega\sigma_3 x_4}$  turns the solution to the periodic one, which reads after all as

$$A_\mu(x) = \Omega \left\{ \frac{\phi}{2} \operatorname{Re} [(\bar{\eta}_{\mu\nu}^1 - i\bar{\eta}_{\mu\nu}^2)(\sigma_1 + i\sigma_2)\partial_\nu\chi] + \frac{\sigma_3}{2}\bar{\eta}_{\mu\nu}^3\partial_\nu \ln \phi \right\} \Omega^\dagger - i\Omega\partial_\mu\Omega^\dagger. \quad (60)$$

Here, one should be careful of Re being defined by  $\operatorname{Re}W = \frac{1}{2}(W + W^\dagger)$ . The  $\sigma_3$  direction is intact from the standard caloron, while the  $\sigma_1$  and  $\sigma_2$  terms involve new functions defined as follows;

$$\phi(x) \equiv \frac{\psi(x)}{\hat{\psi}(x)}, \quad \chi(x) \equiv \frac{1}{\psi(x)} \left[ e^{-i4\pi T\bar{\omega}x_4} \frac{\pi T\rho^2}{s} \sinh(4\pi T\omega s) + e^{i4\pi T\omega x_4} \frac{\pi T\rho^2}{r} \sinh(4\pi T\bar{\omega}r) \right], \quad (61)$$

where  $\bar{\omega} = 1/2 - \omega$ , and for this solution there are two relative position variables of ‘‘instanton quarks’’, i.e.  $r^2 = x^2 + y^2 + (z + 2\pi T\rho^2\omega)^2$  and  $s^2 = x^2 + y^2 + (z - 2\pi T\rho^2\bar{\omega})^2$ . These relative positions of  $r$  and  $s$  are aligned on the  $z$  axis due to a gauge choice. The definitions of dimensionless functions  $\psi(x)$  and  $\hat{\psi}(x)$  are,

$$\hat{\psi}(x) \equiv -\cos(2\pi T x_4) + \cosh(4\pi T\bar{\omega}r) \cosh(4\pi T\omega s) + \frac{r^2 + s^2 - (\pi T\rho^2)^2}{2rs} \sinh(4\pi T\bar{\omega}r) \sinh(4\pi T\omega s), \quad (62)$$

and

$$\begin{aligned} \psi(x) \equiv \hat{\psi}(x) &+ \frac{(\pi T\rho^2)^2}{rs} \sinh(4\pi T\bar{\omega}r) \sinh(4\pi T\omega s) \\ &+ \frac{\pi T\rho^2}{r} \sinh(4\pi T\bar{\omega}r) \cosh(4\pi T\omega s) + \frac{\pi T\rho^2}{s} \cosh(4\pi T\bar{\omega}r) \sinh(4\pi T\omega s). \end{aligned} \quad (63)$$

It is easy to make sure that the  $\omega \rightarrow 0$  limit correctly reduces these expressions to Eqs. (57) and (58) using  $\chi \rightarrow 1 - \phi^{-1}$  and  $\phi\partial_\nu\phi^{-1} = -\phi^{-1}\partial_\nu\phi$ . The  $s$  dependence disappears in this limit.

Shortly after the discovery of the KvBLL caloron, it has been recognized that monopoles constitute it [51, 52]; more precisely speaking, for the winding number  $k$  KvBLL caloron, there are  $kN_c$  dyons so that the total monopole charge is zero and the caloron is a magnetic neutral object. Let us now see the Polyakov loop profile in the presence of one KvBLL caloron for the SU(2) case for simplicity; some examples for this case are found in Ref. [53]. The 4th component of the ‘‘algebraic’’ gauge potential is,

$$A_4(x) = \sigma_1 \left( \frac{\phi}{2} \partial_1 \operatorname{Re}\chi + \frac{\phi}{2} \partial_2 \operatorname{Im}\chi \right) + \sigma_2 \left( -\frac{\phi}{2} \partial_1 \operatorname{Im}\chi + \frac{\phi}{2} \partial_2 \operatorname{Re}\chi \right) + \sigma_3 \left( \frac{1}{2} \partial_3 \ln \phi \right), \quad (64)$$

which is gauge transformed with  $\Omega$ , and then the Polyakov loop  $L$  should be multiplied by  $e^{-i2\pi\omega\sigma_3}$ . Now, for confinement physics, the most interesting choice of the asymptotic boundary condition is

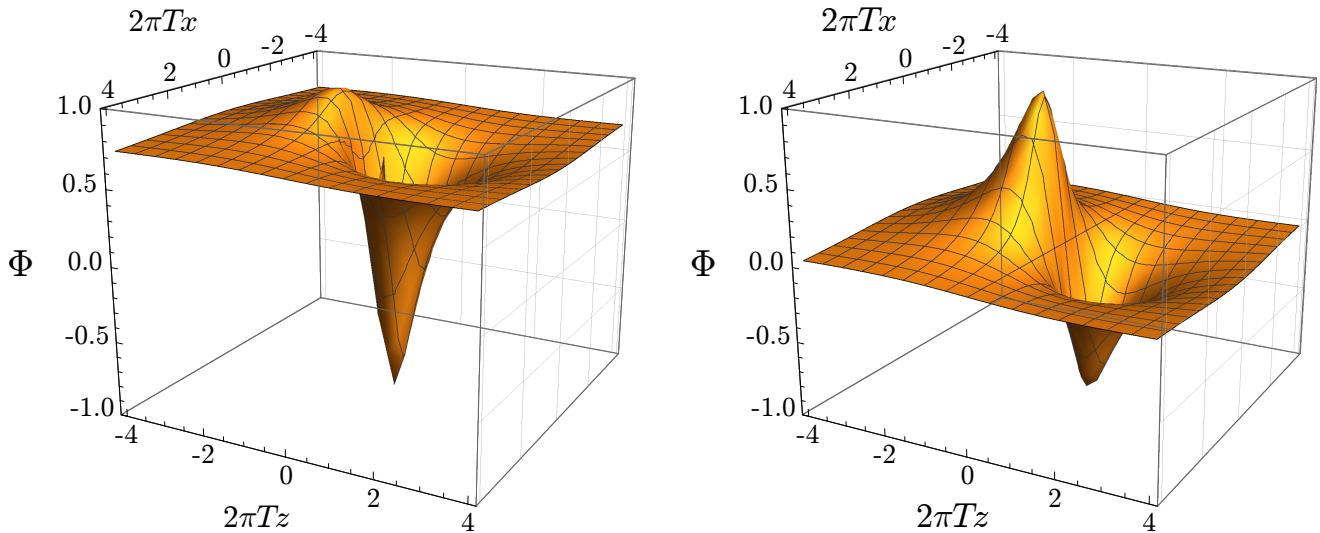


Figure 5: Polyakov loop distribution in the presence of the KvBLL caloron for  $\rho = 1/(2\pi T)$  and  $\omega = 1/8$  (left) and the maximal holonomy  $\omega = 1/4$  (right) as a function of  $2\pi Tx$  and  $2\pi Tz$  at  $y = 0$ .

$\omega = 1/4$ , which is usually referred to as the maximal holonomy. In this case the asymptotic value of the Polyakov loop away from the caloron center becomes zero, i.e.  $\Phi \rightarrow 0$  at  $r \rightarrow \infty$ . Then, as shown in the right of Fig. 5, two peaks in the Polyakov loop distribution appear corresponding to  $N_c$  dyon constituents. For a smaller value of  $\omega$ , as seen in the left of Fig. 5 that depicts the result for  $\omega = 1/8$ , the shape tends to reduce to that of the conventional caloron as in the right of Fig. 4.

It has been known analytically and numerically that the dyon contents become more explicit for  $\rho T < 1$ , while they come close to be degenerate for  $\rho T > 1$ . This observation implies that confinement may be caused by dyons in the KvBLL caloron at  $T < 1/\rho$ , and indeed, it has been found that a gas of the KvBLL calorons with  $\omega = 1/4$  leads to confinement [53]. The explanation, however, still awaits to be given for dynamical determination of the most favorable value of  $\omega$  (for an example of recent calculations of the holonomy potential, see Refs. [54, 55]).

### 3 Phase Transition in the Pure Gluonic Theory

We have discussed the Polyakov loop expectation value from various approaches, and it was so far only the strong coupling expansion that could describe a phase transition in the pure gluonic theory. One can extract the essential feature of such a description to build a more generic model, that is, the Polyakov loop matrix theory. Sometimes even further simplification on the matrix model is useful, which gives us a parametrized form of the Polyakov loop potential. The phase transition in the pure gluonic theory has been studied in detail and one of the most non-trivial but well-defined questions is the nature of phase transition for large  $N_c$ . Physically, the deconfinement phase transition is of second order only for the color  $SU(2)$  case, while it is of first order for the color  $SU(N_c \geq 3)$  case in general. Moreover, the latent heat increases for larger  $N_c$ , meaning that the first-order phase transition becomes stronger if  $N_c$  gets larger. Once physical quantities are rescaled with  $N_c$ , however, it is no longer such easy to make a conclusion about the order of the phase transition, and there is a theoretical suggestion that a third-order phase transition may occur. We will take a close look at this possibility using an effective matrix theory of the Polyakov loop.

### 3.1 Polyakov Loop Models

We introduce three models here. The first one is a parametrized Polyakov loop potential, which is a common ingredient for the Polyakov loop augmented chiral models as we will elucidate later. The second one is an inverted Weiss potential. This special form of the Polyakov loop potential is not a frequent choice but the underlying physics picture provides us with a consistent view of confinement with an interesting link between the perturbative calculation, the strong coupling expansion, and the propagator studies. The last is the Polyakov loop matrix model, which is quite successful for its simple appearance.

#### 3.1.1 Parametrizing the Polyakov loop potential

The first strategy to capture the Polyakov loop dynamics is to find a reasonable parametrization of the Polyakov loop potential instead of calculating it. The guiding principle to optimize the parametrization is the numerical outputs from the lattice simulation [56, 57, 58]. The Polyakov loop and the pressure (from which other thermodynamic quantities are derived) as functions of  $T$  have been already well known in the pure gluonic sector. Then, we can make a guess about the minimal number of parameters to reproduce the lattice numerical outputs; one needs to adjust at least where the phase transition takes place, namely,  $T_c$ , and how large the Polyakov loop and the pressure are then, namely,  $\Phi(T_c)$  and  $p(T_c)$ . Also the large- $T$  behavior of the Polyakov loop (i.e.  $\Phi \rightarrow 1$ ) and the pressure (i.e. the Stefan-Boltzmann limit) should be taken into account. Once we treat these large- $T$  conditions as constraints to eliminate parameters, the minimal number of parameters should be three corresponding to  $T_c$ ,  $\Phi(T_c)$ , and  $p(T_c)$ .

This program to establish a parametrized Polyakov loop potential was addressed in Ref. [59] with an Ansatz of the power expansion in terms of  $t = T/T_c$ . The SU(3) potential then reads,

$$T^{-4}V_{\text{glue}}(\Phi, \bar{\Phi}; T) = -\frac{b_2(T)}{2}\bar{\Phi}\Phi - \frac{b_3}{6}(\Phi^3 + \bar{\Phi}^3) + \frac{b_4}{4}(\bar{\Phi}\Phi)^2, \quad (65)$$

and the temperature dependence is assumed to appear only in the quadratic coefficient as

$$b_2(T) = a_0 + a_1t^{-1} + a_2t^{-2} + a_3t^{-3}. \quad (66)$$

We note that  $\bar{\Phi} = \Phi$  results from the variation of the potential. In this effective potential there are six parameters, one of which is constrained by the Stefan-Boltzmann limit for the pressure;  $T^{-4}V_{\text{glue}}|_{T \rightarrow \infty} \rightarrow a_0/2 - b_3/3 + b_4/4 = -16 \cdot (\pi^2/90) \simeq -1.75$ . Another constraint is  $\Phi \rightarrow 1$  at high  $T$ . In the limit of  $t^{-1} = 0$ , we can calculate the Polyakov loop as  $\Phi \rightarrow (b_3 + \sqrt{b_3 + 4a_0b_4})/(2b_4) = 1$ , which imposes a condition;  $a_0 + b_3 - b_4 = 0$ . The common parameter set [59] is

$$a_0 = 6.75, \quad a_1 = -1.95, \quad a_2 = 2.625, \quad a_3 = -7.44, \quad b_3 = 0.75, \quad b_4 = 7.5. \quad (67)$$

We note that we can safely take the high- $T$  limit because the temperature dependence in the coefficients is only through the power of  $t^{-1}$ , and this feature is consistent with the functional form from the strong coupling expansion;  $b_2/2 \propto e^{-\beta\sigma a}$ .

The above-mentioned parametrization still has redundancy and ideally we could have found a better parametrization with two fewer parameters. Later a simpler and better parametrization with less parameters was found as [60]

$$T^{-4}V_{\text{glue}}(\Phi, \bar{\Phi}; T) = -\frac{a(T)}{2}\bar{\Phi}\Phi + b(T) \ln[1 - 6\bar{\Phi}\Phi + 4(\bar{\Phi} - 3 + \Phi^3) - 3(\bar{\Phi}\Phi)^2] \quad (68)$$

with four parameters in

$$a(T) = a_0 + a_1t^{-1} + a_2t^{-2}, \quad b(T) = b_0t^{-3}. \quad (69)$$

In this case the Stefan-Boltzmann constraint is quite simple;  $T^{-4}V_{\text{glue}}|_{T \rightarrow \infty} \rightarrow -a_0/2$ , which immediately leads to  $a_0 = 3.51$ . Then, there are only three parameters to be fixed by the lattice data, and the well tuned values are [60]

$$a_0 = 3.51, \quad a_1 = -2.47, \quad a_2 = 15.2, \quad b = -1.75. \quad (70)$$

This latter parametrization (68) has three advantages over the former (65); the number of parameters is minimal,  $\Phi$  (and  $\bar{\Phi}$ ) never exceeds the group theoretical upper bound, i.e.  $\Phi \leq 1$ , and the role by the SU(3) Haar measure (see Eqs. (33) and (35)) is manifest in Eq. (68). The comparison to the lattice simulation data is found for example in the review of Ref. [7]. The agreement is remarkable; the pure gluonic dynamics for *any*  $T > T_c$  is almost perfectly characterized by only three free parameters.

We also make a comment on  $T_c$  here. Strictly speaking,  $T_c$  should be counted as another model parameter, and  $T_c = 270$  MeV is a common choice based on the lattice simulation of the pure gluonic theory. Later, with dynamical quarks, we will come back to the determination of this parameter  $T_c$  that should take a backreaction effect from the quark loops.

It is always a tempting idea to derive such a Polyakov loop potential from the first-principle approach. For recent discussions on improving the Polyakov loop potential, see Refs. [61, 62, 63], and for lattice determination, see Refs. [64, 65, 66].

### 3.1.2 Inverted Weiss potential

The ghost or the SU(3) Haar measure causes confinement in the strong coupling expansion, and the successful parametrization in Eq. (68) indeed implements the Haar measure form. Hence, the modern picture of confinement implies the ghost dominance in the infrared regime. This situation of the ghost dominance makes a sharp contrast to the perturbative calculation, in which the ghost and the longitudinal gluon contributions exactly cancel out.

The cancellation no longer holds once we take account of non-perturbative propagators of the ghost and the gluons. Such a procedure to compute the non-perturbative Polyakov loop potential was first suggested in Ref. [67]. Schematically, the effective potential can be written as [see Eq. (43)]

$$V_{\text{glue}}[q] = \frac{1}{2} \text{tr} \ln D_{\mu\nu}(p) - \text{tr} \ln G(p), \quad (71)$$

where  $D_{\mu\nu}(p)$  and  $G(p)$  represent the gluon and the ghost full propagators, respectively. In the Landau gauge these propagators are parametrized by the dressing functions, apart from the trivial color index that is simply the unit matrix in color space, as

$$D_{\mu\nu}(p) = Z_A(p^2)(p^2\delta_{\mu\nu} - p_\mu p_\nu) + \frac{1}{\xi} Z_L(p^2) p_\mu p_\nu, \quad (72)$$

$$G(p) = Z_C(p^2) p^2. \quad (73)$$

As long as  $T$  is low, it is natural to anticipate that the infrared momentum region would be dominant in the integration in Eq. (71). Then, to capture the qualitative feature of the Polyakov loop potential in the confined phase, the so-called scaling solution should be useful, which is numerically known to behave as [68, 69, 70]

$$Z_A(p^2 \sim 0) \simeq (p^2)^{\kappa_A}, \quad Z_L \simeq 1 + \xi, \quad Z_C(p^2 \sim 0) \simeq (p^2)^{\kappa_C}. \quad (74)$$

One might mind about the formal correctness of the scaling solution; the lattice simulation seems to have falsified the exact scaling solution in the  $p^2 \rightarrow 0$  limit, but still, for small but finite  $p^2$ , the scaling solution makes sense qualitatively and even quantitatively. It is not important whether  $Z_C(p^2 \rightarrow \infty)$



strictly diverges or not. We note that  $\kappa_A = -2\kappa_C$  follows from the non-renormalization property of the ghost-gluon vertex at vanishing momentum in the Landau gauge. From the lattice simulation and the functional method,  $\kappa_C \simeq 0.6$  approximately holds [70]. Then, the power of the momentum dependence of the propagator is modified, so that the weight for the gluon part (counting the polarization sum) changes from 4 to  $3(1 + \kappa_A) + 1$  and the weight for the ghost part from 1 to  $1 + \kappa_C$ . Then, the non-perturbative effective potential becomes,

$$V_{\text{glue}}^{\text{non-perturbative}}[q] = (1 - 4\kappa_C)V_{\text{glue}}^{\text{Weiss}}[q] \simeq -1.4V_{\text{glue}}^{\text{Weiss}}[q]. \quad (75)$$

Because of the overall minus sign, the perturbative Weiss potential is *inverted* and the potential minimum is then located at the confined phase with  $\Phi = 0$ , as is obvious from Fig. 2 for the SU(2) case. This is one of the simplest pictures to understand how confinement is realized. It should be noted that, if the theory has adjoint fermions satisfying the periodic boundary condition, the simple one-loop calculation leads to the inverted Weiss potential as above, and the perturbative confinement is realized [71].

The phase transition temperature  $T_c$  is characterized by a typical scale in the ghost and the gluon dressing functions. For momenta larger than such a typical scale the propagators are expected to approach the perturbative ones. If  $T$  is greater than this scale, contributions from higher momentum regions should dominate the calculation, and then the Polyakov loop effective potential should reduce to the Weiss potential that embodies the deconfined phase. Thus, to quantify  $T_c$ , we need more information on the propagators over wide momentum ranges.

A short-cut approach is a hybrid calculation of the one-loop integration using the non-perturbative propagators numerically measured on the lattice. Such a combination of the ‘‘perturbative’’ loop integration and the ‘‘non-perturbative’’ propagators might have sounded weird, but this can be understood as an extension of the ordinary mean-field type approximation. Usually, in the mean-field approximation, all the interaction effects are assumed to be renormalized into the non-perturbative propagator, and then the precise form of the propagator is self-consistently determined to minimize corrections from the interaction effects. Instead of solving the self-consistency condition or the gap equation, why shouldn’t we jump to the full propagators already available from the lattice simulation? Of course we can, and we in principle need the lattice propagators at all temperatures in order to locate  $T_c$  precisely. Looking at the lattice data, we would recognize that only the transverse gluons show moderate  $T$  dependence. It is remarkable that one can hardly see any qualitative difference associated with the first-order deconfinement transition in the ghost and the gluon propagators [72]. Therefore, it is not a bad approximation to utilize even the zero- $T$  propagators for finite- $T$  loop calculations.

Interestingly enough, as demonstrated in Ref. [73], the effective potential calculated in such a way successfully captures even quantitative properties of the deconfinement phase transition, i.e. the phase transition temperature is correctly reproduced. We also note that, instead of using the lattice propagator, an introduction of the gauge mass term can capture the essential features of the phase transitions as discussed in Ref. [74] and the systematic expansion in general SU( $N_c$ ) group has been developed in Refs. [75, 76, 77].

### 3.1.3 Mean-field approximation of a matrix model

Here let us discuss an extended version of the mean-field approximation that correctly takes care of the group integration properties according to Ref. [32]. So far, we implicitly assumed a stronger approximation than the mean-field approximation, that is,  $\Phi = \langle \ell[A_0] \rangle = \ell[\langle A_0 \rangle]$ . Such a treatment would sometimes lead to unphysical results; the most obvious example of pathological behavior is found in the Polyakov loop calculation in color superconductivity, in which a non-zero color charge emerged even in normal quark matter, which is just an artifact from improper approximation [60, 78, 79].

To make the following discussions concrete, we adopt a Polyakov loop effective theory in the strong coupling limit, where the partition function is given by the group integration in Eq. (30). We would

emphasize that the idea itself is quite general, as implemented in Refs. [79, 80]. Precisely speaking, the treatment in Sec. 2.3 was the tree-level approximation, and quantum fluctuations should have been taken into account self-consistently in the genuine mean-field approximation. To formulate the mean-field approximation, we define the mean-field action as

$$S_{\text{mf}}[\ell; z] = -\frac{1}{2} \sum_{\mathbf{x}} [z^* \ell(\mathbf{x}) + z \ell^*(\mathbf{x})] \quad (76)$$

with mean-field variables  $z$  and  $z^*$ . We next define the mean-field average for arbitrary functions of  $L$  as

$$\langle \mathcal{O}[L] \rangle_{\text{mf}} \equiv \frac{\int \mathcal{D}L e^{-S_{\text{mf}}[\ell]} \mathcal{O}(L)}{\int \mathcal{D}L e^{-S_{\text{mf}}[\ell]}}. \quad (77)$$

For the theoretical foundation of the mean-field approximation the most important relation is the convexity condition, that is,  $\langle e^{\mathcal{O}} \rangle_{\text{mf}} \geq e^{\langle \mathcal{O} \rangle_{\text{mf}}}$  (see Ref. [81] for detailed discussions). From this inequality the full partition function is bounded by the mean-field approximated one as

$$Z \geq \exp\{\langle -S[\ell] + S_{\text{mf}}[\ell; z] \rangle_{\text{mf}}\} \cdot \int \mathcal{D}L e^{-S_{\text{mf}}[\ell; z]}, \quad (78)$$

where  $S[\ell] = -J \sum \ell^*(\mathbf{x}') \cdot \ell(\mathbf{x})$  is the original action that defines the matrix theory. Our goal is to find an analytical expression of the right-hand side of the above inequality. Let us introduce a function of the mean-field variables;

$$I(z^*, z) \equiv \int dL e^{-S_{\text{mf}}[\ell; z]}. \quad (79)$$

Then, it is easy to rewrite the mean-field expectation values as

$$\langle S[\ell] \rangle_{\text{mf}} = -V_3 \cdot 6J \cdot \frac{2\partial \ln I}{\partial z} \cdot \frac{2\partial \ln I}{\partial z^*}, \quad (80)$$

and

$$\langle S_{\text{mf}}[\ell] \rangle_{\text{mf}} = -\frac{1}{2} V_3 \left( z^* \frac{2\partial \ln I}{\partial z^*} + z \frac{2\partial \ln I}{\partial z} \right), \quad (81)$$

where  $V_3$  represents the spatial (three dimensional) site number, and 6 appears from the number of nearest neighbor sites in three dimensional space. By taking the logarithm of the right-hand side of the inequality (78), we can evaluate the mean-field grand potential  $\Omega_{\text{mf}}$  that gives the upper bound of the true grand potential. In this way, the mean-field grand potential is found to be

$$\begin{aligned} \beta \Omega_{\text{mf}}(z^*, z)/V_3 &= \langle S[\ell] \rangle_{\text{mf}} - \langle S_{\text{mf}}[\ell; z] \rangle_{\text{mf}} - \ln \int \mathcal{D}L e^{-S_{\text{mf}}[\ell; z]} \\ &= -6J \cdot \frac{2\partial \ln I}{\partial z} \cdot \frac{2\partial \ln I}{\partial z^*} + \frac{1}{2} \left( z^* \frac{2\partial \ln I}{\partial z^*} + z \frac{2\partial \ln I}{\partial z} \right) - \ln I. \end{aligned} \quad (82)$$

As long as the charge parity symmetry is unbroken (that is broken for example in a system at finite density), we can set  $z = z^* = x$ , which simplifies the above mean-field grand potential as

$$\beta \Omega_{\text{mf}}(x)/V_3 = -6J \left[ \frac{d}{dx} \ln I(x) \right]^2 + x^2 \frac{d}{dx} \left[ \frac{1}{x} \ln I(x) \right]. \quad (83)$$

The stationary condition to minimize the grand potential gives a relation,  $x = 12J \langle \ell \rangle$ , which manifests the fact that  $x$  is a mean-field variable corresponding to the Polyakov loop expectation value. We still

need to perform the group integration to find an explicit form of  $I(x)$ . For this purpose it is useful to use an alternative expression for the Haar measure;

$$H = \left| \epsilon_{i_1 \dots i_{N_c}} e^{i2\pi q_1(N_c - i_1)} \dots e^{i2\pi q_{N_c}(N_c - i_{N_c})} \right|^2. \quad (84)$$

With this expression it is possible to find the analytical expression as (see Ref. [82] for detailed derivations)

$$I(x) = \int dL e^{\frac{\mathbb{R}}{2}(\ell + \ell^*)} = N_c! \sum_m \det_{ij} I_{m-i+j}(x/N_c). \quad (85)$$

Here,  $I_n(x)$  is the modified Bessel function of the first kind. Now we can proceed to numerics using these expressions; for  $N_c = 3$  the critical coupling is found to be  $J_c \simeq 1.21$ , which shows a sizable difference from  $J_c \simeq 0.773$  in the tree-level approximation seen in Sec. 2.3.

Because calculations are far more involved as compared to the Polyakov loop potential approach in Sec. 3.1.1, the above analysis is not very much preferred, but can be useful for theoretical investigations as demonstrated in Refs. [79, 83].

## 3.2 Large $N_c$ Limit

It is generally hard to find an analytical answer in the non-perturbative sector of QCD, and then it is useful to consider a modified version of QCD that would have desirable properties for analytical purposes. Some examples include two-dimensional QCD, two-color QCD, QCD in the strong coupling limit, many-flavor QCD, and so on. The most successful idea along these lines is to increase the number of colors,  $N_c$ , to infinity. In particular two-dimensional QCD at  $N_c \rightarrow \infty$  is called 't Hooft model [84] that resembles QCD. It is a widely accepted folklore that the  $N_c = 3$  real world may share most of non-perturbative aspects with the  $N_c \rightarrow \infty$  simplified world. In this subsection we address what is known so far about the pure gluonic dynamics and the phase transition in the large  $N_c$  limit.

### 3.2.1 Gross-Witten phase transition

In two spacetime dimensions, the dynamics of the  $SU(N_c)$  pure gluonic theory is significantly simpler than that in four dimensions owing to the absence of the transverse dimensions and associated gluon excitations. In a lattice formulation of the theory, this simplification is reflected by an independence of the plaquette variables. We can understand this in the Weyl gauge in which the independence is obvious; all temporal link variables are trivial and consequently the spatial links can be represented as a time-ordered product of independent plaquette variables. Thus the partition function (28) reduces to

$$Z = \left\{ \int dU \exp \left[ \frac{1}{g^2} \text{tr}_c(U + U^\dagger) \right] \right\}^{N_p}, \quad (86)$$

where  $N_p = V_2/a^2$  is the number of plaquettes with  $a$  and  $V_2$  denoting the lattice spacing and the two-dimensional spacetime volume, respectively. Here, the integration is performed over a single unitary matrix,  $U \in U(N_c)$ <sup>1</sup>. Hence the problem is reduced to the computation of the single-site partition function;

$$z = \int dU \exp \left[ \frac{1}{g^2} \text{tr}_c(U + U^\dagger) \right]. \quad (87)$$

The integrand depends on the eigenvalues of  $U$ , which we denote by  $q_i$  with  $i = 1, \dots, N_c$ . By a unitary transformation  $T$ , the matrix  $U$  can be rewritten as  $TDT^\dagger$  with a diagonal matrix,  $D =$

<sup>1</sup>In the large  $N_c$  limit, the difference between  $U(N_c)$  and  $SU(N_c)$  can be ignored.

$\text{diag}(e^{i2\pi q_1}, \dots, e^{i2\pi q_{N_c}})$ . The integration measure is thus expressed in the form of the Vandermonde determinant as follows;

$$dU \propto dT \prod_i dq_i \prod_{i<j} |e^{i2\pi q_i} - e^{i2\pi q_j}|^2, \quad (88)$$

modulo an irrelevant normalization factor. Therefore the partition function is proportional to

$$z \propto \int d^{N_c} q \exp \left\{ N_c^2 \left[ \frac{2}{\lambda} \cdot \frac{1}{N_c} \sum_{i=1}^{N_c} \cos(2\pi q_i) + \frac{1}{N_c^2} \sum_{i \neq j} \ln |e^{i2\pi q_i} - e^{i2\pi q_j}| \right] \right\}, \quad (89)$$

where we introduced the 't Hooft coupling as  $\lambda = g^2 N_c$ . We take the large  $N_c$  limit keeping  $\lambda$  constant, and then we can replace the discrete sums with the continuous integrals as

$$\frac{1}{N_c} \sum_i \rightarrow \int_0^1 dx, \quad \frac{1}{N_c^2} \sum_{i \neq j} \rightarrow \text{P} \int_0^1 dx dy, \quad (90)$$

where P denotes the Cauchy principal value. In what follows below, to simplify the notation, we denote the large  $N_c$  limit of  $q_i$  by  $q_x$ . Then, the steepest descent method yields the energy as a function of the coupling  $\lambda$  as

$$-E(\lambda) = \lim_{N_c \rightarrow \infty} \frac{\ln z}{N_c^2} = \frac{2}{\lambda} \int dx \cos(2\pi q_x) + \text{P} \int dx dy \ln |\sin[\pi(q_x - q_y)]| \quad (91)$$

with the most probable  $q_x$  given by the stationarity condition,

$$\frac{2}{\lambda} \sin(2\pi q_x) = \text{P} \int dy \cot[\pi(q_x - q_y)]. \quad (92)$$

We can solve this equation by introducing a positive-definite density of eigenvalues that is defined by

$$\rho(q) = \frac{dx}{dq}, \quad (93)$$

satisfying a proper normalization condition

$$\int_{-q_0}^{q_0} dq \rho(q) = \int_0^1 dx = 1, \quad (94)$$

where we assumed that the eigenvalues may be separated by a single gap, i.e.  $q^2 \leq q_0^2 \leq 1/4$ . Then, Eq. (92) can be rewritten into the following equivalent form,

$$\frac{2}{\lambda} \sin(2\pi q) = \text{P} \int dq' \rho(q') \cot[\pi(q - q')]. \quad (95)$$

It is instructive to rewrite this in terms of the complex variables;  $z = e^{i2\pi q}$  and  $z' = e^{i2\pi q'}$ , that is,

$$\frac{2i}{\lambda} \left( \frac{z - z^{-1}}{2} \right) + i = \frac{1}{\pi} \text{P} \int_C dz' \frac{\rho(z')}{z' - z}. \quad (96)$$

For a given contour  $C$ , the inversion of this equation, also known under the rubric of the Hilbert transform, is a very well-known mathematical problem (see Ref. [85]).

In the strong coupling regime,  $\lambda \geq 2$ , the eigenvalues are expected to be distributed over the entire circle, that implies  $q_0 = 1/2$ . In this case  $C$  is a closed contour on  $|z'| = 1$ , so that the inversion of

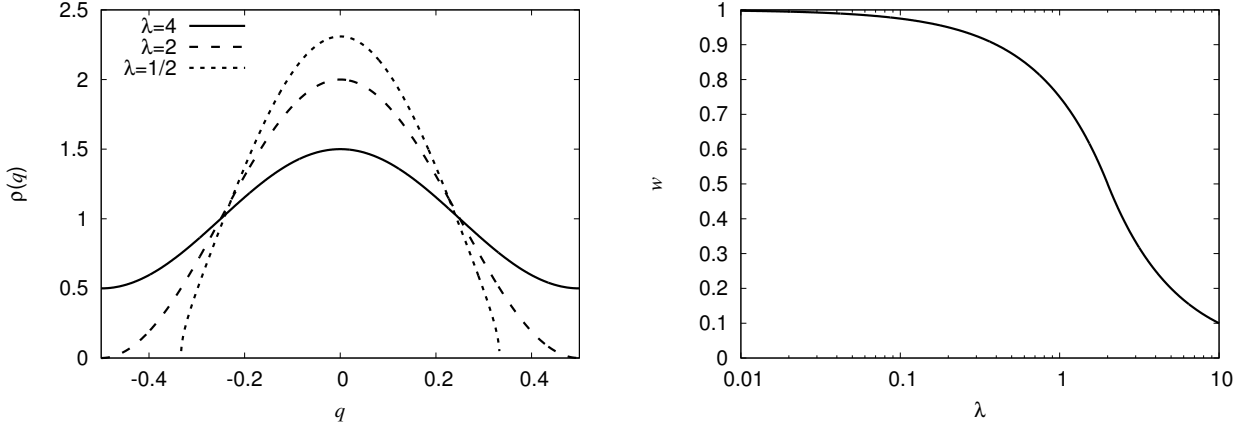


Figure 6: Eigenvalue distribution for different values of the coupling constant (left) and the expectation value of the Wilson loop as a function of the coupling constant (right).

Eq. (96) trivially results in  $\rho(q) = 1 + \frac{2}{\lambda} \cos(2\pi q)$ . We note that the distribution of the eigenvalues is properly normalized and is positive for any  $\lambda \geq 2$ .

In the weak coupling regime,  $\lambda < 2$ , one has to solve the problem for  $q_0 < 1/2$ . Hence, the contour  $C$  represents an arc and the solution is given by  $\rho(q) = \frac{4}{\lambda} \cos(\pi q) \cdot \sqrt{\frac{\lambda}{2} - \sin^2(\pi q)}$ . At  $\lambda = \lambda_c \equiv 2$ , two solutions in the strong and the weak coupling regimes coincide to yield the distribution;  $\rho(q) = 1 + \cos(2\pi q)$ .

Hence, to summarize the above, it has been established that the distribution of the eigenvalues is given by two distinct analytic functions;

$$\rho(q) = \begin{cases} \frac{4}{\lambda} \cos(\pi q) \cdot \sqrt{\frac{\lambda}{2} - \sin^2(\pi q)} & \text{with } \sin^2(\pi q_0) = \frac{2}{\lambda} & \text{for } \lambda < 2, \\ 1 + \frac{2}{\lambda} \cos(2\pi q) & \text{with } q_0 = \frac{1}{2} & \text{for } \lambda \geq 2. \end{cases} \quad (97)$$

We can see the behavior of  $\rho(q)$  for different values of  $\lambda$  in the left panel of Fig. 6. The corresponding expectation value of the traced Wilson loop, that is given by  $\omega = \int dq \rho(q) \cos(2\pi q)$  in the large  $N_c$  limit, takes the following expressions,

$$\omega = \begin{cases} 1 - \frac{\lambda}{4} & \text{if } \lambda < 2, \\ \frac{1}{\lambda} & \text{if } \lambda \geq 2, \end{cases} \quad (98)$$

whose behavior is seen in the right panel of Fig. 6. Here, we refer to Ref. [86] for the interpretation of the phase transition in terms of ‘‘saddle’’ condensation.

Now we can proceed to the calculation of the energy by solving the stationary condition. Indeed, we can immediately integrate Eq. (95) with respect to  $q$  in the range from 0 to  $q$ . Then, we multiply this integrated function of  $q$  by  $\rho(q)$  and finally perform the integration over  $q$  in the range from  $-q_0$  to  $q_0$  to reach,

$$P \int dq dq' \rho(q) \rho(q') \ln |\sin[\pi(q - q')]| = P \int dq \rho(q) \ln |\sin(\pi q)| - \frac{1}{\lambda} \left[ \int dq \rho(q) \cos(2\pi q) - 1 \right], \quad (99)$$

and, we can therefore rewrite the energy into the following form,

$$-E(\lambda) = \frac{1}{\lambda} \left[ \int dq \rho(q) \cos(2\pi q) + 1 \right] + P \int dq \rho(q) \ln |\sin(\pi q)|. \quad (100)$$

Computing the elementary integrals in the above expression we finally get a simple expression for the energy as

$$-E(\lambda) = \begin{cases} \frac{2}{\lambda} + \frac{1}{2} \ln \frac{\lambda}{8} - \frac{3}{4} & \text{if } \lambda < 2, \\ \frac{1}{\lambda^2} - \ln 2 & \text{if } \lambda \geq 2. \end{cases} \quad (101)$$

This energy expression has an interesting property. As a function of  $\lambda$ , the energy, its first, and second derivatives are all continuous functions. The third derivative,  $E'''(\lambda)$ , turns out to be discontinuous. Hence, the critical coupling  $\lambda_c = 2$  is actually a critical point for a *third-order* phase transition. So far, the above results are relevant for the large  $N_c$  pure gluonic theory in two spacetime dimensions, but it can be generalized to four dimensional cases under certain conditions; namely, if the large  $N_c$  limit could be interchangeable with the strong coupling expansion, the pure gluonic theory in four dimensions may exhibit the same third-order phase transition in the large  $N_c$  limit [87].

### 3.2.2 Effective matrix theory

Section 3.2.1 was a review for the analytical results known for the lattice Wilson action in two dimensions. Here, we consider a matrix model for the Polyakov loops in four dimensions and explain how the theory may exhibit novel behavior in the large  $N_c$  limit.

The Polyakov loop potential can be computed analytically in several limits including the high-temperature limit as we already saw in Sec. 2.4 and the small-sphere limit as we will see in Sec. 3.2.3 later. Here, let us adopt a simple and general setup to perform an effective potential analysis. We shall ignore fluctuations and kinetic terms constituting  $1/N_c$  corrections, and then we can express the partition function in a form of the group integration as follows,

$$Z = \int \mathcal{D}L e^{-N_c^2 V(L)}, \quad (102)$$

where the Polyakov loop potential is postulated to have a power-series form in  $|\ell_3|^2$ , i.e.

$$V(L) = -m^2 |\ell_3|^2 + \kappa_4 |\ell_3|^4 + \kappa_6 |\ell_3|^6 + \dots \quad (103)$$

Our goal is to carry out the group integration with respect to  $L$  in Eq (102) except for  $\ell_3$ . In order to achieve this, we use a common trick to construct the so-called constrained effective potential [36] introducing a delta function as

$$Z = \int \mathcal{D}L \int d\gamma \delta(\gamma - \ell_3) e^{-N_c^2 V(\gamma)}. \quad (104)$$

Replacing the order of integration and using the Fourier representation for the delta function we obtain,

$$Z = \int \frac{\omega}{2\pi} \int d\gamma e^{-iN_c^2 \omega \gamma - N_c^2 V(\gamma)} \int \mathcal{D}L e^{iN_c^2 \omega \ell_3}. \quad (105)$$

Now the group integration simplifies with the Haar measure or the Vandermonde determinant taken into account explicitly, leading to

$$\int \mathcal{D}L e^{iN_c^2 \omega \ell_3} = \int d\ell \exp[iN_c^2 \omega \ell - N_c^2 V_{\text{Vdm}}(\ell)], \quad (106)$$

and then the partition function after the  $\omega$  and the  $\gamma$  integrations should read,

$$Z = \int d\ell e^{-N_c^2 V_{\text{eff}}(\ell)} \quad (107)$$



with the effective potential defined by

$$V_{\text{eff}}(\ell) = V(\ell) + V_{\text{Vdm}}(\ell) . \quad (108)$$

From this expression it is clear that  $V_{\text{Vdm}}(\ell)$ , the explicit form of which we will discuss soon later, corresponds to  $-\ln H$  we have encountered in the strong coupling calculation in Sec. 2.3. It is noted that the determination of  $H$  for the SU(2) and the SU(3) cases was straightforward directly from the Vandermonde determinant (33), but what we should consider here is to find it for the general SU( $N_c \rightarrow \infty$ ) case. To this end, we compare the left-hand and the right-hand sides of Eq. (106). Because  $N_c$  is infinitely large, the stationary point approximation should work for the  $\ell$  integration, and the stationary condition with respect to  $\ell$  leads to

$$\tilde{\omega} \equiv i\omega = \frac{\partial V_{\text{Vdm}}}{\partial \ell} . \quad (109)$$

This is a condition to fix  $\ell(\omega)$ , but we can conversely solve  $\omega$  for a given  $\ell$ . Then, we shall consider the left-hand side of Eq. (106) for a real-valued  $\tilde{\omega}$ . Such a replacement of  $\omega \rightarrow \tilde{\omega}$  enables us to make use of the results in the previous subsection, particularly the solution (97) and (98) with the mapping  $2/\lambda \rightarrow \tilde{\omega}$ . Thus, the stationary point solution reads,

$$\ell_3(\tilde{\omega}) = \begin{cases} 1 - \frac{1}{2\tilde{\omega}} & \text{if } \tilde{\omega} > 1 , \\ \frac{\tilde{\omega}}{2} & \text{if } \tilde{\omega} \leq 1 . \end{cases} \quad (110)$$

We can eliminate  $\tilde{\omega}$  by combining Eqs. (109) and (110) to arrive at an equation to be integrated for  $V_{\text{Vdm}}$ . In this way we can fix the explicit form of  $V_{\text{Vdm}}$  and the final results are

$$V_{\text{Vdm}}(\ell) = \begin{cases} \ell^2 & \text{if } \ell < 1/2 , \\ -\frac{1}{2} \ln[2(1 - \ell)] + \frac{1}{4} & \text{if } \ell \geq 1/2 . \end{cases} \quad (111)$$

The Vandermonde potential  $V_{\text{Vdm}}(\ell)$  can also be interpreted as the Legendre transform of the left-hand side of Eq. (106) with  $i\omega$  playing a role of external field. The original eigenvalue repulsion inherent in the Vandermonde determinant is translated into a logarithmic singularity at  $\ell = 1$ , which guarantees that the Polyakov loop stays below the unity for any  $V(L)$  or any coefficients in the parametrization (103) in the total effective potential (108).

The most remarkable property of the Vandermonde potential is that  $V_{\text{Vdm}}(\ell)$ ,  $V'_{\text{Vdm}}(\ell)$ , and  $V''_{\text{Vdm}}(\ell)$  are continuous functions, while the third derivative,  $V'''_{\text{Vdm}}(\ell)$  is discontinuous at  $\ell = 1/2$ .

The analysis of the phase diagram for the effective potential (108) can be readily done. Let us consider only non-zero quadratic term first, that is,  $m^2 \neq 0$  and  $\kappa_n = 0$  in Eq. (103). In the large  $N_c$  limit the stationary point approximation or the mean-field approximation would be exact, and we can simply identify the minimum of the effective potential as the expectation value  $\Phi = \langle \ell \rangle$ . The confining vacuum with a stable minimum at  $\Phi = 0$  is favored for any  $m^2 < 1$ . The potential around this minimum has only quadratic term. For  $m^2 > 1$  the sign of the quadratic term changes leading to the deconfined phase with the expectation value given by

$$\Phi = \frac{1}{2} \left( 1 + \sqrt{1 - \frac{1}{m^2}} \right) . \quad (112)$$

The behavior of the effective potential around the critical point is depicted in the left of Fig. 7. Also, we see that the Polyakov loop jumps from 0 to 1/2 at the phase transition at  $m^2 = 1$ , which is clearly seen in the right panel of Fig. 7.

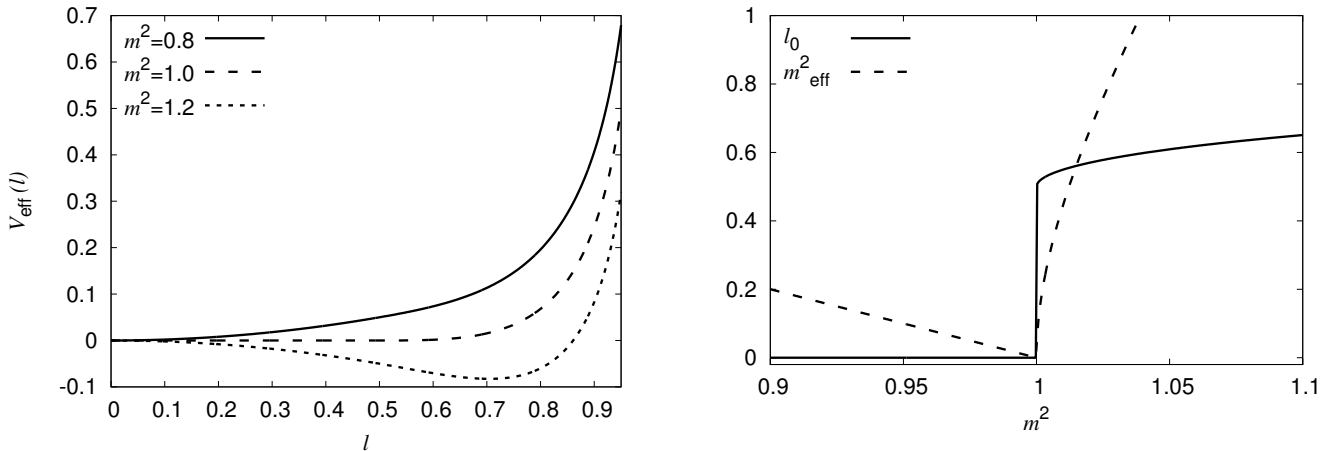


Figure 7: Effective potential at the transition as a function of the Polyakov loop (left) and the expectation value of the Polyakov loop and the effective mass squared as a function of  $m^2$  (right).

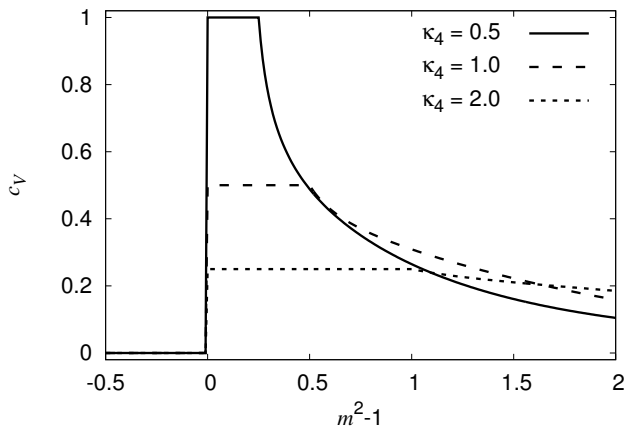


Figure 8: The specific heat,  $c_V$ , as a function of  $m^2 - 1$  for positive quartic couplings.

As shown by the dashed line in the left panel of Fig. 7 the potential behavior at  $m^2 = 1$  is quite peculiar; it is flat and constantly vanishing for  $\ell < 1/2$ . Near the onset, for  $\ell \rightarrow 1/2^+$ , the potential arises from zero as  $\sim 4/3(\ell - 1/2)^3$ . The effective mass (i.e. the potential curvature mass of the Polyakov loop) inferred from  $m_{\text{eff}}^2 = \partial^2 V_{\text{eff}} / \partial \ell^2 |_{\ell=\Phi}$  is continuous and goes to zero regardless of whether the critical point is approached by  $m^2 \rightarrow 1^+$  or  $m^2 \rightarrow 1^-$  as illustrated in the right panel of Fig. 7. Therefore, we can say that the  $m^2 = 1$  point exhibits aspects of both first- and second-order phase transitions. Additionally, when the transition is approached by  $m^2 \rightarrow 1^+$ , the expectation value of the Polyakov loop demonstrates critical behavior associated with the second-order transition;  $\Phi - 1/2 \propto (\delta t)^\beta$  with a critical exponent  $\beta = 1/2$ , where we introduce the dimensionless temperature as  $m^2 - 1 \propto \delta t \equiv T/T_c - 1$ . Moreover, the specific heat diverges at  $m^2 \rightarrow 1^+$  as  $c_v \propto (\delta t)^{-\alpha}$  with  $\alpha = 1/2$ , while it is vanishing for  $m^2 < 1$ . By adding an external field<sup>2</sup>, we can extract another critical exponent as  $\delta = 2$ . It is remarkable that the critical exponents satisfy ordinary Griffith's scaling relation;  $2 - \alpha = \beta(1 + \delta)$ . For this reason this phase transition is often referred to as a *critical first-order* phase transition.

Before closing this subsection, let us discuss effects of non-zero  $\kappa_4$  in the potential (103). For  $\kappa_4 > 0$  some simple computations show that there is an ordinary second-order phase transition at  $m^2 = 1$ ;

<sup>2</sup>For any non-zero external field the transition is of third order. This is due to flatness of the potential, i.e. the absence of the potential barrier at the transition for zero external field [88, 89, 90].

this conclusion is not affected by the non-polynomial part of the Vandermonde potential because the expectation value of the Polyakov loop develops continuously from zero. What is special about the system is that there is one more phase transition at  $m^2 = 1 + \kappa_4/2$ . At this latter critical value of  $m^2$ , the expectation value of the Polyakov loop is  $1/2$  and the third derivative of the effective potential with respect to  $m^2$  is discontinuous. Thus, this transition at  $m^2 = 1 + \kappa_4/2$  is of third order. A more detailed analysis presented in Ref. [91] shows that this transition is associated with non-zero expectation values of the higher order Polyakov loops, defined as  $\text{tr}(L^n)$  with  $n > 1$ . Indeed, for  $m^2 < 1 + \kappa_4/2$ , the higher order Polyakov loops vanish; their values are nonzero only for  $m^2 > 1 + \kappa_4/2$ .

We illustrate the transition behavior by plotting  $c_V$  as a function of  $m^2$  (which is physically interpreted as the temperature) in Fig. 8. As is common in the mean-field approximation, the specific heat is discontinuous at the second-order phase transition,  $m^2 = 1$ , due to vanishing critical exponent for the specific heat. The third-order phase transition at  $m^2 = 1 + \kappa_4/2$  leads to a kink structure in the specific heat. The maximum of  $c_V$  is proportional to  $1/\kappa_4$ ; thus when  $\kappa_4$  approaches zero, two transitions meet at  $m^2 = 1$  and  $c_V$  diverges there.

For  $\kappa_4 < 0$ , there is a single transition of first order at  $m^2 < 1$ . For the first-order phase transition in general, the transition line can be found from the energy comparison of two minima of the effective potential. This results in a parametric form,

$$m^2 = \frac{e^{2v}}{(2e^v - 1)^2} (3 + 4v - 2e^v), \quad (113)$$

$$\kappa_4 = \frac{8e^{4v}}{(2e^v - 1)^4} (1 + v - e^v) \quad (114)$$

with some  $v$  ranging from 0 to  $\infty$ . In this case, at the phase transition, the Polyakov loop jumps from 0 to a value greater than  $1/2$ . We summarize these observations in the phase diagram illustrated in Fig. 9. All three transitions meet at a supercritical point, where the system exhibits properties of both first- and second-order phase transitions, as we already stated.

In the next subsection, we consider a weakly coupled theory on a small 3-sphere, i.e.  $S^1 \times S^3$ ; although the derivation is more cumbersome, the main features are essentially the same as those in the simple matrix model discussed above, including the structure of the phase diagram presented in Fig. 9. We note that a similar effective theory with a quadratic deformation of the perturbative action was considered in Ref. [92]. Although some quantitative aspects of the phase transition are different (e.g. the critical exponents significantly differ), the qualitative pattern of the phase transition and the phase diagram share the same features with what we have seen in this subsection.

### 3.2.3 Weakly coupled theory on a small 3-sphere

As was discussed in Sec. 2.4 the pure gluonic thermodynamics allows for an analytical treatment only at very high temperature. At temperatures in the vicinity of the deconfinement temperature, the numerical methods on lattice discretized spacetime are most useful [93, 94, 56], for the coupling constant is not necessarily small enough there. Nevertheless, there is a theoretical possibility to study the thermodynamics and the deconfinement phenomenon in the weak coupling limit using perturbative approaches, if the theory is formulated on a compact space; more specifically a three-dimensional sphere  $S^3$  with finite radius  $R$ . This provides us with an additional parameter  $R$  or a dimensionless combination,  $R\Lambda_{\text{QCD}}$ , which interpolates between the strong coupling regime for large  $R$  and the weak coupling regime for small  $R$ . In particular, we can anticipate that the perturbation theory should work when the compactification radius is much smaller than the strong interaction scale, i.e.  $R\Lambda_{\text{QCD}} \ll 1$ .

Phase transitions for a theory on a compact manifold should be always continuous and thermodynamic quantities are non-singular due to a limited number of degrees of freedom in a finite volume. There is a notable exception of  $N_c \rightarrow \infty$  that makes the number of degrees of freedom infinite regardless

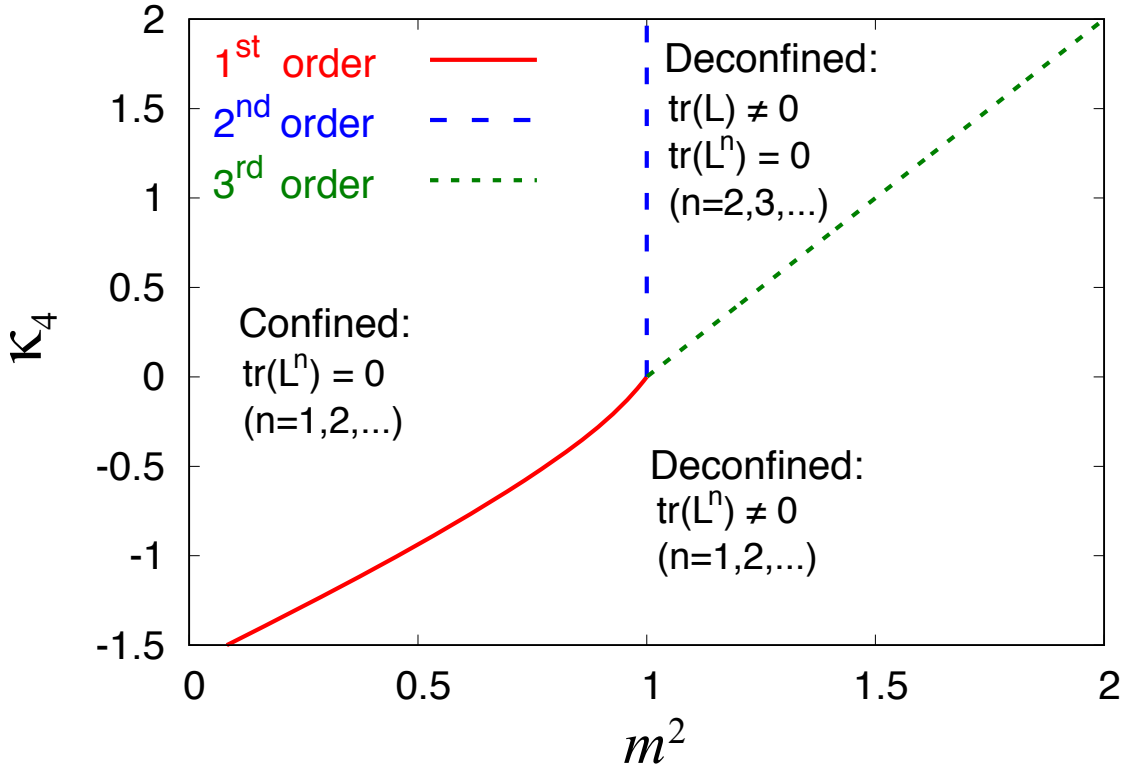


Figure 9: The phase diagram for the effective potential with non-zero quartic coupling.

of the volume of the system; in what follows below we consider the phase transition of a weakly coupled theory on a small 3-sphere in the “thermodynamic limit” in a sense of the  $N_c \rightarrow \infty$  limit.

At weak 't Hooft coupling  $\lambda = g^2 N_c$ , the partition function can be reduced to an integral with respect to a single unitary matrix by leaving the zero mode only after integrating out heavier modes with a gap of order of  $1/R$ . Alternatively, the leading order results of the perturbative expansion in  $\lambda$  (i.e. free theory) can also be obtained by counting the gauge invariant states in free Yang-Mills theory, as was done in Refs. [91, 95]. Here we follow the former approach along the lines outlined in Sec. 2.4.

The pure gluonic or Yang-Mills partition function can be expressed as

$$Z = \int d\alpha \int \mathcal{D}A_i \Delta_A \Delta_\alpha e^{-S_{\text{YM}}(A, \alpha)}, \quad (115)$$

where  $\Delta_A$  is the Faddeev-Popov determinant associated with the partial gauge fixing,  $\partial_i A^i = 0$ , while  $\Delta_\alpha$  corresponds to the residual gauge fixing,  $\partial_0 \alpha = 0$ , where the zero-mode gauge potential is defined as  $\alpha(t) \equiv \frac{1}{V_3} \int_{S^3} A_0$ . An explicit evaluation of  $\Delta_\alpha$  gives  $d\alpha \Delta_\alpha = dU$ , where  $dU$  represents a group integration for the unitary matrix  $U = e^{i\beta\alpha}$  with  $\beta$  being a period of temporal  $S^1$ . Therefore, the partition function can be rewritten as follows;

$$Z = \int dU e^{-S_{\text{eff}}(\alpha)} \quad \text{with} \quad e^{-S_{\text{eff}}(\alpha)} = \int \mathcal{D}A_i \Delta_A e^{-S_{\text{YM}}(A, \alpha)}. \quad (116)$$

The effective action  $S_{\text{eff}}(\alpha)$  can be evaluated diagrammatically as a power-series of the coupling constant. The lowest order calculation is rather straightforward and repeats the one-loop computation with only one minor difference; the eigenvalues of the Laplacian operator should be replaced with those for vector spherical harmonics, which is denoted by  $\Delta^2$  here. On a sphere  $S^3$ , the eigenvalues are degenerate, and for an integer  $\Delta \geq 1$ , the degeneracy factor is given by  $n_\Delta = 2(\Delta^2 - 1)$ . From now on, we rescale all quantities to absorb the mass dimension by the appropriate power of  $R$ ; in other words, we choose a

special unit with which  $S^3$  is a unit-radius sphere. One-loop calculation immediately leads us to

$$S_{\text{eff}}(\alpha) = \frac{1}{2} \text{tr}_c \sum_{\Delta} n_{\Delta} [\beta\Delta + \ln(1 - e^{-\beta\Delta+i\beta\alpha}) + \ln(1 - e^{-\beta\Delta-i\beta\alpha})] , \quad (117)$$

where  $\text{tr}_c$  is a trace over the color adjoint representation that  $\alpha$  belongs to. A more transparent representation of the effective action emerges once the logarithms are expanded. We can then take the summation with respect to the Laplacian eigenvalues  $\Delta$ , and we also switch to the fundamental representation. Then, we find,

$$S_{\text{eff}}(\alpha) = \frac{1}{2} \beta N_c^2 \sum_{\Delta} \Delta n_{\Delta} - \sum_{n=1}^{\infty} \frac{z(e^{-\beta n})}{n} \text{tr}(U^n) \text{tr}(U^{\dagger n}) , \quad (118)$$

where

$$z(e^{-\beta n}) = \sum_{\Delta=1}^{\infty} n_{\Delta} e^{-\beta\Delta n} = 2 \frac{3e^{-2\beta n} - e^{-3\beta n}}{(1 - e^{-\beta n})^3} . \quad (119)$$

Using these results, the partition function can be readily evaluated. In terms of the eigenvalues of the unitary matrix [see Eq. (88)], the partition function takes the following form;

$$Z = \int dU e^{-S_{\text{eff}}} = \int dq_i \exp \left\{ - \sum_{i \neq j} \ln |\sin[\pi(q_i - q_j)]| - \sum_{i,j} \sum_n \frac{z(e^{-\beta n})}{n} \cos[2n\pi(q_i - q_j)] \right\} . \quad (120)$$

We note that both terms can be combined into a common infinite sum by virtue of

$$\ln |\sin(\pi x)| = -\ln 2 - \sum_{n=1}^{\infty} \frac{1}{n} \cos(2n\pi x) . \quad (121)$$

In the large  $N_c$  limit, the saddle point approximation becomes exact and the partition function and the distribution of the eigenvalues can be found analytically; see Refs. [91, 95] for details. Numerical analysis for finite  $N_c$  was performed in Ref. [96] (see also Ref. [97] for higher order extensions).

Close to the deconfinement transition  $z(e^{-\beta c}) = 1$ , where the sign of  $|\text{tr}L|^2$  changes rendering an instability of the trivial solution, the partition function can be approximated by the effective matrix model described in the previous subsection with a non-trivial quadratic coupling. Actually, by taking into account the first perturbative correction to the free limit, we get the effective matrix theory with negative  $\kappa_4$  [98]. The analysis of the phase structure thus repeats the previous subsection.

## 4 Coupling to Quarks

QCD has not only gluons but quarks also, and the inclusion of quarks would drastically change confinement argument based on center symmetry. Quarks explicitly break center symmetry since the center twisted gauge transformation changes the boundary condition for fermions; after the transformation they no longer satisfy the anti-periodic boundary condition but are multiplied by a center element; the transformed field,  $V(x)\psi(x)$ , with the boundary condition (18) satisfies,

$$V(x_4 = \beta)\psi(x_4 = \beta) = -z_k \cdot V(x_4 = 0)\psi(x_4 = 0) , \quad (122)$$

so that  $\psi(x)$  is sensitive to the center. This also means that quark excitations are significantly affected by the realization of center symmetry in a gluonic medium.

In this section, we will first see how quark contributions would change the perturbative Polyakov loop potential, and next we will turn our view point over to discuss how the Polyakov loop background can in effect capture color screening effects on quarks. This latter observation underlies the Polyakov loop augmented building of chiral effective models. The idea can be easily generalized to not only color fundamental quarks but also color adjoint gluons.

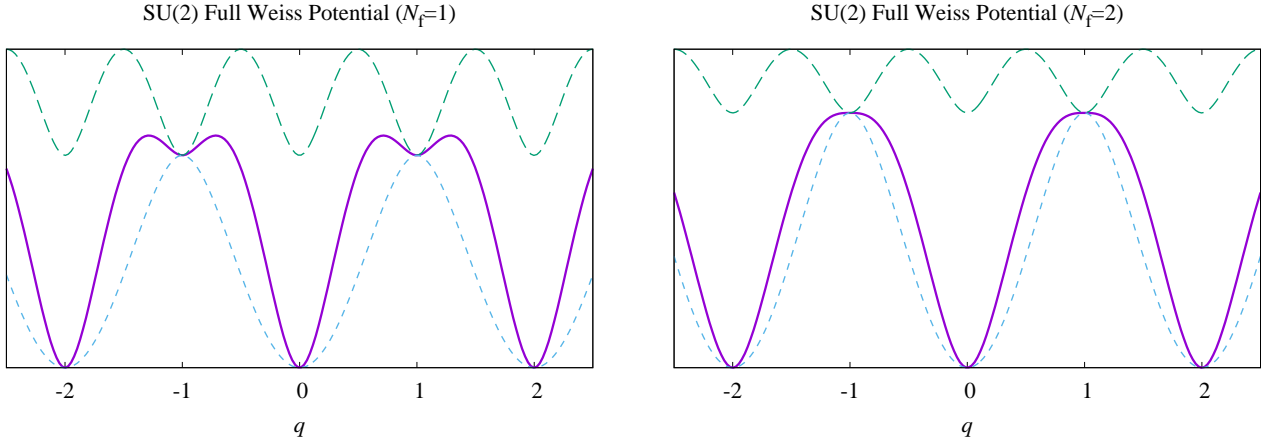


Figure 10: SU(2) full Weiss potential with the gluonic contribution (shown by the dashed lines) together with the quark contribution (shown by the dotted lines) for  $N_f = 1$  (left) and  $N_f = 2$  (right) at  $\mu = 0$ .

#### 4.1 Polyakov Loop Potential from Quarks

Even without concrete calculations, it is straightforward to rewrite Eq. (44) to infer the quark one-loop contribution to the Polyakov loop potential [38]. In Eq. (44) gluons belong to the adjoint representation, and this is why  $q_{ij}$  appears there. For quarks  $q_{ij}$  should be replaced with  $q_i$  in the fundamental representation. For  $N_f$  massless quarks including also a finite chemical potential  $\mu$ , the potential contribution immediately reads from such a mapping as

$$\begin{aligned}
 V_{\text{quark}}[q] &= -2N_f T V \int \frac{d^3 p}{(2\pi)^3} \sum_{i=1}^{N_c} \left[ \ln(1 + e^{-\beta(|\mathbf{p}|-\mu)+2\pi i q_i}) + \ln(1 + e^{-\beta(|\mathbf{p}|+\mu)-2\pi i q_i}) \right] \\
 &= -N_f V \frac{4\pi^2}{3\beta^4} \sum_{i=1}^{N_c} \left( q_i + \frac{1}{2} - i \frac{\beta\mu}{2\pi} \right)_{\text{mod}1}^2 \left[ \left( q_i + \frac{1}{2} - i \frac{\beta\mu}{2\pi} \right)_{\text{mod}1} - 1 \right]^2. \quad (123)
 \end{aligned}$$

This additional contribution to the Weiss potential manifestly breaks translational symmetry and thus center symmetry.

To visualize the center symmetry breaking more transparently, we make a plot for the SU(2) full (i.e. gluonic + quark) Weiss potential for  $N_f = 1$  and  $N_f = 2$  in Fig. 10 in the  $\mu = 0$  case. As is clearly noticed in Fig. 10 the perturbative vacuum at  $q = 0$  is still a global minimum of the effective potential, while the center transformed point at  $q = 1$  is at best only a local potential minimum due to the center symmetry breaking. Interestingly, for  $N_f = 1$  as in the left panel of Fig. 10, there still remains a meta-stable state corresponding to a local minimum at  $q = 1$ . With  $N_f = 2$  flavors the local minimum disappears and only the perturbative vacuum is energetically allowed.

From the potential curvature around  $q = 0$  we can deduce the Debye mass correction from quarks (including  $\mu$ ). The perturbative vacuum becomes more stabilized by an increase in the Debye mass by

$$\delta m_E^2 = N_f \left( \frac{g^2 T^2}{6} + \frac{g^2 \mu^2}{2\pi^2} \right), \quad (124)$$

which correctly reproduces the expression for the Debye screening mass arising from quark one-loop contributions at finite  $T$  and  $\mu$ . Now, one may be naturally tempted to look more closely at global structures of the finite- $\mu$  Weiss potential away from the perturbative vacuum. However, Eq. (123) is complex for non-zero  $\mu$ , and then we can no longer interpret it as a thermodynamic potential. In other words, for complex  $V_{\text{quark}}[q]$ , the most favored  $q$  is not uniquely determined energetically from thermodynamic principles.



The origin of theoretical difficulties from complex  $V_{\text{quark}}[q]$  would be more understandable if we express Eq. (123) in a different but equivalent way. To write explicit expressions down, let us consider the QCD ( $N_c = 3$ ) case specifically below (note that the Polyakov loop is always real in the  $N_c = 2$  case and the sign problem becomes serious for  $N_c \geq 3$ ). In this case with  $N_c = 3$ , it is easy to take the sum over  $i = 1, \dots, N_c = 3$  explicitly before the momentum integration in Eq. (123), so that we finally arrive at

$$\begin{aligned} V_{\text{quark}}[q] &= -2N_f TV \int \frac{d^3p}{(2\pi)^3} \text{tr} \left[ \ln[1 + L e^{-\beta(\varepsilon_p - \mu)}] + \ln[1 + L^\dagger e^{-\beta(\varepsilon_p + \mu)}] \right] \\ &= -2N_f TV \int \frac{d^3p}{(2\pi)^3} \left[ \ln(1 + 3\ell e^{-\beta(\varepsilon_p - \mu)} + 3\ell^* e^{-2\beta(\varepsilon_p - \mu)} + e^{-3\beta(\varepsilon_p - \mu)}) \right. \\ &\quad \left. + \ln(1 + 3\ell^* e^{-\beta(\varepsilon_p + \mu)} + 3\ell e^{-2\beta(\varepsilon_p + \mu)} + e^{-3\beta(\varepsilon_p + \mu)}) \right], \end{aligned} \quad (125)$$

where a finite mass is introduced through  $\varepsilon_p \equiv \sqrt{p^2 + m^2}$ . We can then precisely spot what makes  $V_{\text{quark}}[q]$  complex. In general  $\ell$  is a complex number, but as long as  $\mu = 0$ , the first and the second lines of Eq. (125) are complex conjugate to each other and the sum of them takes a real number. A finite  $\mu$  would destroy this balance and the complex nature of  $V_{\text{quark}}[q]$  is attributed to complex  $\ell$  and  $\ell^*$  with unbalanced weights. Such an observation of complex  $V_{\text{quark}}[q]$  is a very concrete realization of the sign problem, which we will closely discuss later in Sec. 4.3.

## 4.2 Polyakov Loop in Chiral Models

It is worth noting that the general form of  $V_{\text{quark}}[q]$  in Eq. (125) is a result from the one-loop quark integration, and nevertheless, it is a full expression in the quark sector for given gauge (Polyakov loop) configurations. Therefore, the validity region of Eq. (125) is not necessarily restricted to the perturbative regime only but can be extended to more general regimes where the quasi-particle picture makes sense.

This opens a wider range of applications of Eq. (125) beyond the perturbative Weiss potential. Here, we will see a successful example of utilizing Eq. (125) in quark models to consider the Polyakov loop effects on chiral symmetry.

### 4.2.1 PNJL model

The effective potential (125) (together with the gluonic contributions) is supposed to be minimized to determine the expectation value of  $q$ , and at the same time, we can make another interpretation for Eq. (125); for a given  $q$ , this expression represents how the quark excitations are affected in the presence of the Polyakov loop background. Actually, the physical meaning of Eq. (125) would become even clearer in such an interpretation; in fact,  $\ell$  and  $\ell^*$  emerge in Eq. (125) as colored chemical potentials.

If  $\ell$  and  $\ell^*$  are just the unity, the logarithmic terms simplify as  $\ln[1 + 3e^{-\beta(\varepsilon_p \mp \mu)} + 3e^{-2\beta(\varepsilon_p \mp \mu)} + e^{-3\beta(\varepsilon_p \mp \mu)}] = 3 \ln[1 + e^{-\beta(\varepsilon_p \mp \mu)}]$ . Thus,  $V_{\text{quark}}[q = 1]$  is nothing but the grand canonical partition function for free quarks. On the other hand, in the limit of vanishing  $\ell$  and  $\ell^*$ ,  $V_{\text{quark}}[0]$  is reduced to the grand canonical partition function for free particles with an effective temperature lowered by factor 3. In this case of  $\ell = \ell^* = 0$ , all single-quark-type excitations ( $\propto e^{-\beta(\varepsilon_p \mp \mu)}$ ) and diquark-type excitations ( $\propto e^{-2\beta(\varepsilon_p \mp \mu)}$ ) are diminished by color screening and only color-singlet combinations of three quarks survive.

It is obvious from the above arguments that, if some sort of phase transition occurs for  $\ell = 1$  at  $T = T_c$  by quasi-quark excitations, the phase transition under  $\ell = 0$  would be delayed to  $T > 3T_c$ . (The underlying mechanism for the increase in the transition temperature parallels the canonical ensemble approach; see Refs. [99, 100].) One direct implication from this observation would be the finite- $T$  chiral phase transition affected by external  $\ell$  and  $\ell^*$ . This possibility was pioneered in Ref. [101] by means

of the Nambu–Jona-Lasinio (NJL) model to describe the chiral sector. It was then Ref. [102] that first demonstrated a successful treatment of both the chiral order parameter and the Polyakov loop as dynamical degrees of freedom, which was later named as the PNJL (i.e. Polyakov loop augmented Nambu–Jona-Lasinio) model in Ref. [59]. For chiral symmetry in QCD and the details about the NJL model, Refs. [20, 21, 22] are comprehensive reviews. For more modern view points including recent highlights from the lattice-QCD simulations, see Ref. [7], and for a related attempt of the first successful treatment of both the Polyakov loop and the glueball states. see Ref. [103]. Here, since the main focus in this review is the Polyakov loop physics, we shall give a minimal explanation about chiral symmetry and its breaking. If there are  $N_f$  massless Dirac fermions, they are decomposed into  $N_f$  right-handed Weyl fermions and  $N_f$  left-handed Weyl fermions. The Dirac operator is invariant under unitary rotations in  $N_f$  flavor space. Thus, an idealized version of QCD with  $N_f$  massless flavors would accommodate the following global symmetry:

$$U(N_f)_L \times U(N_f)_R = SU(N_f)_L \times SU(N_f)_R \times U(1)_A \times U(1)_V . \quad (126)$$

Chiral symmetry refers to  $SU(N_f)_L \times SU(N_f)_R$ , which is spontaneously broken down to a vectorial subgroup,  $SU(N_f)_V$ , that is a symmetry under simultaneous rotations of right-handed and left-handed fermions. We note that  $U(1)_A$  is explicitly broken by the axial anomaly. These symmetry breaking patterns constrain how the low-energy limit of QCD should look like. In this way, chiral symmetry and its breaking provide us with an important guiding principle to build low-energy effective models of QCD. A condensate of quark and anti-quark, commonly called the chiral condensate, is an order parameter for the spontaneous breaking of chiral symmetry, i.e. chiral order parameter. We will denote it as  $\langle \bar{q}q \rangle$  in the general context, or sometimes use  $\langle \bar{u}u \rangle$ ,  $\langle \bar{d}d \rangle$ , and  $\langle \bar{s}s \rangle$  when different flavors need to be distinguished.

The first physics motivation to build such a model with both the chiral order parameter and the Polyakov loop was a challenge to understand why two (approximate) critical temperatures are located so closely to each other as observed in the lattice-QCD simulation. The chiral phase transition is associated with an in-medium change in terms of dressed quark masses including interaction clouds, while colored excitations are liberated at the deconfinement phase transition. These are apparently different physics phenomena, and there is no *a priori* reason why they are strongly entangled. One might think that QCD has a unique scale,  $\Lambda_{\text{QCD}}$ , which would explain a single  $T_c$ . However, such an argument would not be strong enough to constrain anything beyond order estimates. As explained above, chiral symmetry is exact only when all quark masses are zero, i.e.  $m = 0$ , and center symmetry exists only in a pure gluonic medium, i.e.  $m = \infty$ . Hence, two phenomena belong to two opposite limits from QCD, and the critical temperatures may well be different by a factor. Summarizing this makes the following table;

$$\begin{array}{ccc} \boxed{m = \infty \text{ limit}} & & \boxed{0 < m < \infty} & & \boxed{m = 0 \text{ limit}} \\ \text{Center Symmetry} & \longleftarrow & \text{No Exact Symmetry} & \longrightarrow & \text{Chiral Symmetry} \\ \text{broken at } T_D(m = \infty) & & T_D(m) \simeq T_\chi(m) & & \text{broken at } T_\chi(m = 0) \end{array}$$

It is very important to keep in mind that the critical temperatures,  $T_D$  for deconfinement and  $T_\chi$  for chiral restoration, are well-defined only in the quenched ( $m = \infty$ ) and the chiral ( $m = 0$ ) limits, respectively. A finite (non-zero and non-diverging) mass induces explicit symmetry breaking as if it were like a magnetic field in spin systems. There is then no clear way to define the critical temperature for smooth crossover, unless a first-order phase transition persists. Usually some “prescription” to defined the so-called pseudo-critical temperature is employed to define  $T_D$  and  $T_\chi$  for  $0 < m < \infty$ . One of the most reasonable choices is the peak temperature of the order parameter susceptibility  $\chi(T)$ ; the pseudo-critical temperature  $T_c$  maximizes  $\chi(T)$ . Another choice would be the inflection temperature of the order parameter;  $T_c$  maximizes the  $T$ -derivative of the order parameter. The lattice-QCD simulation for various quark masses strongly suggests that  $T_D(m) \simeq T_\chi(m)$  for any  $m$ .

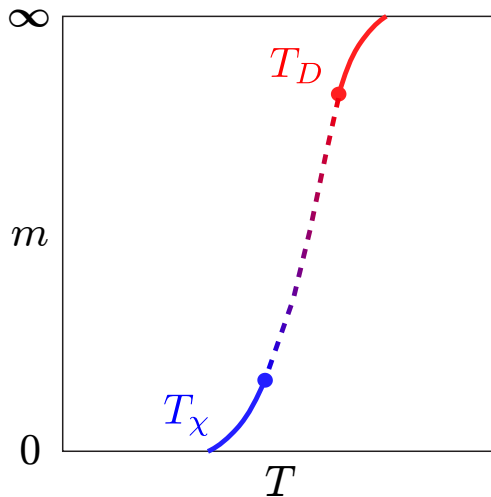


Figure 11: Schematic picture of a scenario on the possible connection between the chiral and the deconfinement critical lines.

Such a tight connection between two crossovers is schematically illustrated in Fig. 11. The deconfinement point at  $m = \infty$  starts with a first-order phase transition for  $N_c \geq 3$  and the first-order line ends at a critical point (which will be more explained later in Sec. 4.2.3). On the other hand, at  $m = 0$  the chiral phase transition is in general of first order again for  $N_f \geq 3$  and the first-order line again ends at a critical point. It is likely that these two critical points of deconfinement and chiral restoration are connected by a *single* line of crossover, which is a scenario proposed in Ref. [104]. In physics language the scenario in Fig. 11 implies that the sigma meson and the glueball are mixed together leading to a single critical field out of the chiral condensate and the Polyakov loop. According to this scenario, it is expected that the low-lying scalar glueball should become light near the critical point, as partially confirmed in the lattice QCD simulation [105].

One appreciable feature of the PNJL model is that it can provide us with a quantitative tool to investigate simultaneous phase transitions of chiral symmetry restoration and quark deconfinement, which goes far beyond a qualitative conjecture in Ref. [104] and a parametrization in Ref. [106]. To see the pragmatic strength of the PNJL model, let us elaborate the model details below according to Ref. [107].

In the conventional NJL model the QCD interaction is approximated by a point-like four-quark vertex. The simplest chiral symmetric combination of four-quark interaction is,

$$\mathcal{L}_S = \frac{g_S}{2} \sum_{a=0}^{N_f^2-1} \left[ (\bar{\psi} \lambda_a \psi)^2 + (\bar{\psi} i \gamma_5 \lambda_a \psi)^2 \right]. \quad (127)$$

For the  $N_f = 3$  case  $\lambda_a$  are Gell-Mann matrices in flavor space. This interaction is invariant under flavor rotations having  $U(N_f)_L \times U(N_f)_R$  symmetry. Among this flavor symmetry,  $U(1)_A$  must be broken by the axial anomaly as mentioned above, and the explicit breaking can be incorporated by the Kobayashi-Maskawa-'t Hooft (KMT) interaction [108, 109] whose explicit form is,

$$\mathcal{L}_A = g_D [\det \bar{\psi} (1 - \gamma_5) \psi + \text{h.c.}] , \quad (128)$$

where the determinant is taken with respect to flavor indices. Let us concretely address the  $N_f = 3$  case specifically including strange quarks for later convenience.

For  $N_f = 3$  there are three independent chiral condensates, namely,  $\langle \bar{u}u \rangle$ ,  $\langle \bar{d}d \rangle$ , and  $\langle \bar{s}s \rangle$ . Non-zero values of these condensates break chiral symmetry  $SU(3)_L \times SU(3)_R$  (if  $m_u = m_d = m_s = 0$ ) down to

SU(3)<sub>V</sub> leading to 8 Nambu-Goldstone (NG) bosons. In the mean-field approximation, four-fermionic interactions are approximated as

$$(\bar{u}u)^2 = [(\bar{u}u - \langle \bar{u}u \rangle) + \langle \bar{u}u \rangle]^2 \simeq -\langle \bar{u}u \rangle^2 + 2\langle \bar{u}u \rangle \bar{u}u \quad (129)$$

in the  $u$ -quark sector of Eq. (127) and similar terms appear in the  $d$ -quark and the  $s$ -quark sectors. The first term in Eq. (129) represents a  $u$ -quark contribution to the condensation energy,  $V_{\text{cond}}$ , and the sum over three flavors yields,

$$V_{\text{cond}}[\langle \bar{q}q \rangle] = g_S(\langle \bar{u}u \rangle^2 + \langle \bar{d}d \rangle^2 + \langle \bar{s}s \rangle^2) + 4g_D \langle \bar{u}u \rangle \langle \bar{d}d \rangle \langle \bar{s}s \rangle, \quad (130)$$

where the last term arises from the KMT interaction (128). The second term in Eq. (129) represents a mass correction by the mean-field interaction. Together with additional mass corrections from the KMT interaction (128), the mean-field masses can be expressed as

$$M_i = m_i - 2g_S \langle \bar{q}_i q_i \rangle - g_D \epsilon^{ijk} \langle \bar{q}_j q_j \rangle \langle \bar{q}_k q_k \rangle, \quad (131)$$

where  $i, j, k$  run in flavor space,  $u, d, s$ . Once the mean-field masses are fixed, the vacuum energy from the zero-point oscillation can be written down in the following form,

$$V_{\text{zero}}[\langle \bar{q}q \rangle] = -2N_c \sum_{i=u,d,s} \int \frac{d^3p}{(2\pi)^3} \varepsilon_i(p) \quad (132)$$

with  $\varepsilon_i(p) = \sqrt{p^2 + M_i^2}$ . The above momentum integration does not converge and we need to introduce a regularization for the momentum integration. The choice of the regularization is a part of the model definition, and the simplest choice would be a sharp momentum cutoff at  $p = \Lambda$ . We note that, when the gauge symmetry is concerned, a better regularization such as the proper-time regularization and the Pauli-Villars regularization would be an indispensable choice. With a sharp cutoff, we can carry out the analytical integration, which after all reads,

$$V_{\text{zero}} = -\frac{N_c \Lambda^4}{4\pi^2} \sum_{i=u,d,s} \left[ \left(1 + \frac{\xi_i^2}{2}\right) \sqrt{1 + \xi_i^2} - \frac{\xi_i^4}{2} \sinh^{-1} \xi_i \right], \quad (133)$$

where we defined a dimensionless mass parameter,  $\xi_i \equiv M_i/\Lambda$ . The vacuum energy,  $V_{\text{zero}}$ , tends to make  $\xi$  or  $M$  larger, while the condensation energy,  $V_{\text{cond}}$ , tends to make  $M$  smaller, and the energetically most favored value of the dynamical mass  $M$  is determined as a result of the competition between these two energies. The analysis would be quite easy if  $g_D = 0$  or  $N_f = 2$  (for which the KMT interaction is also a four-fermionic term) and  $m_i = 0$  (i.e. chiral limit). Under such simplification the total energy can be expanded for small  $\xi$  as

$$V_{\text{zero}} + V_{\text{cond}} \simeq -\frac{9\Lambda^4}{4\pi^2} \left[ 1 + \left(1 - \frac{\pi^2}{3g_S\Lambda^2}\right) \xi^2 \right]. \quad (134)$$

From this expression it is clear that  $\xi \neq 0$  is energetically favored for strong coupling,  $g_S\Lambda^2 > \pi^2/3$ . This is how chiral symmetry is spontaneously broken by a BCS-like mechanism in the QCD vacuum. So far, we implicitly assumed a second-order phase transition in coupling space, but once the condensation energy from the KMT interaction is taken into account, it generates a cubic term with respect to the chiral condensate as seen in Eq. (130), and the order of the phase transition must be first [110]. For more discussions on the order of the chiral phase transition and the possible QCD critical point (that are not covered by the present review), see Refs. [7, 11].

In the standard NJL model, the medium effect is implemented by the grand canonical partition function in the quasi-particle approximation, and in the PNJL model, this part is augmented with

the Polyakov loop coupling. Therefore, the finite- $T$  and the finite- $\mu$  terms acquire the Polyakov loop dependence via the following replacement;

$$\begin{aligned} V_{\text{medium}} &= -2N_c T \sum_{i=u,d,s} \int \frac{d^3 p}{(2\pi)^3} \left\{ \ln[1 + e^{-\beta(\varepsilon_i - \mu)}] + \ln[1 + e^{-\beta(\varepsilon_i + \mu)}] \right\} \\ &\rightarrow -2T \sum_{i=u,d,s} \int \frac{d^3 p}{(2\pi)^3} \text{tr} \left\{ \ln[1 + L e^{-\beta(\varepsilon_i - \mu)}] + \ln[1 + L^\dagger e^{-\beta(\varepsilon_i + \mu)}] \right\}, \end{aligned} \quad (135)$$

which is inspired from Eq. (125). We can explicitly take the color trace as in Eq. (125). In many cases the mean-field approximation is assumed, in which  $\ell$  and  $\ell^\dagger$  are replaced, respectively, with  $\Phi$  and  $\bar{\Phi}$ . Then, the medium part of the energy finally reads,

$$\begin{aligned} V_{\text{medium}}[\langle \bar{q}q \rangle, \Phi, \bar{\Phi}] &= -2T \sum_{i=u,d,s} \int \frac{d^3 p}{(2\pi)^3} \left\{ \ln[1 + 3\Phi e^{-\beta(\varepsilon_i - \mu)} + 3\bar{\Phi} e^{-2\beta(\varepsilon_i - \mu)} + e^{-3\beta(\varepsilon_i - \mu)}] \right. \\ &\quad \left. + \ln[1 + 3\bar{\Phi} e^{-\beta(\varepsilon_i + \mu)} + 3\Phi e^{-2\beta(\varepsilon_i + \mu)} + e^{-3\beta(\varepsilon_i + \mu)}] \right\}. \end{aligned} \quad (136)$$

This expression may look equivalent to Eq. (125), but we must use caution here. In the above it is assumed that the Polyakov loop fluctuations are negligible. If the logarithmic terms are expanded, there are higher order terms involving  $\ell^n$  ( $n > 1$ ), and in general,  $\langle \ell^n \rangle \neq \Phi^n$ . Once  $\Phi$  develops a substantial value in the deconfined phase,  $\langle \ell^n \rangle \simeq \Phi^n$  can hold in a good approximation, but such a treatment may badly break down when  $\Phi \simeq 0$  in the confined phase. Then, a better formulation of the mean-field approximation involving the group integration, as discussed in Sec. 3.1.3, would be much more desirable. Such sophisticated treatments of the Polyakov loop can be found in Refs. [79, 80].

To make use of the PNJL model to study quantitative estimates in the physical energy unit, we should fix the NJL model parameters;

$$m_u, \quad m_d, \quad m_s, \quad g_S, \quad g_D, \quad \Lambda \quad (137)$$

to reproduce the hadronic properties in the QCD vacuum, namely,  $m_\pi, m_\sigma, m_K, m_\eta, f_\pi$  and an empirical value of the constituent quark mass. The standard choice of parameters can be found in Refs. [107, 111]. With a favorite choice of the gluonic potential,  $V_{\text{glue}}[\Phi, \bar{\Phi}]$ , the total energy to be minimized is,

$$V_{\text{PNJL}} = V_{\text{glue}}[\Phi, \bar{\Phi}] + V_{\text{zero}}[\langle \bar{q}q \rangle] + V_{\text{cond}}[\langle \bar{q}q \rangle] + V_{\text{medium}}[\langle \bar{q}q \rangle, \Phi, \bar{\Phi}]. \quad (138)$$

In the NJL setup the sharp momentum cutoff in  $V_{\text{zero}}$  restricts the validity region up to energies below  $\Lambda$ , but this can be relaxed by replacing the cutoff with the momentum-dependent form factor. Such an extended version of the model is referred to as the non-local (P)NJL model; see Refs. [112, 113, 114, 115, 116].

In this review we would not address QCD phase diagram studies using the PNJL model, for the results cannot avoid model-dependent assumptions. Instead, we focus on rather general features of the model, especially on the relation between chiral restoration and deconfinement. (See Refs. [117, 118, 119] for analytical and lattice numerical studies on the Dirac eigenvalue distributions affected by the Polyakov loop.) We note that the medium part (136) does not require any ultraviolet regularization. We can of course define a model with a regularization imposed on the medium part too, but then the Stefan-Boltzmann limit would not be correctly satisfied. In a special case of  $\Phi = 1$  (i.e.  $L$  is a unit matrix) and  $\mu = 0$ , the above (without  $\Lambda$ ) can be expanded for small  $\xi$  as

$$V_{\text{zero}} + V_{\text{cond}} + V_{\text{medium}}[\Phi = 1] \simeq -\frac{9\Lambda^4}{4\pi^2} \left[ 1 + \left( 1 - \frac{\pi^2}{3g_S\Lambda^2} - \frac{\pi^2 T^2}{3\Lambda^2} \right) \xi^2 \right]. \quad (139)$$

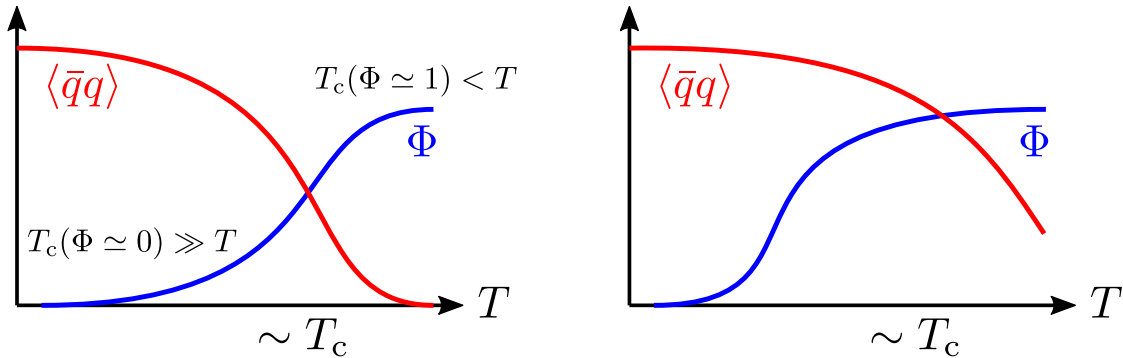


Figure 12: Schematic picture for simultaneous changes of two order parameters, i.e. the chiral condensate  $\langle \bar{q}q \rangle$  and the Polyakov loop expectation value  $\Phi$ . If  $\Phi$  arises at temperatures larger than  $T_c(\Phi \simeq 1)$ ,  $\langle \bar{q}q \rangle$  decreases simultaneously (left). It is also possible in the model that  $\langle \bar{q}q \rangle$  starts decreasing at temperatures greater than the onset of  $\Phi$  (right).

This immediately leads to the second-order phase transition temperature given by

$$T_c(\Phi = 1) = \Lambda \sqrt{\frac{3}{\pi^2} - \frac{1}{g_s \Lambda^2}}, \quad (140)$$

at which the chiral condensate goes zero. In the same way for  $\Phi = 0$ , the transition temperature is reduced as

$$T_c(\Phi = 0) = 3\sqrt{3}T_c(\Phi = 1). \quad (141)$$

Here, 3 appears from the effectively reduced temperature by factor 3 as is obvious in Eq. (125), and  $\sqrt{3}$  is from the overall coefficient of  $V_{\text{medium}}$ .

The fact that the small Polyakov loop would push the chiral phase transition toward higher temperature can give us an intuitive argument to explain how the chiral restoration occurs almost simultaneously as deconfinement. As schematically illustrated in the left panel of Fig. 12, the traced Polyakov loop  $\ell$  or its expectation value  $\Phi$  is small at low temperature, and as long as  $\Phi \simeq 0$  the critical temperature is  $3\sqrt{3}$  times larger, so that  $T$  cannot reach the critical temperature. Therefore, the chiral condensate,  $\langle \bar{q}q \rangle$ , is hardly affected by the temperature and the chiral restoration is hindered by small  $\Phi$  in this way. At high temperature, center symmetry is broken in the deconfined phase and  $\Phi \simeq 1$  is approached. Then, the critical temperature becomes the standard one without the Polyakov loop suppression, and for  $T_c(\Phi \simeq 1) < T$ , quark excitations destroy the chiral condensate and chiral symmetry can be restored. In this picture, therefore, the Polyakov loop expectation value,  $\Phi$ , is a control parameter that governs the behavior of  $\langle \bar{q}q \rangle$ . Thus, rising  $\Phi$  triggers the sizable change in  $\langle \bar{q}q \rangle$  as sketched in the left panel of Fig. 12.

Roughly speaking, one may well describe the situation as follows; in the PNJL model, chiral symmetry restoration does not occur as long as confinement, i.e.  $\Phi \simeq 0$ , holds. If  $T_\chi(m = 0)$  without the Polyakov loop effect is smaller than  $T_D(m = \infty)$ , the chiral restoration temperature is pushed up by  $\Phi$ . This is a quite robust argument to explain  $T_\chi(m) \simeq T_D(m)$  without parameter tuning. Indeed, field-theoretical and phenomenological arguments suggest that the confined phase must break chiral symmetry. If such a relation between confinement and chiral symmetry persists to finite temperature,  $\langle \bar{q}q \rangle$  cannot go to zero as long as  $\Phi$  is vanishingly small, as is exactly the situation in the PNJL model.

It is worth mentioning that there is no reason why chiral restoration *should* happen in the deconfined phase. More specifically, if  $T_\chi(m = 0)$  without the Polyakov loop effect were greater than  $T_D(m = \infty)$ , there might have been a new phase where quarks are deconfined but chiral symmetry is still spontaneously broken as shown in the right panel of Fig. 12. This is not a fictitious imagination, but one can shift the chiral restoration temperature by imposing external magnetic fields that primarily



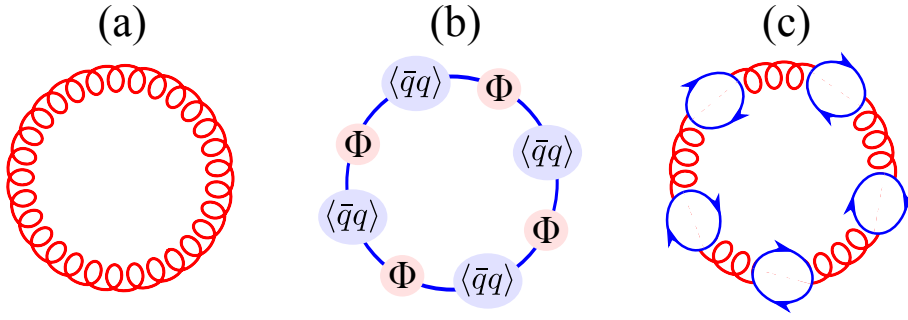


Figure 13: Diagrammatic representation for the building blocks in the PNJL model; (a) Polyakov loop potential from the gluon loop. (b) Medium part with coupling between the Polyakov loop and the chiral condensate. (c) Missing contribution from the back-reaction of the quark polarization.

couple to quarks rather than gluons. The lattice-QCD simulation under strong magnetic fields [120, 121], however, have revealed that two crossovers occur like not the right but the left panel of Fig. 12. This important lattice-QCD observation tells us that deconfinement and chiral restoration are locked together more tightly than realized in the mean-field PNJL model, presumably through the back-reaction of the quark polarization in the Polyakov loop potential. Actually, the back-reaction is always non-negligible for phenomenological applications of the PNJL model.

Here, we give a brief discussion on the back-reaction. From the diagrammatic point of view the first term in the model ingredients (138) represents gluonic loop contributions as shown in Fig. 13 (a). The second and the third terms represent quark loop contributions, and the last term of the medium effect arises from the quark propagation on top of the Polyakov loop background; see Fig. 13 (b). What is missing in a plain version of the PNJL model is the back-reaction or the polarization effects from the processes as in Fig. 13 (c). Because such screening diagrams involving quark loops are suppressed in the large- $N_c$  limit, one may say that the standard PNJL model implicitly assumes partial decoupling between the gluonic and the quark sectors in such a way similar to the large- $N_c$  limit.

Once the polarization diagrams are considered for the computation of the Polyakov loop potential, it would promote the strong coupling constant to the running one with the gluon momentum. As a result of the gluon momentum integration, a typical energy scale in the running coupling constant would be picked up, which turns into the scale characterizing  $T_0$  in the Polyakov loop potential. If there are many quark flavors, the strong coupling becomes smaller for a fixed gluon momentum. This means that the energy scale in the running coupling should be smaller to keep the strong coupling unchanged for a fixed gluon momentum. The change in the energy scale should be specified according to the QCD  $\beta$ -function, which is translated into  $T_0$ . In this way, the diagram (c) can be incorporated in part into the phenomenological Polyakov loop potential as an  $N_f$ -dependent  $T_0$ , as first argued in Ref. [122]. Using the QCD  $\beta$ -function coefficient in the leading order,  $b = (11N_c - 2N_f)/6\pi$ , the Polyakov loop potential scale is given as

$$T_0(N_f) = T_\tau e^{-1/(\alpha_0 b)}, \quad (142)$$

where  $\alpha_0 = 0.304$  is the strong coupling at the ultraviolet scale and  $T_\tau = 1.770$  GeV. This parametrization describes the pure gluonic scale  $T_0(0) = 270$  MeV that is screened down to  $T_0(N_f = 3) = 178$  MeV. This shift is very important for the PNJL and similar models to quantify physically interested temperatures on the level to compare with the lattice-QCD results.

Before closing this subsection, let us make a remark on confinement in the PNJL model. One might be tempted to identify the last term of Eq. (125) and Eq. (136) as a color-singlet excitation of baryon. This interpretation is, however, misleading. We can understand the problem by performing a variable

change, apart from the flavor sum, as

$$\int \frac{d^3p}{(2\pi)^3} f(N_c \sqrt{p^2 + m^2} - N_c \mu) = \frac{1}{N_c^3} \int \frac{d^3p'}{(2\pi)^3} f(\sqrt{p'^2 + M^2} - \mu_B), \quad (143)$$

for an arbitrary function  $f$ , where  $p' = N_c p$  is the new integration variable,  $M = N_c m$  approximates the baryon mass, and  $\mu_B = N_c \mu$  is the baryon chemical potential. The precise form of  $f$  is irrelevant in discussions below. Now, as is clear from the above variable change,  $V_{\text{medium}}[\Phi = 0]$  can be surely translated into a form of the baryonic partition function, but it is multiplied by a suppression factor  $1/N_c^3$ . So, the PNJL model cannot reproduce correct thermodynamics of baryonic degrees of freedom but significantly underestimate it. This failure of underestimating baryonic contributions by  $1/N_c^3$  is attributed to incomplete confinement in the model. For  $\Phi = 0$ , genuine confinement demands that three quarks be localized within a baryon radius, while the PNJL model only describes the situation that three quarks have zero triality (that is a discrete charge associated with center symmetry) overall and these quarks can travel far from each other. In this sense, confinement implemented in the PNJL model is sometimes called the *statistical confinement*.

The lack of local confinement is not a flaw of the model itself, but it simply results from the mean-field treatment of the Polyakov loop. If the Polyakov loop at each spatial point is treated including the spatial correlations, as is the case in the strong coupling expansion [32, 33], the model should, in principle, be capable of grasping more realistic natures of confinement, giving rise to mesons and baryons dynamically.

To extend the validity region of the PNJL model toward the hadronic phase, it would be essential to think of the problem of how to include the mesonic and the baryonic degrees of freedom. As long as we treat the Polyakov loop using  $\Phi$  and  $\bar{\Phi}$  in the mean-field approximation, the statistical confinement has nothing to do with hadrons. If we go into quark two loops, we can incorporate hadrons as collectively resonating states. Such a program to improve the PNJL model is technically involving. For the pions the higher-loop calculations have been done [123], but an extension to the baryons along the same lines as Ref. [123] would be too complicated. One might then think that the hadrons could be introduced by hand as extra degrees of freedom. However, it is a physical requirement that such composite states should dissolve at high enough temperature or at high energy scales in general. In fact, in proper calculations as in Ref. [123], the pions should disappear due to the momentum dependent self-energy or the wave-function renormalization.

#### 4.2.2 PQM model

The Polyakov-loop augmented quark-meson (PQM) model is an efficient approach to take account of the mesonic loops. This is a chiral model in which the pions  $\vec{\pi}$  and the sigma meson  $\sigma$  are introduced as point particles. Instead of four-point fermionic vertices, fermions interact via interacting meson exchanges. One may well think that such mesonic fields and original quark fields overcount physically active degrees of freedom unless finite- $T$  dissociation is somehow implemented. The PQM model is designed in a very nice way to avoid this problem.

The self-interaction of mesons in the PQM model is given by the potential that exhibits spontaneous breaking of chiral symmetry. The standard choice would be,

$$V_{\text{QM}}[\sigma, \vec{\pi}] = \frac{m_\sigma^2}{8f_\pi^2} (\sigma^2 + \vec{\pi}^2 - f_\pi^2)^2 + f_\pi m_\pi^2 \sigma, \quad (144)$$

from which  $\sigma$  acquires a non-zero expectation value  $\sim f_\pi$  and  $\vec{\pi}$ 's become light as the NG bosons. At high temperature, chiral symmetry is restored, and then the above potential is changed to a symmetric shape, with which both  $\sigma$  and  $\vec{\pi}$ 's acquire masses of order  $T$  on top of the vacuum contributions. Because

mesons become heavier than quarks in the symmetric phase at high  $T$  or high energies in general, they are effectively decoupled from the dynamics.

Such a procedure to incorporate mesons is systematically formulated in a framework of the functional renormalization group (FRG) equation [124, 125]. In the FRG language, the potential like Eq. (144) is an infrared output as a result of the RG flow, and the original input potential at the ultraviolet scale,  $\Lambda$ , should be symmetric and  $\sigma$  and  $\vec{\pi}$ 's are as massive as  $\sim \Lambda$ . This should be so, because the relevant degrees of freedom must be quarks and gluons only in the ultraviolet sector. Solving the FRG equations with QCD+mesons can establish a firm theoretical connection between the PQM model and the QCD-based calculations [126, 127].

We comment a little more on the necessity of the FRG treatment of the (P)QM model. It used to be a long standing problem how to avoid an artificial first-order phase transition in the linear sigma model beyond the mean-field approximation [128, 129]. Higher order loops may cure the problem, but momentum dependent self-energies generally have complicated analytical structures [130] and it is not realistic to tackle this problem diagrammatically. The basic equations in the FRG framework is amazingly simple particularly in the local potential approximation and with Litim's optimized cutoff [131]. These technical advances have modernized the (P)QM model.

The PQM model is a more suitable approach to study the QCD phase diagram than the PNJL model for two reasons. The first reason is that the PQM model has mesonic fluctuations and so not only the thermodynamics in the low- $T$  hadronic phase but also the critical properties around  $T_c$  can be correctly reproduced. The latter has a significant phenomenological impact especially for the size of the QCD criticality region [132, 133, 134]. Another reason is that the recent developments in the FRG application to QCD has been clarifying the mapping between the PQM model and QCD if the baryon density is low. The FRG-QCD phase diagram is found in Ref. [126]. Also see Refs. [135, 136]. for the related functional approach to the QCD phase diagram based on the Dyson-Schwinger equations<sup>3</sup>. We also make a brief comment that the inclusion of heavier hadrons and resonances may eventually allow for a dual description in which the Polyakov loop would be dictated by the hadron spectrum [139].

Now, one might wonder about the treatment of meson dissociation in the PQM model; that is, being heavy is not the same as being unstable, is it? At high temperature, as already explained,  $\sigma$  and  $\vec{\pi}$ 's are heavy enough to decouple, but physically speaking, they must be unstable and decay into quarks. These two descriptions seem to be different, but actually, they are not. If mesons are not dynamical, the kinetic term is vanishing, or the wave-function renormalization,  $Z_\phi$ , should be vanishingly small. We can understand this from the NJL model; the meson fields can be introduced as auxiliary fields through the Hubbard-Stratonovich transformation, and at this point, they are not yet dynamical and simply non-propagating fields to replace the fermionic interactions. The important point is that the wave-function renormalization and the mass are related to each other. If the kinetic term for a meson  $\phi$  behaves like  $\tilde{Z}_\phi p^2 \phi^2$  with a dimensionless  $\tilde{Z}_\phi$ , and the potential curvature  $V'' \phi^2$  is non-zero, the physical mass (after rescaling  $\phi \rightarrow \tilde{\phi} = \tilde{Z}_\phi^{1/2} \phi$ ) should be  $m^2 = V''/\tilde{Z}_\phi \rightarrow \infty$  as  $\tilde{Z}_\phi \rightarrow 0$ . Thus, the field is physically very massive if it corresponds to non-propagating mode. We can also understand the decay into quarks in the same way. If the original Yukawa coupling is  $g\bar{q}\phi q$ , the rescaling to  $\tilde{\phi}$  gives the physical Yukawa coupling that diverges as  $g/\tilde{Z}_\phi^{1/2} \rightarrow \infty$  in the limit of  $\tilde{Z}_\phi \rightarrow 0$ , so that the decay is enhanced as it should be.

To deal with composite states in general within the framework of the FRG equation, the wave-function renormalization plays an essential role, which can be explicitly seen in the argument of the so-called rebosonization procedure [140]. In principle, such an idea to treat mesons using the rebosonization procedure can be applied to diquarks and also baryons. The major problem in the inclusion of baryons in the PQM-type models is that they do not necessarily become massive at high density unlike mesons at high temperature. As a cutoff effective description for nuclear matter, as attempted in Ref. [141],

---

<sup>3</sup>As a side remark, in Dyson-Schwinger approach there is a way to extract the Polyakov loop, see Refs. [137, 138].

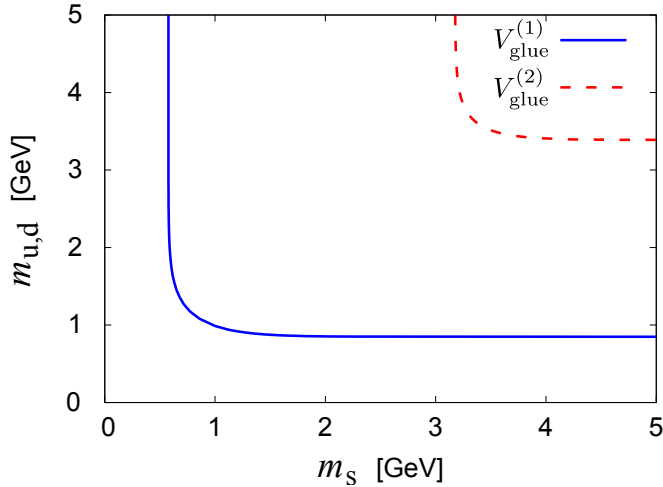


Figure 14: The upper right corner of the Columbia plot. The lines correspond to the second order phase transition.  $V_{\text{glue}}^{(1)}$  denotes the model defined by Eq. (65) and  $V_{\text{glue}}^{(2)}$  by Eq. (68).

the FRG approach is still useful, but to establish a connection to QCD in the high-density region, the baryonic counterpart of the rebosonization (which might be called the rebaryonization) must be addressed. Such a program is still under investigations.

### 4.2.3 Critical point with heavy quarks

So far, we have seen the coupling between the Polyakov loop and the dynamical quarks in the light-flavor sector, to discuss how chiral restoration is affected by the Polyakov loop dynamics. Now, let us turn to the heavy-flavor sector and consider how the Polyakov loop dynamics is influenced perturbatively by massive quarks.

For a pure gluonic theory with  $N_c = 3$  and no dynamical quarks, the deconfinement phase transition is of first order. By adding (heavy) dynamical quarks we can control the  $Z(3)$  symmetry breaking and weaken the transition; in this respect quarks act as a background  $Z(3)$  breaking field. As the quark mass decreases, the first-order phase transition turns into a crossover; hence there is a critical value of the quark mass where the first-order boundary terminates at a deconfining critical point of the second order phase transition.

The location of this critical point is a sensitive probe of the Polyakov loop potential; it reveals the properties of the pure gluonic Polyakov loop potential beyond the expectation value or the curvature computed at the expectation value.

The deconfining critical point is located at rather heavy quark masses, where we can use the Boltzmann approximation for the quark thermodynamic potential. Hence we have to go back to the quark contribution to the effective potential, Eq. (125), and proceed with expansion of each logarithm into a power series (at zero chemical potential), i.e.

$$\text{tr} \ln(1 + L e^{-\beta \epsilon_p}) = \text{tr} L e^{-\beta \epsilon_p} - \frac{1}{2} \text{tr}(L^2) e^{-2\beta \epsilon_p} + \mathcal{O}(e^{-3\beta \epsilon_p}), \quad (145)$$

where the higher order terms are suppressed exponentially. We will keep only the first term in the expansion, which corresponds to the Boltzmann approximation or the leading order in the hopping parameter expansion. The momentum integration can be performed analytically to yield,

$$V_{\text{quark}}[q] \approx - \sum_i \frac{m_i^2 T V}{\pi^2} K_2\left(\frac{m_i}{T}\right) (\text{tr} L + \text{tr} L^\dagger), \quad (146)$$

where  $i$  makes the summation with respect to the flavors. The advantage of having masses as parameters is that by varying the quark masses, one can tilt the Polyakov loop potential and probe it at different values of the order parameter. Thus it is not surprising that, as was demonstrated in Ref. [142], the critical values of the mass differs significantly in the models described by Eq. (65) and Eq. (68). The calculations at  $N_f = 3$  shows that, for the former, the critical mass is 3.5 GeV; for the latter, it is about 1 GeV. A model of Ref. [143] constrained by the Polyakov loop susceptibilities produced yet another value of the critical mass, i.e. 1.48 GeV.

We demonstrate this striking difference by plotting the most upper right corner (that is the region where all quark masses are heavy) of the Columbia plot in Fig. 14. The lines represent the locations of the second-order deconfinement phase transition, which is found by setting first three derivatives of the effective potential with respect to the Polyakov loop to zero. See also Ref. [144] for other approaches to the Columbia plot with a different type of confining potential.

The lattice studies for the critical point of the deconfinement phase transition are available for different number of heavy flavors; see e.g. Ref. [145] and references therein. They, however, were not extrapolated to the continuum; this hinders a direct comparison with the model predictions at present.

### 4.3 Systems at Finite Baryon Density

Once the chemical potential is turned on, the most interested and yet unsolved problem in QCD is the QCD phase diagram. There are many theoretical attempts to explore the QCD phase diagram at finite  $T$  and  $\mu$  using the PNJL and the PQM models. Because baryonic degrees of freedom are underestimated as seen in Eq. (143), it is still a challenging problem to reveal the correct structures of the dense QCD vacuum even on the qualitative level. Also, the system has valence quarks for  $\mu \neq 0$ , and so center symmetry is more broken by those quarks. Therefore, the Polyakov loop would lose its meaning as an approximate order parameter for deconfinement. Nevertheless, the Polyakov loop is a theoretically interesting quantity for the finite-density systems, especially for the analysis of the sign problem in some algebraic approaches.

#### 4.3.1 Sign problem

We start from a short reminder of the sign problem in QCD. At finite baryon or quark density the Dirac operator (apart from the mass term) is no longer anti-Hermitian, and thus the Dirac determinant may have a complex phase. This can be seen from the fact that the Dirac determinant at finite chemical potential is written as

$$\mathcal{M}[A; \mu] = \det(i\mathcal{D} - i\gamma_4\mu - m) . \quad (147)$$

We should recall that in our convention Euclidean  $\gamma_\mu$ 's are chosen as anti-Hermitian matrices. So,  $i\mathcal{D}$  is an anti-Hermitian operator having pure imaginary eigenvalues;  $\pm i\lambda$ . It is then clear that  $-i\gamma_4\mu$  is Hermitian and eigenvalues of such a mixed operator,  $i\mathcal{D} - i\gamma_4\mu$ , are neither pure imaginary nor real.

We can then separate the real part and the imaginary part of the Dirac determinant as

$$\mathcal{M}[A; \mu] = \text{Re}\mathcal{M}[A; \mu] + i\text{Im}\mathcal{M}[A; \mu] , \quad (148)$$

and then we can prove that, under the charge parity transformation;  $A_\mu \rightarrow A_\mu^C = -A_\mu$ , the real part and the imaginary part, respectively, change as

$$\text{Re}\mathcal{M}[A^C; \mu] = \text{Re}\mathcal{M}[A; \mu] , \quad \text{Im}\mathcal{M}[A^C; \mu] = -\text{Im}\mathcal{M}[A; \mu] . \quad (149)$$

We can understand this from the property of  $\mathcal{M}^*[A; \mu] = \det C^{-1}(i\mathcal{D} - i\gamma_4\mu - m)^*C = \mathcal{M}[A^C; \mu]$ , where under the charge parity transformation,  $C^{-1}\gamma_\mu^*C \rightarrow -\gamma_\mu$ . In the functional integration with respect to  $A_\mu$ , any contribution from a certain  $A_\mu$  has a paired contribution from  $A_\mu^C$ , and so after taking the

functional integration over whole  $A_\mu$ , the  $C$ -odd part is averaged away. Therefore, the partition function is,

$$Z = \int \mathcal{D}A_\mu \operatorname{Re}\mathcal{M}[A; \mu] e^{-S_{\text{YM}}[A]}, \quad (150)$$

apart from the gauge fixing. In the same way for a  $C$ -even (real-valued) observable,  $\mathcal{O}_+[A]$ , the expectation value is,

$$\langle \mathcal{O}_+[A] \rangle = \frac{1}{Z} \int \mathcal{D}A_\mu \mathcal{O}_+[A] \operatorname{Re}\mathcal{M}[A; \mu] e^{-S_{\text{YM}}[A]}, \quad (151)$$

and for a  $C$ -odd real-valued observable,  $\mathcal{O}_-[A]$ , the expectation value is,

$$\langle \mathcal{O}_-[A] \rangle = \frac{i}{Z} \int \mathcal{D}A_\mu \mathcal{O}_-[A] \operatorname{Im}\mathcal{M}[A; \mu] e^{-S_{\text{YM}}[A]}. \quad (152)$$

From these arguments we see that the integrand in the functional integrals is always a real-valued function, and what does really matter is the sign changes of  $\operatorname{Re}\mathcal{M}[A; \mu]$  and  $\operatorname{Im}\mathcal{M}[A; \mu]$  at finite  $\mu$ . This is why we commonly refer to this difficulty as the ‘‘sign problem’’, not the complex problem of the Dirac determinant.

It is interesting how the sign problem looks like concretely in the PNJL model. As we already mentioned near Eq. (125), the quark contribution,  $V_{\text{quark}}[q]$ , is complex for  $\mu \neq 0$  if  $\ell$  is complex. In the mean-field approximation,  $\ell$  and  $\ell^*$  are replaced with real-valued expectation values, which are calculated from

$$\langle \operatorname{Re}\ell \pm i\operatorname{Im}\ell \rangle = \frac{1}{Z} \int \mathcal{D}A_\mu (\operatorname{Re}\ell \operatorname{Re}\mathcal{M} \mp \operatorname{Im}\ell \operatorname{Im}\mathcal{M}) e^{-S_{\text{YM}}}. \quad (153)$$

If the Dirac determinant or the quark potential is expanded as in Eq. (146),  $\operatorname{Im}\mathcal{M}$  is proportional to  $\operatorname{Im}\ell$ , and so [146],

$$\bar{\Phi} - \Phi = -2i\langle \operatorname{Im}\ell \rangle \propto \langle (\operatorname{Im}\ell)^2 \rangle_{\text{YM}}. \quad (154)$$

For  $\mu > 0$ , we see  $\bar{\Phi} > \Phi$ , and we can immediately give a physical explanation for this. Since  $\Phi$  is related to an energy excess  $f_q$  induced by a test static quark,  $\bar{\Phi} > \Phi$  means that a test anti-quark costs less energy than a test quark. In other words, we can place an anti-quark more easily than a quark into the finite-density medium, which should be naturally so due to screening effects; see Ref. [147] for lattice-QCD results and physical discussions.

Now, one might think that, once the mean-field approximation is adopted for the Polyakov loop, one may no longer monitor the sign problem. There is no apparent sign problem indeed, but the Polyakov loop potential has only the saddle points then, which should be regarded as a remnant of the sign problem. The saddle point structure was considered in details in Ref. [83]. For the purpose to see the problem, the simplest lowest order would be sufficient. The Polyakov loop potential (65) can be approximated in the confined phase as

$$T^{-4}V_{\text{glue}}(\Phi, \bar{\Phi}) \approx -\frac{b_2}{2}\bar{\Phi}\Phi = -\frac{b_2}{16}[(\bar{\Phi} + \Phi)^2 - (\bar{\Phi} - \Phi)^2]. \quad (155)$$

If we naively take the  $\Phi$  derivative and the  $\bar{\Phi}$  derivative of  $V_{\text{glue}}(\Phi, \bar{\Phi})$ , we have  $\Phi = \bar{\Phi} = 0$  as is reasonable in the confined phase ( $b_2 > 0$ ). However, clearly, the above potential is unstable along the direction of  $\bar{\Phi} - \Phi$ , and  $\Phi = \bar{\Phi}$  is not a potential minimum but a saddle point. Surprisingly, this problem occurs not only at finite density but already at zero density, as soon as we allow for a possibility of  $\bar{\Phi} \neq \Phi$  (which is allowed only at finite density, so the sign problem matters only at finite density anyway). In Ref. [83] it was conjectured that the saddle-point approximation should work, though it cannot be justified from the thermodynamic principles. Recently, the mathematical justification for the saddle-point prescription has been proposed with help of the Lefschetz thimble method [148]. As a final remark it is worth mentioning that the Polyakov loop potential in terms of  $q_i$  (such as the inverted Weiss potential) has no such problem of the saddle-point prescription, but as we already confirmed in Fig. 3, the ground state lies in the global minimum of the potential.



### 4.3.2 Heavy-dense model

Here, let us introduce a very useful model to consider the sign problem. We have seen that the hopping parameter expansion picks up a Polyakov loop in Sec. 4.2.3. There is an interesting limit in which such an expanded form becomes exact while keeping a non-trivial phase structure. A naïve heavy mass limit would justify the expansion, but the coefficient would be too small to cause anything interesting. To compensate such smallness of the coefficient, we can take the high density limit simultaneously. That is, the Dirac determinant (on the lattice) simplifies as

$$\det[i\mathcal{D} - i\gamma_4\mu - m] \rightarrow [\det(1 + \epsilon L)]^{N_f/4}, \quad (156)$$

where the flavor counting is complicated due to the doubler problem. To avoid unnecessary complication, let us limit our considerations below to the simplest case of  $N_f = 4$ . We should take two limits of  $m \rightarrow \infty$  and  $\mu \rightarrow \infty$  so as to keep their combination [149],

$$\epsilon \equiv \left( \frac{e^{\mu a}}{2ma} \right)^{N_\tau}, \quad (157)$$

to be finite. We can intuitively understand the above statement in the following way; in the heavy limit quarks cannot move and the static quark and anti-quark propagation at spatial point  $\mathbf{x}$  is written in terms of  $L(\mathbf{x})$  and  $L^\dagger(\mathbf{x})$ , from which the anti-quark part by  $L^\dagger(\mathbf{x})$  is negligible in the dense limit. Thus, the Dirac determinant should be a function of  $L(\mathbf{x})$  only.

Interestingly, such a simple expression of  $\det(1 + \epsilon L)$  captures the important features of the sign problem. For the color SU(2) case we immediately see that the Dirac determinant is always real. That is, in this case of the color SU(2) group, we can explicitly take the determinant as

$$\det(1 + \epsilon L) = \prod_{\mathbf{x}} [1 + \epsilon^2 + 2\epsilon\ell(\mathbf{x})] \quad [\text{for SU(2)}], \quad (158)$$

which is real because  $\ell(\mathbf{x})$  is real for the SU(2) case. We note that the above determinant is positive definite and this is because we implicitly assumed  $N_f = 4$ .

In contrast to the SU(2) case, the sign problem becomes manifested for the color SU(3) group. The explicit calculation leads to

$$\det(1 + \epsilon L) = \prod_{\mathbf{x}} [1 + \epsilon^3 + 3\epsilon\ell(\mathbf{x}) + 3\epsilon^2\ell^*(\mathbf{x})] \quad [\text{for SU(3)}]. \quad (159)$$

Clearly, except for special values of  $\epsilon = 0$  (i.e. zero density) and  $\epsilon = 1$  (i.e. half-filling), the Dirac determinant generally has a complex phase. We note that the determinant is real for  $\epsilon = 1$  but it can be negative for  $-1 < \ell + \ell^* < -2/3$ . Because this heavy-dense model setup has a duality, i.e. invariance under the transformation,  $\epsilon \leftrightarrow 1/\epsilon$  and  $\ell \leftrightarrow \ell^*$ , the high density region is described as a dilute anti-quark (or diquark with anti-triplet color) medium, which is due to the lattice artifact of saturation.

One can treat the pure gluonic part as it is and simply model it using the matrix model (30), or one can completely drop it assuming the strong coupling limit. There are many applications of the heavy-dense model; for the mean-field study on the sign problem, see Ref. [83]. For the strong-coupling expansion including the heavy-dense model discussions as a special example, see Ref. [150]. For the test of the complex Langevin simulation using the heavy-dense model, see Refs. [151, 152].

### 4.3.3 Roberge-Weiss phase transition with imaginary chemical potential

There is no sign problem for the imaginary chemical potential, which is obvious from Eq. (125);  $\ell e^{\beta\mu}$  and  $\ell^* e^{-\beta\mu}$  are complex conjugate to each other because  $(\mu)^* = -\mu$  then, and so the quark contribution to

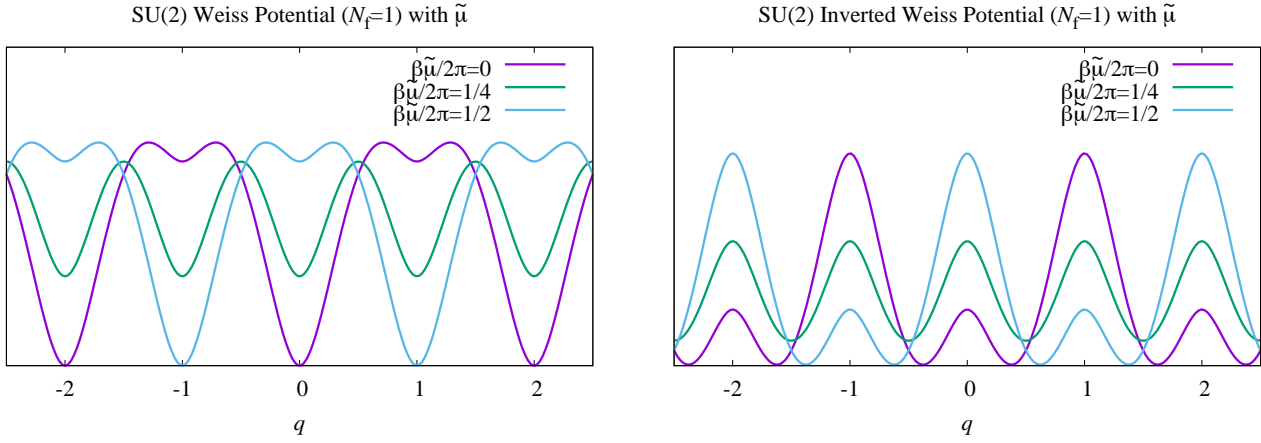


Figure 15: SU(2) Polyakov loop potential with imaginary chemical potential  $\tilde{\mu}$  for the perturbative Weiss potential (left) and the inverted Weiss potential (right).

the potential is real. Although considering the imaginary chemical potential may sound rather academic, the ground state properties at finite imaginary chemical potential have quite intriguing aspects.

We can regard the Polyakov loop as a colored imaginary chemical potential, as we mentioned previously, and so the imaginary chemical potential for the baryon or quark U(1) symmetry is mixed together with a center element of the Polyakov loop. The dependence on the imaginary chemical potential  $\tilde{\mu}$  (where  $\mu = i\tilde{\mu}$ ) appears only through a combination of  $\ell e^{i\beta\tilde{\mu}}$ . The quark effective potential is thus a function of  $\ell e^{i\beta\tilde{\mu}}$  and  $\ell^* e^{-i\beta\tilde{\mu}}$ . We know that the gluonic potential,  $V_{\text{glue}}[\ell, \ell^*]$ , is center symmetric, and there are  $N_c$  degenerate minima. Hence, under the center transformation, the effective potential changes as

$$\begin{aligned} V_{\text{glue}}[\ell, \ell^*] + V_{\text{quark}}[\ell e^{i\beta\tilde{\mu}}, \ell^* e^{-i\beta\tilde{\mu}}] &\rightarrow V_{\text{glue}}[\ell, \ell^*] + V_{\text{quark}}[e^{i2\pi k/N_c} \ell e^{i\beta\tilde{\mu}}, e^{-i2\pi k/N_c} \ell^* e^{-i\beta\tilde{\mu}}] \\ &= V_{\text{glue}}[\ell, \ell^*] + V_{\text{quark}}[\ell e^{i\beta(\tilde{\mu}+2\pi kT/N_c)}, \ell^* e^{-i\beta(\tilde{\mu}+2\pi kT/N_c)}]. \end{aligned} \quad (160)$$

This in turn means that such a shift in the imaginary chemical potential by a multiple of  $2\pi T/N_c$  is absorbed by a  $Z(N_c)$  transformation on the Polyakov loop. At low  $T$ , center symmetry approximately remains and the Polyakov loop distribution is centered around  $\ell = 0$ , which implies that such a  $Z(N_c)$  rotation is possible without any energy barrier. At high  $T$ , on the other hand, center symmetry is largely broken and the Polyakov loop distribution is centered around  $\text{Re} \ell \gg \text{Im} \ell \simeq 0$ . There, we would anticipate an energy barrier associated with the  $Z(N_c)$  rotation. As a matter of fact, such a structure is evident in the perturbative potential (123); by replacing  $\mu$  by  $i\tilde{\mu}$ , we find the quark contribution to the Weiss potential to be a function of  $(q_i + 1/2 + \beta\tilde{\mu}/2\pi)_{\text{mod}1}$ .

In the deconfined phase the SU(2) perturbative Weiss potential is modified by non-zero  $\tilde{\mu}$  as shown in the left of Fig. 15. With increasing  $\tilde{\mu}$  the perturbative vacuum at  $q = 0$  is pushed up, while the center transformed point at  $q = 1$  is pushed down. Eventually, two minima become degenerated at  $\beta\tilde{\mu}/(2\pi) = 1/4$ , and then the absolute minimum jumps from  $q = 0$  to  $q = 1$ , which signifies a first-order phase transition at  $\tilde{\mu} = \pi T/2$ . This first-order phase transition at  $\tilde{\mu} = \pi T/N_c$  for general  $N_c$  is called the Roberge-Weiss phase transition [153]. In the confined phase, in contrast, there is no such first-order phase transition owing to unbroken center symmetry. To see it expressly, we model confinement using the inverted Weiss potential multiplied by  $-1.4$ . Then, as shown in the right of Fig. 15, the absolute minimum continuously moves but no jump occurs in this case. Here we point out an interesting observation. The confined phase corresponds to  $q = 1/2$  (to make  $\Phi = 0$ ) if center symmetry is exact, but the potential minimum generally differs from  $q = 1/2$  due to explicit breaking

of center symmetry in the presence of dynamical quarks. Actually, at  $\tilde{\mu} = 0$ , the potential minimum is located at  $q \simeq 0.377$  leading to  $\Phi \simeq 0.377$ . We can see, however, that the potential minimum goes to  $q = 1/2$  exactly for  $\beta\tilde{\mu}/(2\pi) = 1/4$ , which means that center symmetry is unbroken for this special value of  $\tilde{\mu}$ . We note that with this special value of  $\tilde{\mu}$  the quark distribution function looks like a bosonic one.

It is possible to investigate the phase diagram at finite  $\tilde{\mu}$  using the PNJL model. The location of the Roberge-Weiss point is robust regardless of the model choice, but it would be model dependent at which temperature the Roberge-Weiss phase boundary of first order ends and at which temperature the crossovers of deconfinement and chiral restoration occur for general  $\tilde{\mu}$  away from the Roberge-Weiss point. For (non-local) PNJL analyses, see Refs. [114, 115, 154, 155, 156, 157] for concrete evaluations.

Here, let us point out a suggestive similarity between an imaginary chemical potential and the strong  $\theta$  angle in the light quark sector. We must be careful that the  $\theta$  angle dependence in the pure gluonic sector shows resembling behavior to the light quark sector, but the underlying physics is different [158] (and nevertheless, the light and the heavy sectors could be continuously linked; see Ref. [159]). If the theory has massless fermion, the  $\theta$  dependence is gauged away with help of the  $U(1)_A$  anomaly. For massive quarks, the  $\theta$  angle dependence is sensitive to whether chiral symmetry is broken or not. If chiral symmetry is broken, the phase of the chiral condensate changes with  $\theta$ , and then a first-order phase transition occurs at  $\theta = \pi$  [160]. It should be noted that, after an appropriate  $U(1)_A$  rotation, the  $\theta$  dependence appears only in the quark mass term as  $\bar{q} m e^{-i\theta\gamma_5} q$ , which favors the chiral condensate  $\langle \bar{q}q \rangle$  in a  $\theta$ -tilted direction. One may say that, in analogy to the Roberge-Weiss phase transition, the relationship between center symmetry and the Polyakov loop at finite  $\tilde{\mu}$  is comparable to the relationship between chiral symmetry and the chiral condensate at finite  $\theta$ . For further phase diagram research with finite  $\theta$ , interested readers can see Refs. [161, 162] for the NJL model studies, Refs. [163, 164] for the PNJL model studies, and Refs. [165, 166] for the lattice simulation. Finally we make a note that, even though there are apparent similarities between  $\tilde{\mu}$  and  $\theta$  in the phase structures, the theory at finite  $\tilde{\mu}$  is free from the sign problem, while a finite  $\theta$  term is always a complex phase suffering from the sign problem.

## 4.4 Deformed QCD with Center Symmetry

We have understood that center symmetry is spontaneously broken in the deconfined phase. From this fact, it has been speculated that non-perturbation information on confinement and chiral symmetry breaking could be extracted even *perturbatively* by enforcing center symmetry on QCD. We will introduce several ideas here, and finally we will pay our special attention to deformed QCD in  $R^3 \times S^1$  as a rigorous and successful framework.

### 4.4.1 Canonical ensemble

The first example of deformation that makes QCD preserve center symmetry is the canonical ensemble. There have been controversial arguments about the physical interpretation of the center symmetry breaking at high temperature (see Ref. [9] for critical discussions against regarding the Polyakov loop as a physical quantity; see also Ref. [167] for a related work using solvable models). For field-theoretical objects responsible for the triality screening, see Ref. [168].

Interestingly, it is possible to reformulate hot QCD in such a way that center symmetry is forced to be exact. To understand the point in the easiest manner, let us take a concrete expression of the

symmetry breaking term as Eq. (146) or,  $-h(\ell + \ell^*)$ , simply. Then, the partition function is,

$$\begin{aligned}
Z_{\text{QCD}} &\sim \int \mathcal{D}A_\mu e^{-S_{\text{glue}}[A] - h \int d^3x (\ell + \ell^*)} \\
&= \int \mathcal{D}A_\mu e^{-S_{\text{glue}}[A]} \frac{1}{N_c} \left( e^{-h \int d^3x (\ell + \ell^*)} + e^{-h \int d^3x (\ell + \ell^*)} + \dots \right) \\
&= \int \mathcal{D}A_\mu e^{-S_{\text{glue}}[A]} \frac{1}{N_c} \sum_{k=0}^{N_c-1} e^{-h \int d^3x (z_k \ell + z_k^* \ell^*)} .
\end{aligned} \tag{161}$$

Here, from the second to the third line, we used that the integration measure is center invariant. This superposition of seemingly different but equivalent  $N_c$  integrals is nothing but a projection operator to the zero  $N_c$ -ality (that is a charge associated with  $Z(N_c)$  center group) sector. In other words, the last line of Eq. (161) represents the QCD partition function in the canonical ensemble with respect to the  $N_c$ -ality charge.

This is a surprisingly simple idea and was originally proposed to circumvent the absence of the strict confinement order parameter (see Refs. [100, 169] and references therein). Thanks to the apparently restored center symmetry in the partition function, the naïve expectation was that the Polyakov loop should be no longer an approximate but an exact order parameter. The above way to restore chiral symmetry is somehow an approach opposite to restricting the functional integration to one fundamental modular domain [170, 171, 172], which was also proposed to account for confinement.

Let us explain the idea a bit more using the physics language. In principle, the Dirac determinant can be expanded in terms of gauge invariant gluonic operators, namely, the Wilson loops. The most important trajectories of the Wilson loops in our consideration at finite  $T$  are the ones wrapping around the temporal direction (which is nothing but the Polyakov loop if the trajectory is straight along the temporal axis), which counts the excited quark number in the thermal bath [88]. If the trajectory has one winding, its operator would change non-trivially under the center transformation, but such an expectation value should be just vanishing after the functional integration of entire gluonic configurations. That is, in the example of Eq. (161), if the symmetry breaking term is expanded, the first order term is,

$$\int \mathcal{D}A_\mu e^{-S_{\text{glue}}[A]} (-h) \int d^3x \ell(x) = 0 , \tag{162}$$

from Elitzur's theorem [173], while the second order term contains,

$$\int \mathcal{D}A_\mu e^{-S_{\text{glue}}[A]} \frac{(-h)^2}{2!} \int d^3x d^3y \ell(x) \ell^*(y) \neq 0 , \tag{163}$$

which physically represents a pair of quark at  $x$  and anti-quark at  $y$ . One might want to associate this type of pair excitation with mesons, but just like the statistical confinement in the PNJL model,  $x$  and  $y$  can be independently separated. Also, the  $N_c$ -th order term has a baryonic combination, i.e.

$$\int \mathcal{D}A_\mu e^{-S_{\text{glue}}[A]} \frac{(-h)^{N_c}}{N_c!} \int d^3x_1 \dots d^3x_{N_c} \ell(x_1) \dots \ell(x_{N_c}) \neq 0 , \tag{164}$$

but again,  $N_c$  quarks may be distributed non-locally. We should stress that, even without rewriting the partition function as in Eq. (161), center symmetry seems to be unbroken superficially, and Eq. (161) is simply a way to make it clear.

This argument about unbroken center symmetry is mathematically correct as long as the volume is finite. We should note that the canonical ensemble could be then not equivalent to the grand canonical ensemble, and in this sense, nothing is surprising about such unbroken center symmetry in the canonical ensemble if the volume is finite. The question is the infinite volume limit or the thermodynamic limit, in

which the canonical ensemble should become equivalent to the grand canonical ensemble. This happens in a very singular way, and actually the center symmetric vacuum in the canonical ensemble turned out to be thermodynamically unstable in the large volume limit, as first pointed out in Ref. [174]. Roughly speaking, the instability occurs due to abnormally long-ranged interactions as seen in Eq. (161). If the final form in Eq. (161) is exponentiated, the interaction looks like,

$$S_{\text{int}} = -\ln \left[ \frac{1}{N_c} \sum_{k=0}^{N_c-1} e^{-h \int d^3x (z_k \ell + z_k^* \ell^*)} \right], \quad (165)$$

for which the volume is not simply factored out. Then, in the infinite volume limit, center symmetry in the canonical ensemble is always *spontaneously* broken down into the explicitly broken state in the grand canonical ensemble. Therefore, unfortunately, the canonical ensemble approach to restore center symmetry does not work as naively expected. Moreover, one can learn an important lesson; when the finite-density phase transition is investigated in a small-size canonical ensemble as discussed in Refs. [175, 176], it is difficult to make a reliable conclusion until the thermodynamic limit is taken.

#### 4.4.2 Center twisted flavors

We can avoid the instability of the canonical ensemble once we change the interaction so that the volume factor is correctly factored out. The simplest remedy is to replace the projection sum in Eq. (161) with the projection product [177, 178, 179]. Then, the theory is no longer QCD and the partition function in this ‘‘QCD-like theory’’ reads,

$$Z_{\text{QCD-like}} \sim \int \mathcal{D}A_\mu e^{-S_{\text{glue}}[A]} \prod_{k=0}^{N_c-1} e^{-h \int d^3x (z_k \ell + z_k^* \ell^*)}. \quad (166)$$

In the leading order of the expansion, the above is just a trivial example and the matter parts are averaged away. It should be obvious how this idea can be generalized to unexpanded form of the Dirac operator once we realize that multiplying  $z_k$  on  $\ell$  is equivalent to adding an imaginary chemical potential by  $i2\pi T k/N_c$ . That is, this center symmetric QCD-like theory may be defined as

$$Z_{\text{QCD-like}} = \int \mathcal{D}A_\mu e^{-S_{\text{glue}}[A]} \prod_{k=0}^{N_c-1} \det \mathcal{M}[A; \mu + i2\pi T k/N_c]. \quad (167)$$

Such a deformed QCD as defined above has interesting properties. Because  $N_c$  quarks as a combination do not break center symmetry explicitly, the first-order deconfinement phase transition in the pure gluonic sector survives with a shifted critical point to a lower temperature, just like in QCD-like theories with adjoint fermions. What is quite non-trivial is that chiral symmetry breaking persists at temperatures far above deconfinement (as shown in the right panel of Fig. 12), which is because single quark excitations are projected out as seen in Eq. (166). Moreover, flavor-dependent imaginary chemical potential explicitly breaks chiral symmetry as  $SU(N_c)_L \times SU(N_c)_R \rightarrow U(1)_V^{N_c-1} \times U(1)_A^{N_c-1}$ . Although the introduced deformation changes the theory from QCD, this center symmetric formulation has been attracting interest in connection to the instanton-dyon model of confinement [180], especially to understand the interplay between confinement and chiral symmetry breaking.

#### 4.4.3 Center-stabilized QCD

A more sophisticated idea to impose center symmetry on QCD was proposed in Ref. [181] for the pure gluonic sector on  $R^3 \times S^1$  in the large- $N_c$  limit, and later extended to address continuous chiral symmetry including the matter sector [182] (see Ref. [183, 184] for earlier exact results at large  $N_c$  using

orientifold field theories, and also Ref. [185] for related discussions near the transition temperature). In the original argument in Ref. [181], a toroidal compactification is also discussed, but here, for simplicity, we look over the one dimensional case only and change the notation of the compactification size from  $L$  to  $\beta = 1/T$ . The point of the whole idea is that the perturbation theory inevitably breaks center symmetry as we already saw in Sec. 2.4, but we can deform the pure gluonic theory by adding terms that prevent the theory from breaking center symmetry spontaneously even in the perturbative regime.

For the deformation to stabilize center symmetry, quadratic interactions such as  $|\ell|^2$  and more generally  $|\text{tr}(L^n)|^2$  are added. Then, for high temperature, the perturbation theory should work due to small running coupling, but center symmetry is still unbroken. The key observation in such center-stabilized QCD is that, as long as there is no center symmetry breaking, such deformed QCD at any temperature is smoothly connected to the pure gluonic theory at zero temperature in the large- $N_c$  limit. This opens a possibility that confinement can be perturbatively investigated if the temperature is large enough, i.e.  $T \gg N_c \Lambda_{\text{QCD}}$ .

One can intuitively understand the essence of the correspondences from the following arguments. We know that in the ordinary pure gluonic theory the large- $N_c$  limit makes the low- $T$  and the high- $T$  phases clearly distinct. Below the deconfinement transition temperature, all physical quantities are insensitive to the temperature because the glueball excitations are  $1/N_c^2$  suppressed as compared to the gluon excitations that are prohibited by center symmetry. In the center-stabilized QCD, there is no phase transition, and so the temperature dependence is always suppressed for any temperature. Thus, with imposed center symmetry, the high- $T$  state is equivalent to the low- $T$  state and the latter is naturally connected to the pure gluonic theory only with smooth deformation.

In this way, in Ref. [181], the mass gap and the string tension have been parametrically estimated. For the description of finite mass gap of gauge bosons, the vacuum state is first identified from the condition to minimize the perturbatively obtained energy, which favors a special form of the Polyakov loop matrix as  $L = \text{diag}(1, z_1, z_2, \dots, z_{N_c-1})$  where  $\text{tr}L = 0$  is indeed satisfied. It should be noted that, if each eigenvalue of  $L$  is associated with different quark flavor, a deformed QCD-like theory in Sec. 4.4.2 emerges. This background configuration spontaneously breaks the gauge symmetry from  $\text{SU}(N_c)$  down to  $\text{U}(1)^{N_c-1}$ , i.e. Abelianized, giving a mass gap  $\sim T$  for off-diagonal gauge bosons. Then, including non-perturbative contributions to the diagonal “photons”, the mass gap is found to be  $\sim \Lambda_{\text{QCD}}(N_c \Lambda_{\text{QCD}}/T)^{5/6} |\ln N_c \Lambda_{\text{QCD}}/T|^{9/11}$ . Also, the string tension turns out to be  $\sim \Lambda_{\text{QCD}}^2 (N_c \Lambda_{\text{QCD}}/T)^{-1/6} |\ln N_c \Lambda_{\text{QCD}}/T|^{-3/11}$ . As long as the flavor number is  $\mathcal{O}(1) \ll N_c$ , the above mentioned argument holds with quarks in the fundamental representation included. Then, because chiral symmetry is not broken perturbatively, the deformed QCD at high enough temperature  $\gg N_c \Lambda_{\text{QCD}}$  should accommodate a state with confinement but no chiral symmetry breaking, which suggests a conjecture to relate spontaneous breaking of chiral symmetry to not Abelian but non-Abelian confinement whose critical temperature is of order of  $\sim N_c \Lambda_{\text{QCD}}$  [182].

We shall make a comment on related developments on  $R^3 \times S^1$ . In Ref. [186] a twisted partition function for the gluonic theory with one adjoint Weyl fermion (whose mass is  $m$ ) was considered on  $R^3 \times S^1$ . In the  $m = 0$  limit perturbative confinement realizes, while the ordinary pure gluonic theory is recovered in the  $m \rightarrow \infty$  limit. It is claimed in Ref. [186] that the confinement-deconfinement transition is continuous as  $m$  changes, which means that non-perturbative confinement may be investigated perturbatively with  $m$  as an interpolating variable. An interpretation in terms of monopoles was also given, and then the chiral condensate was calculated analytically in Ref. [187], which shows an interesting connection to the idea of center twisted flavors as we saw in the previous subsection.



## 5 Phenomenological Implications

In this section we will make a brief overview of two selected topics on phenomenological applications of the Polyakov loop physics. There are many relevant topics especially in the context of heavy-ion collisions, but we specifically choose the following: One is the fluctuation measurement which is expected to have good sensitivity to probe a phase transition. The other is an effective description of the so-called strongly-correlated QGP (sQGP) by means of the Polyakov loop, or an alternative of sQGP, which is known as the semi-QGP regime. For other phenomenological applications such as the chiral fluid dynamics [188], the domain-wall dynamics [43], and so on, readers can consult recent proceedings volumes of Quark Matter conference series [189, 190].

### 5.1 Higher Cumulants and Polyakov Loop Fluctuations

The idea is close to the one discussed in Sec. 4.2.3, and the Polyakov loop potential could be probed from the light quark sector. In Sec. 4.2.1, we discussed two limits  $\Phi \rightarrow 1$  and  $\Phi \rightarrow 0$ . In the former limit, we demonstrated that the quark thermodynamics is dominated by free quarks. In the latter limit, we showed that quark and diquark-type excitations are suppressed and only color-singlet combinations of three quarks survive. This radical change in the effective degrees of freedom impacts many observables measurable in the heavy-ion collisions. In particular, the cumulants of the net-baryon number can be very sensitive probes of this change. It is probably worth mentioning that the very first successful example of the PNJL model calculations is the quantitative agreement of the quark number susceptibility with the lattice result [59].

From the mathematical point of view, the thermodynamic pressure is a cumulant generating functional for the net-baryon number fluctuations. Thus, we find the cumulants by differentiating the pressure with respect to the baryon chemical potential,

$$\chi_n^B = \frac{\partial^n (p/T^4)}{\partial (\mu_B/T)^n}. \quad (168)$$

In the same way one can define the cumulants with respect to other quantum numbers such as the strangeness, the electric charge, etc., as QGP probes [191, 192]. We here list first few non-trivial coefficients expressed through the moments as

$$\chi_2^B = \frac{1}{VT^3} \langle (\delta N_B)^2 \rangle, \quad (169)$$

$$\chi_3^B = \frac{1}{VT^3} \langle (\delta N_B)^3 \rangle, \quad (170)$$

$$\chi_4^B = \frac{1}{VT^3} (\langle (\delta N_B)^4 \rangle - 3\langle (\delta N_B)^2 \rangle^2), \quad (171)$$

where  $\delta N_B \equiv N_B - \langle N_B \rangle$  and  $N_B$  is the net-baryon number.

The so-called kurtosis defined by the ratio,  $\chi_4^B/\chi_2^B$ , is known as a good probe of the deconfinement transition; as we demonstrate below, at zero chemical potential, it reflects the quark content of physical degrees of freedom that carry the baryon number [193, 194].

Let us first consider *small temperatures* where  $\Phi \rightarrow 0$  and the spontaneous chiral symmetry breaking results in a dynamical quark mass as  $m \gg T$ . In this limit we can perform the expansion similar to what we saw in the heavy-quark limit; see Eq. (145). For simplicity we assume that all flavors are degenerate, and then we find the quark pressure as

$$p = -\frac{V_{\text{quark}}}{V} = -2TN_f \int \frac{d^3p}{(2\pi)^3} \left\{ e^{-\beta\varepsilon_p} (\text{tr} L e^{\beta\mu} + \text{tr} L^\dagger e^{-\beta\mu}) - \frac{1}{2} e^{-2\beta\varepsilon_p} [\text{tr} L^2 e^{2\beta\mu} + \text{tr} (L^\dagger)^2 e^{-2\beta\mu}] + \frac{1}{3} e^{-3\beta\varepsilon_p} [\text{tr} L^3 e^{3\beta\mu} + \text{tr} (L^\dagger)^3 e^{-3\beta\mu}] + \dots \right\}, \quad (172)$$

where the higher order corrections are suppressed exponentially. Differentiating this expression with respect to the baryon chemical potential ( $\mu_B = 3\mu$ ), setting it to zero, and equating  $\Phi = \bar{\Phi}$ , we arrive in the mean-field approximation at

$$\lim_{T \rightarrow 0} \frac{\chi_4^B}{\chi_2^B} \approx \frac{\int \frac{d^3p}{(2\pi)^3} \left[ \frac{1}{81} e^{-\beta\varepsilon_p} \Phi - \frac{8}{81} e^{-2\beta\varepsilon_p} (3\Phi - 2)\Phi + e^{-3\beta\varepsilon_p} (27\Phi^3 - 27\Phi^2 + 3) \right]}{\int \frac{d^3p}{(2\pi)^3} \left[ \frac{1}{9} e^{-\beta\varepsilon_p} \Phi - \frac{4}{9} e^{-2\beta\varepsilon_p} (3\Phi - 2)\Phi + e^{-3\beta\varepsilon_p} (27\Phi^3 - 27\Phi^2 + 3) \right]}. \quad (173)$$

Now in the limit of vanishing  $\Phi$  we see that only the last terms (containing color-singlet parts) proportional to  $e^{-3\beta\varepsilon_p}$  survive in the numerator and the denominator; therefore, the ratio  $\chi_4^B/\chi_2^B$  goes to the unity, as we expect from the hadron resonance gas model. We can also check that, if we neglect the Polyakov loop coupling of quarks (that is, if we set  $\Phi \rightarrow 1$  in the above), the leading term with  $e^{-\beta\varepsilon_p}$  dominates at small temperature and we get a smaller result of  $\chi_4^B/\chi_2^B \rightarrow 1/9$ .

At *high temperatures*, on the other hand, chiral symmetry is supposed to be restored; hence, we can neglect the quark mass and recover Eq. (123). By differentiating the pressure obtained from Eq. (123), at zero chemical potential and in the perturbative limit ( $q \rightarrow 0$ ), we obtain,

$$\lim_{T \rightarrow \infty} \frac{\chi_4^B}{\chi_2^B} \rightarrow \frac{2}{3\pi^2}. \quad (174)$$

This result is slightly different from 1/9 as considered in Ref. [193]. In fact, 1/9 appears in the Boltzmann approximation that leaves only the leading order of the expansion in  $e^{-\beta\varepsilon_p}$ , but such a treatment is no longer valid once  $T \gg m$  owing to the chiral symmetry restoration at high temperature.

On top of the above discussions on deconfinement, the cumulants are also useful probes to study the chiral dynamics and the effect of the Polyakov loop fluctuations. In order to demonstrate this we have to refine the discussions presented above and consider a mean-field description with the self-consistently defined fields. We here introduce a collective notation,  $\phi \equiv (\Phi, \bar{\Phi}, \sigma)$ , to simplify expressions. The first derivative of the pressure with respect to the chemical potential is

$$\frac{dp}{d\mu_B} = \frac{\partial p}{\partial \mu_B} + \frac{\partial p}{\partial \phi_i} \frac{\partial \phi_i}{\partial \mu_B} = \frac{\partial p}{\partial \mu_B}, \quad (175)$$

where the second equality follows from the equations of motion,  $\partial p/\partial \phi_i = 0$ . Continuing to take the second derivative, we find,

$$\frac{d^2p}{d\mu_B^2} = \frac{\partial^2 p}{\partial \mu_B^2} + \frac{\partial^2 p}{\partial \mu_B \partial \phi_i} \frac{\partial \phi_i}{\partial \mu_B} = \frac{\partial^2 p}{\partial \mu_B^2} + \frac{\partial^2 p}{\partial \mu_B \partial \phi_i} \chi_{ij} \frac{\partial^2 p}{\partial \mu_B \partial \phi_j}, \quad (176)$$

where we defined the susceptibilities,  $\chi_{ij}$ , as the inverse of the mass matrix, i.e.

$$\chi_{ij} \left( -\frac{\partial^2 p}{\partial \phi_j \partial \phi_k} \right) = \delta_{ik}. \quad (177)$$

In Eqs. (176) and (177), we used the equation of motion differentiated with respect to the chemical potential (that is justified by the fact that the equation of motion holds for any  $\mu$ ),

$$\frac{d}{d\mu_B} \frac{\partial p}{\partial \phi_i} = \frac{\partial^2 p}{\partial \mu_B \partial \phi_i} + \frac{\partial^2 p}{\partial \phi_i \partial \phi_j} \frac{\partial \phi_j}{\partial \mu_B} = 0. \quad (178)$$

This relation allows us to eliminate  $\partial \phi_i/\partial \mu_B$  from Eq. (176). Finally, we see that the second cumulant is related to the field susceptibilities  $\chi_{ij}$  as

$$\chi_2^B = \frac{\partial^2 (p_{\text{quark}}/T^4)}{\partial (\mu_B/T)^2} + T^2 \frac{\partial^2 (p_{\text{quark}}/T^4)}{\partial (\mu_B/T) \partial \phi_i} \chi_{ij} \frac{\partial^2 (p_{\text{quark}}/T^4)}{\partial (\mu_B/T) \partial \phi_j}. \quad (179)$$

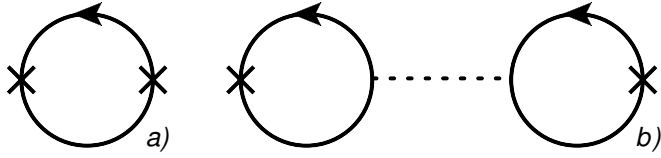


Figure 16: Diagrammatic representation of different contributions to  $\chi_2^B$  in Eq. (179): (a) the one-particle irreducible part and (b) the one-particle reducible part. The dashed line corresponds to the mean-field exchange defined by the inverse of the mass matrix, namely, the susceptibility  $\chi_{ij}$ .

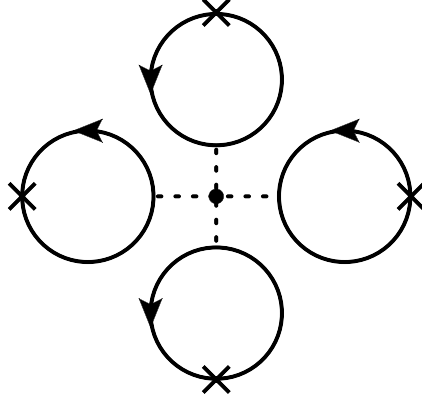


Figure 17: Diagrammatic representation of the divergent contribution to  $\chi_4$  at chiral critical point. The dashed line corresponds to the  $\sigma$  propagator.

Here we replaced the total pressure  $p$  with its quark part  $p_{\text{quark}}$  in the differentiations with respect to the chemical potential. This equation has an intuitive diagrammatic representation as shown in Fig. 16. Clearly, the baryon number fluctuation is affected by the Polyakov loop fluctuations in  $\chi_{\Phi\Phi}$ ,  $\chi_{\Phi\bar{\Phi}}$ , and  $\chi_{\bar{\Phi}\bar{\Phi}}$  as well as the chiral susceptibility.

For even higher-order cumulants the number of contributing diagrams increases and the full expression becomes tedious; at the same time, it would not bring any new theoretical insights beyond those that can already be illustrated in Eq. (179). Here, we point two useful features out below.

*First*, at the chiral critical point, the  $\sigma$  susceptibility diverges and this will be reflected in the second order cumulant via the one-particle reducible contribution [see Fig. 16 (b)]. Actually, based on this argument, it is easy to see why higher-order cumulants exhibit stronger divergence; they include contributions with larger number of the  $\sigma$  propagator, as illustrated in Fig. 17 for an example of the fourth-order contribution. A detailed analysis of the singular contribution to the cumulants shows that the  $n$ -th order cumulant of the net-baryon number fluctuations diverges with the correlation length,  $\xi$ , as [195]

$$\chi_n^{\text{sing}} \propto \xi^{\frac{n\beta\delta}{\nu}-3}, \quad (180)$$

where  $\beta$ ,  $\delta$  and  $\nu$  are the standard notations for critical exponents. The QCD critical point belongs to the Z(2) universality class, and thus  $\beta \approx 0.31$ ,  $\delta \approx 5$ ,  $\nu \approx 0.64$ . Hence the fourth-order cumulant,  $\chi_4^B$ , is proportional to  $\approx \xi^7$  as predicted in Ref. [195]. The sensitivity of the fourth-order cumulant to the correlation length has motivated an experimental search for the QCD critical point. This is an exciting research field and interested readers are guided to see, e.g. Ref. [196] for an overview of the state-of-the-art experimental status.

*Second*, through the one-particle reducible part, the second order cumulant as well as higher orders are all sensitive to the Polyakov loop susceptibilities. This becomes especially important at high temperatures (not necessarily in the vicinity of the critical point), where  $\sigma$  decouples and the details of the Polyakov loop potential significantly affect the whole cumulants. The Polyakov loop potential

including fluctuation effects was proposed in Ref. [63], and recently, the FRG-QCD calculations [197] imply that the experimental data for the kurtosis  $\chi_4^B/\chi_2^B$  can be best reproduced with this proposed Polyakov loop potential. This is the first experimental (other than the numerical experiment of the lattice QCD) indication to provide us with very concrete information on the Polyakov loop physics.

## 5.2 Semi-QGP Regime

In the previous subsection we discussed the effect of the Polyakov loop on the equilibrium static observables. Here we also consider how the Polyakov loop may change the out-of-equilibrium observables such as the shear viscosity, the collisional energy loss, and the production of direct photons and dileptons.

Experimentally the heavy-ion collisions at ultra-relativistic energies probe QCD at temperatures above and close to the transition temperature during most of the collision evolution. Collective properties confirmed by experimental measurements (e.g. elliptic flow) demonstrated that the matter created in these collisions can be described well by hydrodynamics with a very small value of the ratio of the shear viscosity,  $\eta$ , to the entropy. At least naïvely, this fact implies that the QCD coupling constant is large near the transition temperature as the extracted value of the shear viscosity ratio is explained by a strongly coupled  $\mathcal{N} = 4$  supersymmetric  $SU(N_c)$  theory [198].

However, strong correlation does not necessarily mean strong coupling, and moreover, EQCD (that is a three-dimensional effective theory of hot QCD) demonstrated that at the transition temperature the coupling constant stays quite moderate, i.e.  $\alpha_s^{\text{EQCD}} \approx 0.3$  [199]. Motivated by this and constrained by the fact that such a transitional thermodynamic region cannot be treated reliably neither by a hadron resonance gas nor by (resummed) QCD perturbation theory, the authors of Ref. [200] explored an alternative explanation for the small value of the shear viscosity even with the moderate/weak coupling constant. To describe the transition, they considered a new regime with a partial ionization of color, called the “semi”-Quark-Gluon Plasma (semi-QGP). This region of partial ionization/deconfinement can naturally be modeled by a non-trivial Polyakov loop. On a small sphere as we discussed in Sec. 3.2.3, one can show that the semi-QGP description is manifestly an appropriate effective theory.

Most of the results concluded from the semi-QGP calculations can be intuitively understood as follows. In Minkowski spacetime, the diagrammatic calculations are formulated as an ordinary perturbation theory, except that the background field  $A_4$  acts like an imaginary chemical potential for color. For a quark with a given color  $a$  and for a gluon with a given color pair  $a$  and  $b$ , the statistical distribution functions are, respectively,  $n_a = [\exp(-\beta\varepsilon + 2\pi i q_a) + 1]^{-1}$  and  $n_{ab} = [\exp(-\beta\varepsilon + 2\pi i q_{ab}) - 1]^{-1}$ . In the Boltzmann approximation, the color-traced distribution function for a single quark (and anti-quark) is suppressed by the Polyakov loop, that is,  $N_c^{-1} \sum_a \exp(-\beta\varepsilon + 2\pi i q_a) \propto \exp(-\beta\varepsilon) \ell$ . For gluons, the suppression is more prominent as  $\exp(-\beta\varepsilon) \ell^2$ . Thus, in this way, any physical observable sensitive to the abundance of color charge in the system will be suppressed in the semi-QGP regime by one or even larger powers of the Polyakov loop.

Let us consider the shear viscosity first. Here we will give a somewhat qualitative account by skipping concrete calculations. For technical details, see the original calculations in Ref. [200] and also see Refs. [201, 202] for the conventional calculations of the transport coefficients in perturbative QCD.

The shear viscosity of a gas is in general proportional to  $\eta \propto n\bar{p}\lambda$ , where  $n$  is the number density,  $\bar{p}$  is the average momentum, and  $\lambda$  is the mean free path. We first consider a conventional plasma of fully-ionized gluons to extract a parametric dependence of the viscosity on the temperature and the coupling constant. The mean average momentum in this case is proportional to the temperature, the mean free path is of the order of  $1/(n\sigma)$  where  $\sigma$  is the cross section. In QCD, the transport cross section is  $\sigma_{\text{pQCD}} \sim g^4 T^{-2} \ln(T/m_{\text{Debye}})$  with the Debye mass of the order of  $gT$ , where the logarithm arises due to an infrared singularity in the forward scattering. Combining everything together, we conclude that the shear viscosity is parametrically given by  $\eta_{\text{pQCD}} \sim T^3/(g^4 \ln 1/g)$ .

Now, we shall consider the semi-QGP regime and show that in this case the counting is somewhat

different. The mean free path should be changed due to the color flow. It is proportional to the average number of the color sources divided by the effective collisional area or the collisional cross section, which leads to

$$\lambda_{\text{semi-QGP}} \propto \frac{\sum_{a,b} n_{ab}}{\sum_{a,b,c,d} n_{ab} n_{cd} \sigma_{ab,cd}}. \quad (181)$$

The gluon density is proportional to  $\ell^2 T^3$  as we discussed above. The denominator in  $\lambda_{\text{semi-QGP}}$ , describing a hard  $2 \leftrightarrow 2$  scattering with a single soft exchange in the  $t$ -channel, is dominated by the planar graph with two of the color indices being equal. This color index contraction leads to a partial cancellation of, say,  $q_b$  in  $n_{ab}$  and  $q_c$  in  $n_{cd}$  in the color sum and results in the parametric result  $\lambda_{\text{semi-QGP}} \propto (\ell^2 T^3)/(\ell^2 T^6 \sigma) = (T^3 \sigma)^{-1}$ , which is approximately  $\ell$  independent.

The shear viscosity of semi-QGP is then  $\eta_{\text{semi-QGP}} \sim T \sum_{a,b} n_{ab}/\lambda_{\text{semi-QGP}} \propto \ell^2 \eta_{\text{pQCD}}$ , so that the shear viscosity as compared to the perturbative result is suppressed by the Polyakov loop squared. In the vicinity of the phase transition in the pure gluonic theory, the Polyakov loop is roughly  $\sim 1/2$ , and thus the viscosity of semi-QGP is smaller than the perturbative estimate by a factor  $\sim 4$ . Interestingly, taking account of quark degrees of freedom does not modify this parametric suppression of the shear viscosity by the Polyakov loop.

Before moving on to the next example of physical observables, we mention on an exceptional case, for which only color singlet states make a contribution. Let us consider the dilepton production and show that it is not sensitive to the Polyakov loop at least at the leading order. This is to be expected since the dilepton rate arises from the annihilation process of a quark and an anti-quark in a color singlet states going into a virtual photon, which can eventually decay into a dilepton pair.

For the sake of simple arguments, we restrict ourselves to the back-to-back dilepton pair, i.e. the momentum of the intermediate photon is  $p = 0$ . In the kinetic theory, the dilepton production rate is given by the product of quark statistical distribution functions and a squared amplitude. The energy conservation requires that each quark carries a half of the dilepton energy,  $E$ , and the expression is parametrized as

$$\frac{d\Gamma}{d^4p} \propto e^2 \sum_{a=1}^{N_c} e^{-\beta E/2 + i2\pi q_a} e^{-\beta E/2 - i2\pi q_a} |M|^2, \quad (182)$$

where  $e$  is the QED coupling and we assumed  $E \gg T$  to justify the Boltzmann approximation for quarks. The eigenvalue,  $q_a$ , enters in the quark/anti-quark distribution functions as a colored imaginary chemical potential, and they naturally contribute with opposite signs. Then, two  $q_a$ 's cancel in the production rate! The probability for a hard virtual photon,  $E \gg T$ , to be produced from a quark/anti-quark annihilation process is, therefore, independent of the Polyakov loop. This makes a sharp contrast to the statistical distribution function for individual quarks and anti-quarks suppressed by the Polyakov loop.

Interestingly enough, explicit calculations in Refs. [203, 204, 205, 206] show that the dilepton production rate for  $\ell < 1$  is not suppressed but always more enhanced than the  $\ell = 1$  case, i.e.

$$\left. \frac{d\Gamma}{dE d^3p} \right|_{\ell} = \frac{f(\ell)}{f(\ell = 1)} \cdot \left. \frac{d\Gamma}{dE d^3p} \right|_{\ell=1} \quad (183)$$

with

$$f(\ell) \equiv 1 - \frac{2T}{3p} \ln \left[ \frac{1 + 3\ell e^{-\beta(E-p)/2} + 3\ell e^{-2\beta(E-p)/2} + e^{-3\beta(E-p)/2}}{1 + 3\ell e^{-\beta(E+p)/2} + 3\ell e^{-2\beta(E+p)/2} + e^{-3\beta(E+p)/2}} \right]. \quad (184)$$

The enhancement due to  $\ell < 1$  is very modest; about 10-20 percent at most. It is therefore unlikely that the enhancement plays any important role in the heavy-ion phenomenology.

Let us now turn our attention to a more Polyakov loop sensitive observable, that is, the real photon production. Now, we consider a real photon with a large momentum,  $E = p \gg T$ . The leading order processes for the photon production consist of the Compton scattering of a quark or an anti-quark and the annihilation of a quark/anti-quark pair. Both processes are proportional to  $e^2 g^2$  and of the same order. There is an additional contribution; a quark scatters with an arbitrary number of soft gluons with energy of order  $gT$ , and emits collinear photons. Such multiple scattering processes are of the same order of  $e^2 g^2$  because of the Bose-Einstein enhancement for the soft gluon, as seen as  $n(gT) \sim 1/g$  if  $\ell = 1$ . In the semi-QGP regime,  $\ell < 1$  by definition, and this Bose-Einstein enhancement is diminished for off-diagonal gluons (see Ref. [205] for calculations of the collinear rate in the semi-QGP regime). At small energies ( $E \ll T$ ) the gluon distribution function is proportional to  $1/(e^{-i2\pi q_a} - 1)$  and is of order the unity if  $q_{ab} = q_a - q_b \sim 1$  for different  $a$  and  $b$ . The contribution of the diagonal ( $a = b$ ) gluons is suppressed by  $1/N_c$ . Hence, up to  $1/N_c$  corrections, the production of real photons is dominated by  $2 \leftrightarrow 2$  processes in the semi-QGP regime. To illustrate the effect of the non-trivial Polyakov loop on the photon production, let us consider the case of quark/anti-quark annihilation into a gluon and a photon; the conclusion we will draw is also valid for the Compton scattering. In the Boltzmann approximation, the rate of the real photon production is proportional to

$$E \frac{d\Gamma_\gamma}{d^3p} \propto e^2 g^2 \sum_{a,b} e^{-\beta\varepsilon_1 - i2\pi q_a} e^{-\beta\varepsilon_2 + i2\pi q_b} |M^{ab}|, \quad (185)$$

where  $\varepsilon_1$  and  $\varepsilon_2$  are the energies of the color  $a$  quark and the color  $b$  anti-quark, respectively. The matrix element of the process is denoted by  $M^{ab}$ . In the perturbative limit,  $q_a, q_b \rightarrow 0$ , and the rate is simply proportional to  $e^2 g^2 N_c^2$ . In states near the confined phase, the sum  $\sum_a e^{-i2\pi q_a}$  goes to zero, as it is nothing but the traced Polyakov loop, so that only  $a = b$  terms in Eq. (185) make finite contributions. This immediately results in a suppression factor of  $1/N_c$ . Moreover, the matrix element  $M^{ab}$  involves a quark-gluon vertex giving an additional suppression factor of  $1/N_c$  for  $a = b$ . This amounts to an overall  $1/N_c^2$  suppression factor in the confined phase! Such a large suppression of the real photon production in the semi-QGP regime can have a significant impact on the phenomenological observables; this mechanism is considered to be potentially responsible for resolving the puzzle of the photon azimuthal anisotropy, as argued in Ref. [204].

Similarly, the calculations of the collisional energy loss show that, at the leading order, the energy loss can be also suppressed by powers of the Polyakov loop. For small values of the Polyakov loop, this suppression behavior is linear for the light-quark scattering, and is quadratic for the gluon scattering or the Compton scattering. This results can be directly attributed to the number of the colored object in the semi-QGP regime, as we discussed above. For a concrete phenomenological setup, for example, see Ref. [207] in which a semi quark gluon monopole plasma is assumed.

There are many other transport coefficients calculable in the semi-QGP regime, such as the heat conductivity, the electric conductivity, the bulk viscosity, etc. However, they have not yet been considered in the literature and remain to be explored in the future.

## 6 Summary

In writing this review, we followed a rather orthodox approach; we gave a minimal description about the quantization procedure for QCD at finite temperature, which is indispensable for understanding the physical meaning of the Polyakov loop and its relation to the realization of center symmetry. Then, we introduced monumental examples of the Polyakov loop calculations that were milestones in the history of the Polyakov loop physics. We made a quick review of Polyakov's original arguments and calculations in the strong coupling limit of the pure gluonic theory. We also covered more extensive strong coupling analysis to discuss the explicit forms of the Polyakov loop potentials in the confined phase.



An asymptotic limit of weak coupling realizing at high temperatures, where quarks and gluons are deconfined and the perturbation theory can be applied, serves as an important example of the Polyakov loop calculation. In this case, the calculation self-consistently leads to center symmetry breaking and we confirmed that the center broken vacuum is stabilized by a finite Debye screening mass. An interesting and non-trivial question is how these two asymptotic phases of confined and deconfined matter transition from one to the other as the temperature approaches the critical value. Similarly to the formation of magnetic domains in spin systems, the  $Z(N_c)$  domain walls may be identified as the physical interfaces between the two phases. A domain-wall classical configuration can be easily found from the equation of motion obtained from the perturbative potential. In QCD, however, the vacuum can accommodate other, more non-trivial configurations called instantons; the center elements are disturbed by instantons and anti-instantons as well as by the  $Z(N_c)$  domain walls. We shortly reviewed a special class of finite- $T$  instantons with a non-trivial holonomy (a non-unity Polyakov loop). In this context, for the advance of the confinement physics, it was important to recognize that the finite- $T$  instantons are the bound states of dyons. Up to this point all discussions were based on first-principle QCD calculations.

Even if it is impenetrable to extract information on the Polyakov loop directly from first-principle theory, we can still make use of the Polyakov loop as a representative variable to characterize the hot QCD system. In this way, full thermodynamic behavior in the pure gluonic theory could be well dictated by a Polyakov loop potential parametrized by a few coefficients. Such an ad-hoc parametrization procedure not only results in successful fitting of lattice results but also suggests the validity of an underlying physical picture that the Haar measure or the ghost singularity is responsible for confinement. To improve upon this ad-hoc approach, one can pursue a more ambitious goal of deriving the Polyakov loop potential directly from QCD supplemented by some approximations; thus, a goal of extending our understanding to the new, more fundamental, and QCD-based level. We selected and described two methods along these lines. The first one, the inverted Weiss potential, is a very simple but powerful idea providing a qualitatively concrete description of the confining vacuum. The ingredients necessary for the inverted Weiss potential are the one-loop perturbative expression from QCD calculations, in which the propagators are slightly modified to implement a clear observation of ghost dominance seen in the lattice QCD or in the strong coupling expansion. This method can be regarded as a hybrid approach to confinement, for it is based on the perturbative technique supplemented by the non-perturbative input. The second method we discussed is the Polyakov loop matrix model. This effective description is derived from QCD by the strong coupling expansion with an assumption that higher-order Polyakov loop interactions can be neglected. The theory of the  $SU(N_c)$  matrix model has interesting properties on its own; for instance, we can formulate the mean-field approximation in such a way as to manifest the group integration nature, which is useful to guarantee gauge invariance.

The most profound application of the Polyakov loop matrix model is found in the large  $N_c$  limit. Although some analytical studies are possible for large- $N_c$  QCD, the nature of the phase transition is not yet fully revealed. We showed that rich phase structures of first, second, and third order phase boundaries emerge as coefficients in the Polyakov loop potential vary. Such a phase structure is relevant also to QCD in a different setup, namely, QCD on a small sphere. The running coupling constant is small on a small 3-sphere just like in the high temperature environment justifying the perturbation theory approach. Perturbative calculations result in an effective theory of the Polyakov loop matrix model.

Coupling to quarks turns the Polyakov loop physics into a quite fertile research field. The biggest unsolved puzzle is the structure of the QCD phase diagram at finite temperature and density. For this purpose various chiral models have predicted various phase boundaries associated with chiral symmetry restoration. These models can be augmented with the Polyakov loop potential and the coupling to the quarks; such augmented models provide handy theoretical tools for a discussion of the interplay between chiral restoration and deconfinement. Instead of presenting model-dependent examples of the phase diagrams, we focused on model-independent features of the Polyakov loop coupling to quarks. For

further quantifying the model studies, it is crucial to establish a precise determination of the Polyakov loop potential. We introduced an idea to constrain the Polyakov loop potential from the heavy quark sector.

Even with sufficient knowledge on the Polyakov loop potential, the sign problem prevents us from making any reliable prediction at finite density. In particular, the Polyakov loop and the anti-Polyakov loop are sensitive to quark and anti-quark excitations in the medium, so that the Polyakov loop model can be a minimal setup that shares the same sign problem with original QCD. For one example we gave a brief explanation of one of the simplest and thus most frequently used models called the heavy-dense model. To circumvent the sign problem, it is a common strategy to change the underlying theory such that to evade the issue. This can be done in several ways, and one of the most well-understood is to analytically continue the chemical potential to imaginary values. QCD with imaginary chemical potential shows a different pattern of the phase structure from the finite-density QCD, and we exemplified it by the perturbative Weiss potential, which exhibits the Roberge-Weiss phase transition, and by the inverted Weiss potential.

Not only the external parameter such as the chemical potential but also the definition of the theory itself could be deformed in such a way as to make it convenient for theoretical considerations. The deformed QCD, although related to the original theory, does not describe physical QCD and should be regarded as a QCD-like model; nevertheless, it offers a useful insight to deepen our understanding on the non-perturbative nature of QCD. In QCD, chiral symmetry breaking and confinement are entangled in a complicated way, which is of course the most interesting aspect of QCD; a disentanglement of these transitions opens a possibility to investigate the confinement physics *exclusively*. In order to achieve this, one has to deform the theory or introduce the matter fields in such a way as to keep the center symmetry unbroken and, consequently, as to preserve the status of the Polyakov loop as the exact order parameter. In this review, we selected three approaches out of many existing ones in the literature. We made this specific choice based on relevance to the other parts of this review and based on their future prospects.

The Polyakov loop is gauge invariant and thus physically observable, but since the Polyakov loop is defined in Euclidean spacetime, one may conclude that it hardly has any relevance for experimentally measurable quantities. This is not correct; the Polyakov loop is not an academic phantom as it does affect experimental observables measured in the relativistic heavy-ion collisions. We took a quick look at two examples; one is the baryon number fluctuations and the other is the so-called semi-QGP regime. The baryon number fluctuations play an important role of a signature for deconfinement, which is naturally sensitive to the Polyakov loop. Moreover, the baryon number fluctuations provide a possible measure to detect and locate the QCD critical point; experimental data at various collision energies are already available (to be precise, not the baryon number but rather the proton number is measurable). Because the Polyakov loop has a direct coupling to quark, the baryon number fluctuations receive a contribution from the Polyakov loop fluctuations or the curvature of the Polyakov loop potential. One should now notice that not only the Polyakov loop fluctuations but the expectation value of the Polyakov loop can change the real-time physical observables including the transport coefficients. This is the idea of the semi-QGP regime, which is applicable more generally near the QCD crossover. We know that around the QCD phase transition temperature the Polyakov loop is still small, and this means, that the quark and the anti-quark excitations are significantly screened by the effect of the Polyakov loop. Since gluons are colored particles, small Polyakov loops also suppress gluonic excitations, which could be an alternative description of the strongly correlated QGP with small shear viscosity to the entropy density ratio.

In this review we stressed that the Polyakov loop is not just another observable measured in the lattice-QCD simulation; as in theoretical studies it is sometimes useful to regard the Polyakov loop as a control parameter to access the confining sector of QCD. It is even possible to treat the Polyakov loop as a theoretical device to establish an intuitive understanding of hot gluonic medium, similar to the

concept of a constituent quark in hadronic physics. We chose the topics covered in this review so that our discussions bear some degree of generality and could be applied not only to QCD but also to other systems, e.g. condensed matter systems with emergent gauge symmetry. This is the reason why we did not cover important but rather specific subjects including higher-order perturbative calculations of the Polyakov loop expectation value [208, 209], subtleties in the renormalization prescriptions [210, 211, 212] (see Ref. [213] for latest results with the  $Q\bar{Q}$  renormalization procedure), Casimir scaling [214, 215], magnetic field coupling to the Polyakov loop [216, 217], etc.

We close this review by reiterating that there is a common consensus that the Polyakov loop is an approximate order parameter for the deconfinement phase transition in QCD. The traditional way of treating the Polyakov loop was to use it to characterize a thermal system away from confinement rather than coping with the low- $T$  confinement problem itself. However, in view of the recent developments, the Polyakov loop is becoming an increasingly more important player in the arena of confinement physics. We hope that this review makes a strong case for the paramount significance of the Polyakov loop as the quantity defining the properties of pure gluonic theory and QCD near zero as well as near the transition temperature.

## Acknowledgments

The authors thank Jens Braun, Yoshi Hatta, Yoshimasa Hidaka, Hiroaki Kouno, Larry D. McLerran, Hiromichi Nishimura, Jan M. Pawłowski, Rob Pisarski, Janos Polonyi, Bernd-Jochen Schaefer, Edward Shuryak, Yuya Tanizaki, Mithat Ünsal, and Wolfram Weise for discussions. K. F. was partially supported by JSPS KAKENHI Grant No. 15H03652 and 15K13479.

## References

- [1] A. M. Polyakov, “Thermal properties of gauge fields and quark liberation,” *Phys. Lett.* **B72** (1978) 477–480.
- [2] K. G. Wilson, “Confinement of quarks,” *Phys. Rev.* **D10** (1974) 2445–2459.
- [3] C. G. Callan, Jr., R. F. Dashen, and D. J. Gross, “The Structure of the gauge theory vacuum,” *Phys. Lett.* **B63** (1976) 334–340.
- [4] C. G. Callan, Jr., R. F. Dashen, and D. J. Gross, “Toward a theory of the strong interactions,” *Phys. Rev.* **D17** (1978) 2717.
- [5] B. Svetitsky, “Symmetry aspects of finite temperature confinement transitions,” *Phys. Rept.* **132** (1986) 1–53.
- [6] B. Svetitsky and L. G. Yaffe, “Critical behavior at finite temperature confinement transitions,” *Nucl. Phys.* **B210** (1982) 423.
- [7] K. Fukushima and C. Sasaki, “The phase diagram of nuclear and quark matter at high baryon density,” *Prog. Part. Nucl. Phys.* **72** (2013) 99–154, [arXiv:1301.6377 \[hep-ph\]](#).
- [8] D. J. Gross, R. D. Pisarski, and L. G. Yaffe, “QCD and instantons at finite temperature,” *Rev. Mod. Phys.* **53** (1981) 43.
- [9] A. V. Smilga, “Physics of thermal QCD,” *Phys. Rept.* **291** (1997) 1–106, [arXiv:hep-ph/9612347 \[hep-ph\]](#).

- [10] D. H. Rischke, “The Quark gluon plasma in equilibrium,” *Prog. Part. Nucl. Phys.* **52** (2004) 197–296, [arXiv:nucl-th/0305030 \[nucl-th\]](#).
- [11] K. Fukushima and T. Hatsuda, “The phase diagram of dense QCD,” *Rept. Prog. Phys.* **74** (2011) 014001, [arXiv:1005.4814 \[hep-ph\]](#).
- [12] P. Braun-Munzinger, V. Koch, T. Schaefer, and J. Stachel, “Properties of hot and dense matter from relativistic heavy ion collisions,” *Phys. Rept.* **621** (2016) 76–126, [arXiv:1510.00442 \[nucl-th\]](#).
- [13] J. Kapusta and C. Gale, *Finite-Temperature Field Theory: Principles and Applications*. Cambridge University Press, 2006.
- [14] M. Le Bellac, *Thermal Field Theory*. Cambridge University Press, 2000.
- [15] J. Letessier and J. Rafelski, *Hadrons and Quark-Gluon Plasma*. Cambridge University Press, 2002.
- [16] K. Yagi, T. Hatsuda, and Y. Miake, *Quark-Gluon Plasma: From Big Bang to Little Bang*. Cambridge Monographs on Particle Physics, Nuclear Physics and Cosmology. Cambridge University Press, 2005.
- [17] H.-T. Ding, F. Karsch, and S. Mukherjee, “Thermodynamics of strong-interaction matter from Lattice QCD,” *Int. J. Mod. Phys.* **E24** (2015) no. 10, 1530007, [arXiv:1504.05274 \[hep-lat\]](#).
- [18] C. Ratti, “Lattice QCD: bulk and transport properties of QCD matter,” *Nucl. Phys.* **A956** (2016) 51–58, [arXiv:1601.02367 \[hep-lat\]](#).
- [19] S. Borsanyi, “Frontiers of finite temperature lattice QCD,” in *12th Conference on Quark Confinement and the Hadron Spectrum (Confinement XII) Thessaloniki, Greece, August 28-September 4, 2016*. 2016. [arXiv:1612.06755 \[hep-lat\]](#).  
<https://inspirehep.net/record/1505186/files/arXiv:1612.06755.pdf>.
- [20] S. P. Klevansky, “The Nambu-Jona-Lasinio model of quantum chromodynamics,” *Rev. Mod. Phys.* **64** (1992) 649–708.
- [21] T. Hatsuda and T. Kunihiro, “QCD phenomenology based on a chiral effective Lagrangian,” *Phys. Rept.* **247** (1994) 221–367, [arXiv:hep-ph/9401310 \[hep-ph\]](#).
- [22] M. Buballa and S. Carignano, “Inhomogeneous chiral condensates,” *Prog. Part. Nucl. Phys.* **81** (2015) 39–96, [arXiv:1406.1367 \[hep-ph\]](#).
- [23] Y. Nambu and G. Jona-Lasinio, “Dynamical model of elementary particles based on an analogy with superconductivity. 1.,” *Phys. Rev.* **122** (1961) 345–358.
- [24] K. Rajagopal and F. Wilczek, “The Condensed matter physics of QCD,” [arXiv:hep-ph/0011333 \[hep-ph\]](#).
- [25] J. Braun, “Fermion interactions and universal behavior in strongly interacting theories,” *J. Phys.* **G39** (2012) 033001, [arXiv:1108.4449 \[hep-ph\]](#).
- [26] H. Hata and T. Kugo, “An Operator formalism of statistical mechanics of gauge theory in covariant gauges,” *Phys. Rev.* **D21** (1980) 3333.

- [27] L. D. McLerran and B. Svetitsky, “A Monte Carlo study of SU(2) Yang-Mills Theory at finite temperature,” *Phys. Lett.* **B98** (1981) 195.
- [28] L. D. McLerran and B. Svetitsky, “Quark liberation at high temperature: A Monte Carlo study of SU(2) gauge theory,” *Phys. Rev.* **D24** (1981) 450.
- [29] K. A. James and P. V. Landshoff, “Finite temperature field theory in the temporal gauge: The Imaginary time formalism,” *Phys. Lett.* **B251** (1990) 167–174.
- [30] J. Polonyi and K. Szlachanyi, “Phase transition from strong coupling expansion,” *Phys. Lett.* **B110** (1982) 395–398.
- [31] M. Gross, J. Bartholomew, and D. Hochberg, “SU( $N$ ) deconfinement transitions and the  $N$  state clock model,”.
- [32] A. Gocksch and M. Ogilvie, “Finite temperature deconfinement and chiral symmetry restoration at strong coupling,” *Phys. Rev.* **D31** (1985) 877.
- [33] K. Fukushima, “Effects of chiral restoration on the behavior of the Polyakov loop at strong coupling,” *Phys. Lett.* **B553** (2003) 38–44, [arXiv:hep-ph/0209311 \[hep-ph\]](#).
- [34] K. Fukushima, “Relation between the Polyakov loop and the chiral order parameter at strong coupling,” *Phys. Rev.* **D68** (2003) 045004, [arXiv:hep-ph/0303225 \[hep-ph\]](#).
- [35] A. Gocksch and R. D. Pisarski, “Partition function for the eigenvalues of the Wilson line,” *Nucl. Phys.* **B402** (1993) 657–668, [arXiv:hep-ph/9302233 \[hep-ph\]](#).
- [36] C. Korthals Altes, “Constrained effective potential in hot QCD,” *Nucl. Phys.* **B420** (1994) 637–668, [arXiv:hep-th/9310195 \[hep-th\]](#).
- [37] N. Weiss, “The effective potential for the order parameter of gauge theories at finite temperature,” *Phys. Rev.* **D24** (1981) 475.
- [38] N. Weiss, “The Wilson line in finite temperature gauge theories,” *Phys. Rev.* **D25** (1982) 2667.
- [39] E. Megias, E. Ruiz Arriola, and L. L. Salcedo, “The Polyakov loop and the heat kernel expansion at finite temperature,” *Phys. Lett.* **B563** (2003) 173–178, [arXiv:hep-th/0212237 \[hep-th\]](#).
- [40] E. Megias, E. Ruiz Arriola, and L. L. Salcedo, “The Thermal heat kernel expansion and the one loop effective action of QCD at finite temperature,” *Phys. Rev.* **D69** (2004) 116003, [arXiv:hep-ph/0312133 \[hep-ph\]](#).
- [41] A. Dumitru, Y. Guo, and C. P. Korthals Altes, “Two-loop perturbative corrections to the thermal effective potential in gluodynamics,” *Phys. Rev.* **D89** (2014) no. 1, 016009, [arXiv:1305.6846 \[hep-ph\]](#).
- [42] E. Witten, “Cosmic separation of phases,” *Phys. Rev.* **D30** (1984) 272–285.
- [43] M. Asakawa, S. A. Bass, and B. Mueller, “Center domains and their phenomenological consequences,” *Phys. Rev. Lett.* **110** (2013) no. 20, 202301, [arXiv:1208.2426 \[nucl-th\]](#).
- [44] T. Bhattacharya, A. Gocksch, C. Korthals Altes, and R. D. Pisarski, “Interface tension in an SU( $N$ ) gauge theory at high temperature,” *Phys. Rev. Lett.* **66** (1991) 998–1000.

- [45] T. Bhattacharya, A. Gocksch, C. Korthals Altes, and R. D. Pisarski, “ $Z(N)$  interface tension in a hot  $SU(N)$  gauge theory,” *Nucl. Phys.* **B383** (1992) 497–524, [arXiv:hep-ph/9205231 \[hep-ph\]](#).
- [46] G. 't Hooft, “On the phase transition towards permanent quark confinement,” *Nucl. Phys.* **B138** (1978) 1.
- [47] P. de Forcrand and D. Noth, “Precision lattice calculation of  $SU(2)$  't Hooft loops,” *Phys. Rev.* **D72** (2005) 114501, [arXiv:hep-lat/0506005 \[hep-lat\]](#).
- [48] T. C. Kraan and P. van Baal, “Exact T duality between calorons and Taub - NUT spaces,” *Phys. Lett.* **B428** (1998) 268–276, [arXiv:hep-th/9802049 \[hep-th\]](#).
- [49] T. C. Kraan and P. van Baal, “Periodic instantons with nontrivial holonomy,” *Nucl. Phys.* **B533** (1998) 627–659, [arXiv:hep-th/9805168 \[hep-th\]](#).
- [50] K.-M. Lee, “Instantons and magnetic monopoles on  $R^3 \times S^1$  with arbitrary simple gauge groups,” *Phys. Lett.* **B426** (1998) 323–328, [arXiv:hep-th/9802012 \[hep-th\]](#).
- [51] K.-M. Lee and C.-h. Lu, “ $SU(2)$  calorons and magnetic monopoles,” *Phys. Rev.* **D58** (1998) 025011, [arXiv:hep-th/9802108 \[hep-th\]](#).
- [52] T. C. Kraan and P. van Baal, “Monopole constituents inside  $SU(n)$  calorons,” *Phys. Lett.* **B435** (1998) 389–395, [arXiv:hep-th/9806034 \[hep-th\]](#).
- [53] P. Gerhold, E. M. Ilgenfritz, and M. Muller-Preussker, “An  $SU(2)$  KvBLL caloron gas model and confinement,” *Nucl. Phys.* **B760** (2007) 1–37, [arXiv:hep-ph/0607315 \[hep-ph\]](#).
- [54] R. Larsen and E. Shuryak, “Interacting ensemble of the instanton-dyons and the deconfinement phase transition in the  $SU(2)$  gauge theory,” *Phys. Rev.* **D92** (2015) no. 9, 094022, [arXiv:1504.03341 \[hep-ph\]](#).
- [55] M. A. Lopez-Ruiz, Y. Jiang, and J. Liao, “Confinement, Holonomy and Correlated Instanton-Dyon Ensemble I:  $SU(2)$  Yang-Mills Theory,” [arXiv:1611.02539 \[hep-ph\]](#).
- [56] S. Borsanyi, G. Endrodi, Z. Fodor, S. Katz, and K. Szabo, “Precision  $SU(3)$  lattice thermodynamics for a large temperature range,” *JHEP* **1207** (2012) 056, [arXiv:1204.6184 \[hep-lat\]](#).
- [57] L. Giusti and M. Pepe, “Equation of state of a relativistic theory from a moving frame,” *Phys. Rev. Lett.* **113** (2014) 031601, [arXiv:1403.0360 \[hep-lat\]](#).
- [58] L. Giusti and M. Pepe, “Equation of state of the  $SU(3)$  Yang-Mills theory: A precise determination from a moving frame,” *Phys. Lett.* **B769** (2017) 385–390, [arXiv:1612.00265 \[hep-lat\]](#).
- [59] C. Ratti, M. A. Thaler, and W. Weise, “Phases of QCD: Lattice thermodynamics and a field theoretical model,” *Phys. Rev.* **D73** (2006) 014019, [arXiv:hep-ph/0506234 \[hep-ph\]](#).
- [60] S. Roessner, C. Ratti, and W. Weise, “Polyakov loop, diquarks and the two-flavour phase diagram,” *Phys. Rev.* **D75** (2007) 034007, [arXiv:hep-ph/0609281 \[hep-ph\]](#).
- [61] L. M. Haas, R. Stiele, J. Braun, J. M. Pawłowski, and J. Schaffner-Bielich, “Improved Polyakov-loop potential for effective models from functional calculations,” *Phys. Rev.* **D87** (2013) no. 7, 076004, [arXiv:1302.1993 \[hep-ph\]](#).



- [62] C. Sasaki and K. Redlich, “An Effective gluon potential and hybrid approach to Yang-Mills thermodynamics,” *Phys. Rev.* **D86** (2012) 014007, [arXiv:1204.4330 \[hep-ph\]](#).
- [63] P. M. Lo, B. Friman, O. Kaczmarek, K. Redlich, and C. Sasaki, “Polyakov loop fluctuations in SU(3) lattice gauge theory and an effective gluon potential,” *Phys. Rev.* **D88** (2013) 074502, [arXiv:1307.5958 \[hep-lat\]](#).
- [64] J. Greensite and K. Langfeld, “Effective Polyakov line action from strong lattice couplings to the deconfinement transition,” *Phys. Rev.* **D88** (2013) 074503, [arXiv:1305.0048 \[hep-lat\]](#).
- [65] D. Smith, A. Dumitru, R. Pisarski, and L. von Smekal, “Effective potential for SU(2) Polyakov loops and Wilson loop eigenvalues,” *Phys. Rev.* **D88** (2013) no. 5, 054020, [arXiv:1307.6339 \[hep-lat\]](#).
- [66] D. Diakonov, V. Petrov, H.-P. Schadler, and C. Gattringer, “Effective Lagrangian for the Polyakov line on a lattice,” *JHEP* **11** (2013) 207, [arXiv:1308.2328 \[hep-lat\]](#).
- [67] J. Braun, H. Gies, and J. M. Pawłowski, “Quark confinement from color confinement,” *Phys. Lett.* **B684** (2010) 262–267, [arXiv:0708.2413 \[hep-th\]](#).
- [68] D. Zwanziger, “Nonperturbative Landau gauge and infrared critical exponents in QCD,” *Phys. Rev.* **D65** (2002) 094039, [arXiv:hep-th/0109224 \[hep-th\]](#).
- [69] C. Lerche and L. von Smekal, “On the infrared exponent for gluon and ghost propagation in Landau gauge QCD,” *Phys. Rev.* **D65** (2002) 125006, [arXiv:hep-ph/0202194 \[hep-ph\]](#).
- [70] J. M. Pawłowski, D. F. Litim, S. Nedelko, and L. von Smekal, “Infrared behavior and fixed points in Landau gauge QCD,” *Phys. Rev. Lett.* **93** (2004) 152002, [arXiv:hep-th/0312324 \[hep-th\]](#).
- [71] T. Kanazawa, M. Ünsal, and N. Yamamoto, “Phases of circle-compactified QCD with adjoint fermions at finite density,” [arXiv:1703.06411 \[hep-th\]](#).
- [72] R. Aouane, V. G. Bornyakov, E. M. Ilgenfritz, V. K. Mitrjushkin, M. Müller-Preussker, and A. Sternbeck, “Landau gauge gluon and ghost propagators at finite temperature from quenched lattice QCD,” *Phys. Rev.* **D85** (2012) 034501, [arXiv:1108.1735 \[hep-lat\]](#).
- [73] K. Fukushima and K. Kashiwa, “Polyakov loop and QCD thermodynamics from the gluon and ghost propagators,” *Phys. Lett.* **B723** (2013) 360–364, [arXiv:1206.0685 \[hep-ph\]](#).
- [74] K. Fukushima and N. Su, “Stabilizing perturbative Yang-Mills thermodynamics with Gribov quantization,” *Phys. Rev.* **D88** (2013) 076008, [arXiv:1304.8004 \[hep-ph\]](#).
- [75] U. Reinosa, J. Serreau, M. Tissier, and N. Wschebor, “Deconfinement transition in SU( $N$ ) theories from perturbation theory,” *Phys. Lett.* **B742** (2015) 61–68, [arXiv:1407.6469 \[hep-ph\]](#).
- [76] J. Serreau, M. Tissier, and A. Tresmontant, “Covariant gauges without Gribov ambiguities in Yang-Mills theories,” *Phys. Rev.* **D89** (2014) 125019, [arXiv:1307.6019 \[hep-th\]](#).
- [77] U. Reinosa, J. Serreau, M. Tissier, and N. Wschebor, “Two-loop study of the deconfinement transition in Yang-Mills theories: SU(3) and beyond,” *Phys. Rev.* **D93** (2016) no. 10, 105002, [arXiv:1511.07690 \[hep-th\]](#).

- [78] D. Gomez Dumm, D. B. Blaschke, A. G. Grunfeld, and N. N. Scoccola, “Color neutrality effects in the phase diagram of the PNJL model,” *Phys. Rev.* **D78** (2008) 114021, [arXiv:0807.1660 \[hep-ph\]](#).
- [79] H. Abuki and K. Fukushima, “Gauge dynamics in the PNJL model: Color neutrality and Casimir scaling,” *Phys. Lett.* **B676** (2009) 57–62, [arXiv:0901.4821 \[hep-ph\]](#).
- [80] E. Megias, E. Ruiz Arriola, and L. Salcedo, “Polyakov loop in chiral quark models at finite temperature,” *Phys. Rev.* **D74** (2006) 065005, [arXiv:hep-ph/0412308 \[hep-ph\]](#).
- [81] M. Creutz, *Quarks, Gluons and Lattices*. Cambridge Monographs on Mathematical Physics. Cambridge University Press, 1983.
- [82] J. B. Kogut, M. Snow, and M. Stone, “Mean field and Monte Carlo studies of  $SU(N)$  chiral models in three-dimensions,” *Nucl. Phys.* **B200** (1982) 211–231.
- [83] K. Fukushima and Y. Hidaka, “A Model study of the sign problem in the mean-field approximation,” *Phys. Rev.* **D75** (2007) 036002, [arXiv:hep-ph/0610323 \[hep-ph\]](#).
- [84] G. 't Hooft, “A two-dimensional model for mesons,” *Nuclear Physics B* **75** (1974) no. 3, 461 – 470. <http://www.sciencedirect.com/science/article/pii/0550321374900881>.
- [85] N. Muskhelishvili, *Singular Integral Equations: Boundary problems of functions theory and their applications to mathematical physics*. Springer Netherlands, 2012.
- [86] P. V. Buividovich, G. V. Dunne, and S. N. Valgushev, “Complex path integrals and saddles in two-dimensional gauge theory,” *Phys. Rev. Lett.* **116** (2016) no. 13, 132001, [arXiv:1512.09021 \[hep-th\]](#).
- [87] D. J. Gross and E. Witten, “Possible third order phase transition in the large  $N$  lattice gauge theory,” *Phys. Rev.* **D21** (1980) 446–453.
- [88] F. Green and F. Karsch, “Mean field analysis of  $SU(N)$  deconfining transitions in the presence of dynamical quarks,” *Nucl. Phys.* **B238** (1984) 297–306.
- [89] H. J. Schnitzer, “Confinement/deconfinement transition of large  $N$  gauge theories with  $N(f)$  fundamentals:  $N(f)/N$  finite,” *Nucl. Phys.* **B695** (2004) 267–282, [arXiv:hep-th/0402219 \[hep-th\]](#).
- [90] A. Dumitru, J. Lenaghan, and R. D. Pisarski, “Deconfinement in matrix models about the Gross-Witten point,” *Phys. Rev.* **D71** (2005) 074004, [arXiv:hep-ph/0410294 \[hep-ph\]](#).
- [91] O. Aharony, J. Marsano, S. Minwalla, K. Papadodimas, and M. Van Raamsdonk, “The Hagedorn - deconfinement phase transition in weakly coupled large  $N$  gauge theories,” *Adv. Theor. Math. Phys.* **8** (2004) 603–696, [arXiv:hep-th/0310285 \[hep-th\]](#).
- [92] R. D. Pisarski and V. V. Skokov, “Gross-Witten-Wadia transition in a matrix model of deconfinement,” *Phys. Rev.* **D86** (2012) 081701, [arXiv:1206.1329 \[hep-th\]](#).
- [93] G. Boyd, J. Engels, F. Karsch, E. Laermann, C. Legeland, M. Lutgemeier, and B. Petersson, “Thermodynamics of  $SU(3)$  lattice gauge theory,” *Nucl. Phys.* **B469** (1996) 419–444, [arXiv:hep-lat/9602007 \[hep-lat\]](#).
- [94] B. Lucini and M. Panero, “ $SU(N)$  gauge theories at large  $N$ ,” [arXiv:1210.4997 \[hep-th\]](#).

- [95] B. Sundborg, “The Hagedorn transition, deconfinement and  $N = 4$  SYM theory,” *Nucl. Phys.* **B573** (2000) 349–363, [arXiv:hep-th/9908001](#) [hep-th].
- [96] T. J. Hollowood and J. C. Myers, “Deconfinement transitions of large  $N$  QCD with chemical potential at weak and strong coupling,” *JHEP* **10** (2012) 067, [arXiv:1207.4605](#) [hep-th].
- [97] A. S. Christensen, J. C. Myers, and P. D. Pedersen, “Large  $N$  lattice QCD and its extended strong-weak connection to the hypersphere,” *JHEP* **02** (2014) 028, [arXiv:1312.3519](#) [hep-lat].
- [98] O. Aharony, J. Marsano, S. Minwalla, K. Papadodimas, and M. Van Raamsdonk, “A First order deconfinement transition in large  $N$  Yang-Mills theory on a small  $S^3$ ,” *Phys. Rev.* **D71** (2005) 125018, [arXiv:hep-th/0502149](#) [hep-th].
- [99] M. Oleszczuk and J. Polonyi, “Canonical versus grand canonical ensemble in QCD,” *Submitted to: Annals. Phys.* (1992) .
- [100] K. Fukushima, “Thermodynamic limit of the canonical partition function with respect to the quark number in QCD,” *Annals Phys.* **304** (2003) 72–88, [arXiv:hep-ph/0204302](#) [hep-ph].
- [101] P. N. Meisinger and M. C. Ogilvie, “Chiral symmetry restoration and  $Z(N)$  symmetry,” *Phys. Lett.* **B379** (1996) 163–168, [arXiv:hep-lat/9512011](#) [hep-lat].
- [102] K. Fukushima, “Chiral effective model with the Polyakov loop,” *Phys. Lett.* **B591** (2004) 277–284, [arXiv:hep-ph/0310121](#) [hep-ph].
- [103] F. Sannino, “Polyakov loops versus hadronic states,” *Phys. Rev.* **D66** (2002) 034013, [arXiv:hep-ph/0204174](#) [hep-ph].
- [104] Y. Hatta and K. Fukushima, “Linking the chiral and deconfinement phase transitions,” *Phys. Rev.* **D69** (2004) 097502, [arXiv:hep-ph/0307068](#) [hep-ph].
- [105] N. Ishii, H. Suganuma, and H. Matsufuru, “Scalar glueball mass reduction at finite temperature in  $SU(3)$  anisotropic lattice QCD,” *Phys. Rev.* **D66** (2002) 014507, [arXiv:hep-lat/0109011](#) [hep-lat].
- [106] A. Mocsy, F. Sannino, and K. Tuominen, “Confinement versus chiral symmetry,” *Phys. Rev. Lett.* **92** (2004) 182302, [arXiv:hep-ph/0308135](#) [hep-ph].
- [107] K. Fukushima, “Phase diagrams in the three-flavor Nambu-Jona-Lasinio model with the Polyakov loop,” *Phys. Rev.* **D77** (2008) 114028, [arXiv:0803.3318](#) [hep-ph]. [Erratum: *Phys. Rev.* **D78**, 039902(2008)].
- [108] M. Kobayashi and T. Maskawa, “Chiral symmetry and eta-x mixing,” *Prog. Theor. Phys.* **44** (1970) 1422–1424.
- [109] G. ’t Hooft, “Symmetry breaking through Bell-Jackiw anomalies,” *Phys. Rev. Lett.* **37** (1976) 8–11.
- [110] R. D. Pisarski and F. Wilczek, “Remarks on the chiral phase transition in chromodynamics,” *Phys. Rev.* **D29** (1984) 338–341.
- [111] W.-j. Fu, Z. Zhang, and Y.-x. Liu, “2+1 flavor Polyakov-Nambu-Jona-Lasinio model at finite temperature and nonzero chemical potential,” *Phys. Rev.* **D77** (2008) 014006, [arXiv:0711.0154](#) [hep-ph].

- [112] T. Hell, S. Rossner, M. Cristoforetti, and W. Weise, “Thermodynamics of a three-flavor nonlocal Polyakov-Nambu-Jona-Lasinio model,” *Phys. Rev.* **D81** (2010) 074034, [arXiv:0911.3510 \[hep-ph\]](#).
- [113] A. E. Radzhabov, D. Blaschke, M. Buballa, and M. K. Volkov, “Nonlocal PNJL model beyond mean field and the QCD phase transition,” *Phys. Rev.* **D83** (2011) 116004, [arXiv:1012.0664 \[hep-ph\]](#).
- [114] V. Pagura, D. Gomez Dumm, and N. N. Scoccola, “Deconfinement and chiral restoration in nonlocal PNJL models at zero and imaginary chemical potential,” *Phys. Lett.* **B707** (2012) 76–82, [arXiv:1105.1739 \[hep-ph\]](#).
- [115] K. Kashiwa, T. Hell, and W. Weise, “Nonlocal Polyakov-Nambu-Jona-Lasinio model and imaginary chemical potential,” *Phys. Rev.* **D84** (2011) 056010, [arXiv:1106.5025 \[hep-ph\]](#).
- [116] G. Contrera, A. Grunfeld, and D. Blaschke, “Phase diagrams in nonlocal PNJL models constrained by Lattice QCD results,” [arXiv:1207.4890 \[hep-ph\]](#).
- [117] T. G. Kovacs, “Absence of correlations in the QCD Dirac spectrum at high temperature,” *Phys. Rev. Lett.* **104** (2010) 031601, [arXiv:0906.5373 \[hep-lat\]](#).
- [118] F. Bruckmann, T. G. Kovacs, and S. Schierenberg, “Anderson localization through Polyakov loops: lattice evidence and Random matrix model,” *Phys. Rev.* **D84** (2011) 034505, [arXiv:1105.5336 \[hep-lat\]](#).
- [119] G. Cossu and S. Hashimoto, “Anderson Localization in high temperature QCD: background configuration properties and Dirac eigenmodes,” *JHEP* **06** (2016) 056, [arXiv:1604.00768 \[hep-lat\]](#).
- [120] G. S. Bali, F. Bruckmann, G. Endrodi, Z. Fodor, S. D. Katz, S. Krieg, A. Schafer, and K. K. Szabo, “The QCD phase diagram for external magnetic fields,” *JHEP* **02** (2012) 044, [arXiv:1111.4956 \[hep-lat\]](#).
- [121] G. S. Bali, F. Bruckmann, G. Endrodi, Z. Fodor, S. D. Katz, and A. Schafer, “QCD quark condensate in external magnetic fields,” *Phys. Rev.* **D86** (2012) 071502, [arXiv:1206.4205 \[hep-lat\]](#).
- [122] B.-J. Schaefer, J. M. Pawłowski, and J. Wambach, “The phase structure of the Polyakov–Quark-Meson Model,” *Phys. Rev.* **D76** (2007) 074023, [arXiv:0704.3234 \[hep-ph\]](#).
- [123] K. Yamazaki and T. Matsui, “Quark-hadron phase transition in the PNJL model for interacting quarks,” *Nucl. Phys.* **A913** (2013) 19–50, [arXiv:1212.6165 \[hep-ph\]](#).
- [124] B.-J. Schaefer and H.-J. Pirner, “Renormalization group flow and equation of state of quarks and mesons,” *Nucl. Phys.* **A660** (1999) 439–474, [arXiv:nucl-th/9903003 \[nucl-th\]](#).
- [125] O. Bohr, B. J. Schaefer, and J. Wambach, “Renormalization group flow equations and the phase transition in O(N) models,” *Int. J. Mod. Phys.* **A16** (2001) 3823–3852, [arXiv:hep-ph/0007098 \[hep-ph\]](#).
- [126] J. Braun, L. M. Haas, F. Marhauser, and J. M. Pawłowski, “Phase structure of two-flavor QCD at finite chemical potential,” *Phys. Rev. Lett.* **106** (2011) 022002, [arXiv:0908.0008 \[hep-ph\]](#).

- [127] T. K. Herbst, J. M. Pawłowski, and B.-J. Schaefer, “Phase structure and thermodynamics of QCD,” *Phys. Rev.* **D88** (2013) no. 1, 014007, [arXiv:1302.1426 \[hep-ph\]](#).
- [128] G. Amelino-Camelia, “Thermal effective potential of the  $O(N)$  linear sigma model,” *Phys. Lett.* **B407** (1997) 268–274, [arXiv:hep-ph/9702403 \[hep-ph\]](#).
- [129] S. Chiku and T. Hatsuda, “Optimized perturbation theory at finite temperature,” *Phys. Rev.* **D58** (1998) 076001, [arXiv:hep-ph/9803226 \[hep-ph\]](#).
- [130] T. Nishikawa, O. Morimatsu, and Y. Hidaka, “On the thermal sunset diagram for scalar field theories,” *Phys. Rev.* **D68** (2003) 076002, [arXiv:hep-ph/0302098 \[hep-ph\]](#).
- [131] D. F. Litim, “Optimization of the exact renormalization group,” *Phys. Lett.* **B486** (2000) 92–99, [arXiv:hep-th/0005245 \[hep-th\]](#).
- [132] V. Skokov, B. Stokic, B. Friman, and K. Redlich, “Meson fluctuations and thermodynamics of the Polyakov loop extended quark-meson model,” *Phys. Rev.* **C82** (2010) 015206, [arXiv:1004.2665 \[hep-ph\]](#).
- [133] V. Skokov, B. Friman, and K. Redlich, “Quark number fluctuations in the Polyakov loop-extended quark-meson model at finite baryon density,” *Phys. Rev.* **C83** (2011) 054904, [arXiv:1008.4570 \[hep-ph\]](#).
- [134] T. K. Herbst, J. M. Pawłowski, and B.-J. Schaefer, “The phase structure of the Polyakov-quark-meson model beyond mean field,” *Phys. Lett.* **B696** (2011) 58–67, [arXiv:1008.0081 \[hep-ph\]](#).
- [135] C. S. Fischer and J. A. Mueller, “Chiral and deconfinement transition from Dyson-Schwinger equations,” *Phys. Rev.* **D80** (2009) 074029, [arXiv:0908.0007 \[hep-ph\]](#).
- [136] C. S. Fischer, J. Luecker, and C. A. Welzbacher, “Phase structure of three and four flavor QCD,” *Phys. Rev.* **D90** (2014) no. 3, 034022, [arXiv:1405.4762 \[hep-ph\]](#).
- [137] C. Gattringer, “Linking confinement to spectral properties of the Dirac operator,” *Phys. Rev. Lett.* **97** (2006) 032003, [arXiv:hep-lat/0605018 \[hep-lat\]](#).
- [138] E. Bilgici, F. Bruckmann, C. Gattringer, and C. Hagen, “Dual quark condensate and dressed Polyakov loops,” *Phys. Rev.* **D77** (2008) 094007, [arXiv:0801.4051 \[hep-lat\]](#).
- [139] E. Megias, E. Ruiz Arriola, and L. L. Salcedo, “The Polyakov loop and the hadron resonance gas model,” *Phys. Rev. Lett.* **109** (2012) 151601, [arXiv:1204.2424 \[hep-ph\]](#).
- [140] H. Gies and C. Wetterich, “Renormalization flow of bound states,” *Phys. Rev.* **D65** (2002) 065001, [arXiv:hep-th/0107221 \[hep-th\]](#).
- [141] M. Drews and W. Weise, “Functional renormalization group approach to neutron matter,” *Phys. Lett.* **B738** (2014) 187–190, [arXiv:1404.0882 \[nucl-th\]](#).
- [142] K. Kashiwa, R. D. Pisarski, and V. V. Skokov, “Critical endpoint for deconfinement in matrix and other effective models,” *Phys. Rev.* **D85** (2012) 114029, [arXiv:1205.0545 \[hep-ph\]](#).
- [143] P. M. Lo, B. Friman, and K. Redlich, “Polyakov loop fluctuations and deconfinement in the limit of heavy quarks,” *Phys. Rev.* **D90** (2014) no. 7, 074035, [arXiv:1406.4050 \[hep-ph\]](#).



- [144] U. Reinosa, J. Serreau, and M. Tissier, “Perturbative study of the QCD phase diagram for heavy quarks at nonzero chemical potential,” *Phys. Rev.* **D92** (2015) 025021, [arXiv:1504.02916 \[hep-th\]](#).
- [145] **WHOT-QCD** Collaboration, H. Saito, S. Ejiri, S. Aoki, T. Hatsuda, K. Kanaya, Y. Maezawa, H. Ohno, and T. Umeda, “Phase structure of finite temperature QCD in the heavy quark region,” *Phys. Rev.* **D84** (2011) 054502, [arXiv:1106.0974 \[hep-lat\]](#). [Erratum: *Phys. Rev.* **D85**,079902(2012)].
- [146] A. Dumitru, R. D. Pisarski, and D. Zschiesche, “Dense quarks, and the fermion sign problem, in a SU(N) matrix model,” *Phys. Rev.* **D72** (2005) 065008, [arXiv:hep-ph/0505256 \[hep-ph\]](#).
- [147] C. R. Allton, S. Ejiri, S. J. Hands, O. Kaczmarek, F. Karsch, E. Laermann, C. Schmidt, and L. Scorzato, “The QCD thermal phase transition in the presence of a small chemical potential,” *Phys. Rev.* **D66** (2002) 074507, [arXiv:hep-lat/0204010 \[hep-lat\]](#).
- [148] Y. Tanizaki, H. Nishimura, and K. Kashiwa, “Evading the sign problem in the mean-field approximation through Lefschetz-thimble path integral,” *Phys. Rev.* **D91** (2015) no. 10, 101701, [arXiv:1504.02979 \[hep-th\]](#).
- [149] T. C. Blum, J. E. Hetrick, and D. Toussaint, “High density QCD with static quarks,” *Phys. Rev. Lett.* **76** (1996) 1019–1022, [arXiv:hep-lat/9509002 \[hep-lat\]](#).
- [150] J. Langelage, M. Neuman, and O. Philipsen, “Heavy dense QCD and nuclear matter from an effective lattice theory,” *JHEP* **09** (2014) 131, [arXiv:1403.4162 \[hep-lat\]](#).
- [151] G. Aarts and I.-O. Stamatescu, “Stochastic quantization at finite chemical potential,” *JHEP* **09** (2008) 018, [arXiv:0807.1597 \[hep-lat\]](#).
- [152] G. Aarts, F. Attanasio, B. Jäger, E. Seiler, D. Sexty, and I.-O. Stamatescu, “Insights into the heavy dense QCD phase diagram using Complex Langevin simulations,” *PoS LATTICE2015* (2016) 155, [arXiv:1510.09100 \[hep-lat\]](#).
- [153] A. Roberge and N. Weiss, “Gauge theories with imaginary chemical potential and the phases of QCD,” *Nucl. Phys.* **B275** (1986) 734–745.
- [154] Y. Sakai, K. Kashiwa, H. Kouno, and M. Yahiro, “Polyakov loop extended NJL model with imaginary chemical potential,” *Phys. Rev.* **D77** (2008) 051901, [arXiv:0801.0034 \[hep-ph\]](#).
- [155] T. Sasaki, Y. Sakai, H. Kouno, and M. Yahiro, “Quark-mass dependence of the three-flavor QCD phase diagram at zero and imaginary chemical potential: Model prediction,” *Phys. Rev.* **D84** (2011) 091901, [arXiv:1105.3959 \[hep-ph\]](#).
- [156] K. Morita, V. Skokov, B. Friman, and K. Redlich, “Probing deconfinement in a chiral effective model with Polyakov loop at imaginary chemical potential,” *Phys. Rev.* **D84** (2011) 076009, [arXiv:1107.2273 \[hep-ph\]](#).
- [157] D. Scheffler, M. Buballa, and J. Wambach, “PNJL Model Analysis of the Roberge-Weiss Transition Endpoint at Imaginary Chemical Potential,” *Acta Phys. Polon. Supp.* **5** (2012) 971–976, [arXiv:1111.3839 \[hep-ph\]](#).
- [158] E. Witten, “Theta dependence in the large  $N$  limit of four-dimensional gauge theories,” *Phys. Rev. Lett.* **81** (1998) 2862–2865, [arXiv:hep-th/9807109 \[hep-th\]](#).



- [159] K. Mameda, “QCD  $\theta$ -vacua from the chiral limit to the quenched limit,” *Nucl. Phys.* **B889** (2014) 712–726, [arXiv:1408.1189 \[hep-ph\]](#).
- [160] M. Creutz, “Anomalies and chiral symmetry in QCD,” *Annals Phys.* **324** (2009) 1573–1584, [arXiv:0901.0150 \[hep-ph\]](#).
- [161] D. Boer and J. K. Boomsma, “Spontaneous CP-violation in the strong interaction at  $\theta = \pi$ ,” *Phys. Rev.* **D78** (2008) 054027, [arXiv:0806.1669 \[hep-ph\]](#).
- [162] J. K. Boomsma and D. Boer, “The High temperature CP-restoring phase transition at  $\theta = \pi$ ,” *Phys. Rev.* **D80** (2009) 034019, [arXiv:0905.4660 \[hep-ph\]](#).
- [163] Y. Sakai, H. Kouno, T. Sasaki, and M. Yahiro, “Theta vacuum effects on QCD phase diagram,” *Phys. Lett.* **B705** (2011) 349–355, [arXiv:1105.0413 \[hep-ph\]](#).
- [164] T. Sasaki, J. Takahashi, Y. Sakai, H. Kouno, and M. Yahiro, “Theta vacuum and entanglement interaction in the three-flavor Polyakov-loop extended Nambu-Jona-Lasinio model,” *Phys. Rev.* **D85** (2012) 056009, [arXiv:1112.6086 \[hep-ph\]](#).
- [165] M. D’Elia and F. Negro, “ $\theta$  dependence of the deconfinement temperature in Yang-Mills theories,” *Phys. Rev. Lett.* **109** (2012) 072001, [arXiv:1205.0538 \[hep-lat\]](#).
- [166] M. D’Elia and F. Negro, “Phase diagram of Yang-Mills theories in the presence of a  $\theta$  term,” *Phys. Rev.* **D88** (2013) no. 3, 034503, [arXiv:1306.2919 \[hep-lat\]](#).
- [167] T. H. Hansson, H. B. Nielsen, and I. Zahed, “QED with unequal charges: A Study of spontaneous  $Z_n$  symmetry breaking,” *Nucl. Phys.* **B451** (1995) 162–176, [arXiv:hep-ph/9405324 \[hep-ph\]](#). [Erratum: Nucl. Phys. B456,757(1995)].
- [168] J. Polonyi, “Confinement of triality,” *Phys. Lett.* **B213** (1988) 340–346.
- [169] C. E. Detar and L. D. McLerran, “Order parameters for the confinement - deconfinement phase transition in  $SU(N)$  gauge theories with quarks,” *Phys. Lett.* **B119** (1982) 171–173.
- [170] D. Zwanziger, “Fundamental modular region, Boltzmann factor and area law in lattice gauge theory,” *Nucl. Phys.* **B412** (1994) 657–730.
- [171] F. Lenz and M. Thies, “QCD at finite extension,” [arXiv:hep-ph/9703398 \[hep-ph\]](#).
- [172] F. Lenz and M. Thies, “Polyakov loop dynamics in the center symmetric phase,” *Annals Phys.* **268** (1998) 308–358, [arXiv:hep-th/9802066 \[hep-th\]](#).
- [173] S. Elitzur, “Impossibility of spontaneously breaking local symmetries,” *Phys. Rev.* **D12** (1975) 3978–3982.
- [174] R. Hagedorn and K. Redlich, “Statistical thermodynamics in relativistic particle and ion physics: Canonical or grand canonical?,” *Z. Phys.* **C27** (1985) 541.
- [175] A. Alexandru, M. Faber, I. Horvath, and K.-F. Liu, “Lattice QCD at finite density via a new canonical approach,” *Phys. Rev.* **D72** (2005) 114513, [arXiv:hep-lat/0507020 \[hep-lat\]](#).
- [176] A. Li, A. Alexandru, K.-F. Liu, and X. Meng, “Finite density phase transition of QCD with  $N_f = 4$  and  $N_f = 2$  using canonical ensemble method,” *Phys. Rev.* **D82** (2010) 054502, [arXiv:1005.4158 \[hep-lat\]](#).

- [177] H. Kouno, Y. Sakai, T. Makiyama, K. Tokunaga, T. Sasaki, and M. Yahiro, “Quark-gluon thermodynamics with the  $Z(N(c))$  symmetry,” *J. Phys.* **G39** (2012) 085010.
- [178] H. Kouno, T. Misumi, K. Kashiwa, T. Makiyama, T. Sasaki, and M. Yahiro, “Differences and similarities between fundamental and adjoint matters in  $SU(N)$  gauge theories,” *Phys. Rev.* **D88** (2013) no. 1, 016002, [arXiv:1304.3274 \[hep-ph\]](#).
- [179] H. Kouno, K. Kashiwa, J. Takahashi, T. Misumi, and M. Yahiro, “Understanding QCD at high density from a  $Z_3$ -symmetric QCD-like theory,” *Phys. Rev.* **D93** (2016) no. 5, 056009, [arXiv:1504.07585 \[hep-ph\]](#).
- [180] R. Larsen and E. Shuryak, “Instanton-dyon ensembles with quarks with modified boundary conditions,” *Phys. Rev.* **D94** (2016) no. 9, 094009, [arXiv:1605.07474 \[hep-ph\]](#).
- [181] M. Unsal and L. G. Yaffe, “Center-stabilized Yang-Mills theory: Confinement and large  $N$  volume independence,” *Phys. Rev.* **D78** (2008) 065035, [arXiv:0803.0344 \[hep-th\]](#).
- [182] M. Shifman and M. Unsal, “Multiflavor QCD\* on  $R(3) \times S(1)$ : Studying transition from Abelian to non-Abelian confinement,” *Phys. Lett.* **B681** (2009) 491–494, [arXiv:0901.3743 \[hep-th\]](#).
- [183] F. Sannino, “Higher representations: Confinement and large  $N$ ,” *Phys. Rev.* **D72** (2005) 125006, [arXiv:hep-th/0507251 \[hep-th\]](#).
- [184] L. Del Debbio and A. Patella, “Center symmetry and the orientifold planar equivalence,” *JHEP* **03** (2009) 071, [arXiv:0812.3617 \[hep-th\]](#).
- [185] A. Vuorinen and L. G. Yaffe, “ $Z(3)$ -symmetric effective theory for  $SU(3)$  Yang-Mills theory at high temperature,” *Phys. Rev.* **D74** (2006) 025011, [arXiv:hep-ph/0604100 \[hep-ph\]](#).
- [186] E. Poppitz, T. Schaefer, and M. Unsal, “Universal mechanism of (semi-classical) deconfinement and theta-dependence for all simple groups,” *JHEP* **03** (2013) 087, [arXiv:1212.1238 \[hep-th\]](#).
- [187] A. Cherman, T. Schaefer, and M. Unsal, “Chiral Lagrangian from duality and monopole operators in compactified QCD,” *Phys. Rev. Lett.* **117** (2016) no. 8, 081601, [arXiv:1604.06108 \[hep-th\]](#).
- [188] C. Herold, M. Nahrgang, I. Mishustin, and M. Bleicher, “Chiral fluid dynamics with explicit propagation of the Polyakov loop,” *Phys. Rev.* **C87** (2013) no. 1, 014907, [arXiv:1301.1214 \[nucl-th\]](#).
- [189] P. Braun-Munzinger, B. Friman, and J. Stachel, “Proceedings, 24th International Conference on Ultra-Relativistic Nucleus-Nucleus Collisions (Quark Matter 2014),” *Nucl. Phys.* **A931** (2014) pp.1–1266.
- [190] Y. Akiba, S. Esumi, K. Fukushima, H. Hamagaki, T. Hatsuda, T. Hirano, and K. Shigaki, “Proceedings, 25th International Conference on Ultra-Relativistic Nucleus-Nucleus Collisions (Quark Matter 2015),” *Nucl. Phys.* **A956** (2016) pp.1–974.
- [191] M. Asakawa, U. W. Heinz, and B. Muller, “Fluctuation probes of quark deconfinement,” *Phys. Rev. Lett.* **85** (2000) 2072–2075, [arXiv:hep-ph/0003169 \[hep-ph\]](#).
- [192] S. Jeon and V. Koch, “Charged particle ratio fluctuation as a signal for QGP,” *Phys. Rev. Lett.* **85** (2000) 2076–2079, [arXiv:hep-ph/0003168 \[hep-ph\]](#).

- [193] S. Ejiri, F. Karsch, and K. Redlich, “Hadronic fluctuations at the QCD phase transition,” *Phys. Lett.* **B633** (2006) 275–282, [arXiv:hep-ph/0509051 \[hep-ph\]](#).
- [194] F. Karsch and K. Redlich, “Probing freeze-out conditions in heavy ion collisions with moments of charge fluctuations,” *Phys. Lett.* **B695** (2011) 136–142, [arXiv:1007.2581 \[hep-ph\]](#).
- [195] M. A. Stephanov, “Non-Gaussian fluctuations near the QCD critical point,” *Phys. Rev. Lett.* **102** (2009) 032301, [arXiv:0809.3450 \[hep-ph\]](#).
- [196] X. Luo and N. Xu, “Search for the QCD critical point with fluctuations of conserved quantities in relativistic heavy-ion collisions at RHIC : An overview,” [arXiv:1701.02105 \[nucl-ex\]](#).
- [197] W.-j. Fu, J. M. Pawłowski, F. Rennecke, and B.-J. Schaefer, “Baryon number fluctuations at finite temperature and density,” *Phys. Rev.* **D94** (2016) no. 11, 116020, [arXiv:1608.04302 \[hep-ph\]](#).
- [198] P. Kovtun, D. T. Son, and A. O. Starinets, “Viscosity in strongly interacting quantum field theories from black hole physics,” *Phys. Rev. Lett.* **94** (2005) 111601, [arXiv:hep-th/0405231 \[hep-th\]](#).
- [199] M. Laine and Y. Schroder, “Two-loop QCD gauge coupling at high temperatures,” *JHEP* **03** (2005) 067, [arXiv:hep-ph/0503061 \[hep-ph\]](#).
- [200] Y. Hidaka and R. D. Pisarski, “Small shear viscosity in the semi quark gluon plasma,” *Phys. Rev.* **D81** (2010) 076002, [arXiv:0912.0940 \[hep-ph\]](#).
- [201] P. B. Arnold, G. D. Moore, and L. G. Yaffe, “Transport coefficients in high temperature gauge theories. 1. Leading log results,” *JHEP* **11** (2000) 001, [arXiv:hep-ph/0010177 \[hep-ph\]](#).
- [202] P. B. Arnold, G. D. Moore, and L. G. Yaffe, “Transport coefficients in high temperature gauge theories. 2. Beyond leading log,” *JHEP* **05** (2003) 051, [arXiv:hep-ph/0302165 \[hep-ph\]](#).
- [203] C. H. Lee, J. Wirstam, I. Zahed, and T. H. Hansson, “Thermal dileptons from a nonperturbative quark - gluon phase,” *Phys. Lett.* **B448** (1999) 168–173, [arXiv:hep-ph/9809440 \[hep-ph\]](#).
- [204] C. Gale, Y. Hidaka, S. Jeon, S. Lin, J.-F. Paquet, R. D. Pisarski, D. Satow, V. V. Skokov, and G. Vujanovic, “Production and elliptic flow of dileptons and photons in a matrix model of the quark-gluon plasma,” *Phys. Rev. Lett.* **114** (2015) 072301, [arXiv:1409.4778 \[hep-ph\]](#).
- [205] Y. Hidaka, S. Lin, R. D. Pisarski, and D. Satow, “Dilepton and photon production in the presence of a nontrivial Polyakov loop,” *JHEP* **10** (2015) 005, [arXiv:1504.01770 \[hep-ph\]](#).
- [206] D. Satow and W. Weise, “Chiral symmetry breaking and confinement effects on dilepton and photon production around  $T_c$ ,” *Phys. Rev.* **D92** (2015) no. 5, 056001, [arXiv:1505.03869 \[hep-ph\]](#).
- [207] J. Xu, J. Liao, and M. Gyulassy, “Bridging soft-hard transport properties of quark-gluon plasmas with CUJET3.0,” *JHEP* **02** (2016) 169, [arXiv:1508.00552 \[hep-ph\]](#).
- [208] N. Brambilla, J. Ghiglieri, P. Petreczky, and A. Vairo, “The Polyakov loop and correlator of Polyakov loops at next-to-next-to-leading order,” *Phys. Rev.* **D82** (2010) 074019, [arXiv:1007.5172 \[hep-ph\]](#).
- [209] M. Berwein, N. Brambilla, P. Petreczky, and A. Vairo, “Polyakov loop at next-to-next-to-leading order,” *Phys. Rev.* **D93** (2016) no. 3, 034010, [arXiv:1512.08443 \[hep-ph\]](#).

- [210] O. Kaczmarek, F. Karsch, P. Petreczky, and F. Zantow, “Heavy quark anti-quark free energy and the renormalized Polyakov loop,” *Phys. Lett.* **B543** (2002) 41–47, [arXiv:hep-lat/0207002 \[hep-lat\]](#).
- [211] A. Dumitru, Y. Hatta, J. Lenaghan, K. Orginos, and R. D. Pisarski, “Deconfining phase transition as a matrix model of renormalized Polyakov loops,” *Phys. Rev.* **D70** (2004) 034511, [arXiv:hep-th/0311223 \[hep-th\]](#).
- [212] P. Petreczky and H. P. Schadler, “Renormalization of the Polyakov loop with gradient flow,” *Phys. Rev.* **D92** (2015) no. 9, 094517, [arXiv:1509.07874 \[hep-lat\]](#).
- [213] A. Bazavov, N. Brambilla, H. T. Ding, P. Petreczky, H. P. Schadler, A. Vairo, and J. H. Weber, “Polyakov loop in 2+1 flavor QCD from low to high temperatures,” *Phys. Rev.* **D93** (2016) no. 11, 114502, [arXiv:1603.06637 \[hep-lat\]](#).
- [214] S. Gupta, K. Huebner, and O. Kaczmarek, “Renormalized Polyakov loops in many representations,” *Phys. Rev.* **D77** (2008) 034503, [arXiv:0711.2251 \[hep-lat\]](#).
- [215] E. Megias, E. Ruiz Arriola, and L. L. Salcedo, “Polyakov loop in various representations in the confined phase of QCD,” *Phys. Rev.* **D89** (2014) no. 7, 076006, [arXiv:1311.2814 \[hep-ph\]](#).
- [216] F. Bruckmann, P. V. Buividovich, and T. Sulejmanpasic, “Electric charge catalysis by magnetic fields and a nontrivial holonomy,” *Phys. Rev.* **D88** (2013) 045009, [arXiv:1303.1710 \[hep-th\]](#).
- [217] S. Ozaki, T. Arai, K. Hattori, and K. Itakura, “Euler-Heisenberg-Weiss action for QCD+QED,” *Phys. Rev.* **D92** (2015) no. 1, 016002, [arXiv:1504.07532 \[hep-ph\]](#).